12. RADIONUCLIDE TRANSPORT IN THE SATURATED ZONE

The objective of this section is to evaluate the effect of saturated zone (SZ) information collected since the completion of the *Total System Performance Assessment for the Site Recommendation* (TSPA-SR) (CRWMS M&O 2000 [DIRS 153246]). The new information includes new data, revisions of numerical models, sensitivity analyses, and evaluation of multiple lines of evidence to increase confidence in models used to simulate flow and transport processes. A summary of the supplemental models and new analyses is given in Table 12-1.

12.1 INTRODUCTION

The *Saturated Zone Flow and Transport Process Model Report* (SZ PMR) (CRWMS M&O 2000 [DIRS 153168]) provides details of SZ data and modeling that have been conducted in support of the TSPA-SR (CRWMS M&O 2000 [DIRS 153246]). Characterizing and understanding the flow and transport of radionuclides through the SZ is important in assessing the overall strategy for safely storing radioactive materials at the potential Yucca Mountain repository. If radioactive materials in the potential repository escaped from breached waste packages, they would have to migrate approximately 300 m downward through the unsaturated zone (UZ) to reach the water table and then travel horizontally for approximately 20 km to reach the accessible environment. The nature of the rocks encountered by these radioactive particles along the 20-km flow paths in the SZ, and the time it takes for the particles to travel through the SZ, greatly affects the amount and nature of any materials that might be released to the accessible environment. Thus, the SZ reduces the potential for release through the processes of naturally attenuating radionuclide concentrations and delaying the arrival of radionuclides to the accessible environment.

The water table (i.e., the top of the SZ) under the potential repository occurs in volcanic rocks of the Tertiary Crater Flat Group in a hydrostratigraphic unit referred to as the lower volcanic aquifer. The lower volcanic aquifer is composed of three lithologic units: the Tram, Bullfrog, and Prow Pass Tuffs. After infiltrating water reaches the water table, it joins with groundwater in the lower volcanic aquifer and flows away from the potential repository area in a southeasterly direction, remaining in rocks of the Crater Flat Group. The matrix permeability of the unfractured tuffs in the Crater Flat Group is low; consequently, most of the groundwater flow in these rocks occurs in fractures.

The volcanic rocks are about 2,000 m thick beneath the potential repository, but they thin to the south and interfinger with Tertiary and Quaternary sediments. Along the flow path, at a distance somewhere between 10 and 20 km from the potential repository, groundwater close to the water table enters the valley-fill alluvium and then flows in the alluvium (Figure 12.1-1). The exact location of the transition zone from the volcanic aquifer to the alluvium is uncertain. Section 12.3.1.2.2 discusses new data related to the transition zone. Flow in the alluvium is thought to occur through pores between grains rather than in fractures. Because the effective porosity of alluvium is larger than the effective porosity of fractured rocks, the velocity of transport is expected to be slower in the alluvium.

Table 12-1. Summary of Supplemental Models and Analyses

Key Attributes of System	Process Model (Section of S&ER)	Topic of Supplemental Scientific Model or Analysis	Reason For Supplemental Scientific Model or Analysis			Section of Volume 1	Performance Assessment Treatment of Supplemental Scientific Model or Analysis[a]	
			Unquantified Uncertainty Analysis	Update in Scientific Information	Lower-Temperature Operating Mode Analysis		TSPA Sensitivity Analysis	Included in Supplemental TSPA Model
Delay and Dilution of Radionuclide Concentrations by the Natural Barriers	Saturated Zone Radionuclide Flow and Transport (4.2.9)	Groundwater specific discharge	X	X		12.3.1	X	
		Effective diffusion coefficient in volcanic tuffs	X			12.3.2	X	
		Flowing interval spacing				12.3.2	X	
		Flowing interval (fracture) porosity	X			12.3.2	X	
		Effective porosity in the alluvium	X			12.3.2	X	
		Correlation of the effective diffusion coefficient with matrix porosity	X			12.3.2	X	
		Bulk density of the alluvium	X	X		12.3.2	X	X
		Retardation for radionuclides irreversibly sorbed on colloids in the alluvium	X	X		12.3.2	X	
		No matrix diffusion in volcanic tuffs case				12.5.2	X	
		Presence or absence of alluvium				12.5.2	X	
		Sorption coefficient in alluvium for I, Tc	X	X		12.3.2	X	X
		Sorption coefficient in alluvium for Np, U	X	X		12.3.2	X	
		Sorption coefficient for Np in volcanic tuffs	X			12.3.2	X	
		Kc model for groundwater colloid concentrations Pu, Am		X		12.5.2	X	
		Enhanced matrix diffusion in volcanic tuffs				12.5.2	X	
		Effective longitudinal dispersivity	X	X		12.3.2	X	
		New dispersion tensor		X		12.3.2		
		Flexible design			X	12.3.2		
		Different conceptual models of the large hydraulic gradient and their effects on the flow path and specific discharge		X		12.3.1		
		Hydraulic head and map of potentiometric surface		X		12.3.1		

NOTE: S&ER = *Yucca Mountain Science and Engineering Report* (DOE 2001 [DIRS 153849]).

[a] Performance assessment treatment of supplemental scientific model or analysis discussed in SSPA Volume 2 (McNeish 2001 [DIRS 155023]).

Important physical processes relevant to radionuclide transport in the SZ are advection, dispersion, sorption of radionuclides, matrix diffusion in fractured media, colloid-facilitated transport, and radioactive decay and ingrowth (CRWMS M&O 2000 [DIRS 153168]). The following list provides brief definitions of these terms and describes how they relate to the conceptual model of site-scale SZ flow and transport:

- Advection is the process by which solutes (dissolved substances) are transported by the motion of naturally flowing groundwater.

- Dispersion is the spreading and dilution of solutes transported in groundwater that results from mixing due to variations in fluid flow. These variations in flow are caused by heterogeneities in the subsurface materials through which the flow occurs at a variety of scales, ranging from the pore scale to the scale of the thickness of an individual stratum and to the length of structural features (such as faults).

- Sorption is a general term to describe the binding of a solute onto a material (e.g., mineral grains in the matrix of the tuffs, minerals making up the particles of the alluvium, or colloids). Sorption in the rock matrix and the alluvium retards transport, whereas sorption on colloids can facilitate transport.

- Matrix diffusion is the movement of solutes from groundwater flowing in fractures into the relatively stagnant pore water of the rock matrix and is caused by differences in concentration. When a molecule enters the matrix, its velocity effectively goes to zero until Brownian motion carries it back into a fracture. The result is a delay of the arrival of the solute at a downgradient location from what would be predicted if the solute had remained in the fracture. Thus, matrix diffusion is a transport process that tends to retard the migration of radionuclides through the fractures in the moderately to densely welded tuffs of the SZ. This effect can be further enhanced by sorption of a dissolved radionuclide onto the matrix material once it enters the matrix by diffusion.

- Colloids are tiny particles (i.e., clay minerals, metal oxides, viruses, bacteria, and organic macromolecules) that range in size from 1 to 10,000 nm. These particles can be transported as suspended solids in the groundwater flow. Dissolved radionuclides can bind to colloids and be transported with them.

- Ingrowth is the production over time of radionuclides as decay products of other radionuclides. A particular radionuclide will decay into other radionuclides in a certain amount of time, depending on its half-life. This process is simulated with a one-dimensional model used to track radionuclide decay and radionuclide ingrowth so they are accounted for in the modeling predictions.

This section describes new information developed since completion of the initial analysis model reports (AMRs), process model reports (PMRs), the TSPA-SR (CRWMS M&O 2000 [DIRS 153246]), and the *Yucca Mountain Science and Engineering Report* (DOE 2001 [DIRS 153849]). The new information includes:

- New data and analyses to quantify previously unquantified uncertainties and to establish new uncertainty ranges.
- New data, and new technical work at the process-model level.
- Multiple lines of evidence, including natural analogues, hydrochemical and isotopic analyses, and other lines of evidence. The multiple lines of evidence are used to independently support the identification of processes affecting flow and transport, the numerical modeling of the processes, and the modeling predictions.

Much of the new information reported in Section 12 comes from sensitivity analyses. The objectives of these sensitivity analyses include, but are not limited to, examination of previously unquantified uncertainty, scoping calculations, and additional conceptual models. It is anticipated that many of the scoping calculations and sensitivity analyses will not be carried forward to future baseline project documents. Consequently, a fully-documented basis for the assumptions used in these calculations and analyses has not been developed.

Several types of new data and information have been obtained as part of the Nye County Early Warning Drilling Program (NC-EWDP). Under this program, the Nye County Nuclear Waste Repository Project Office, the U.S. Geological Survey (USGS), and the Yucca Mountain Site Characterization Office jointly collect data to characterize the saturated zone down gradient of Yucca Mountain. New measurements of hydraulic head were obtained as described in Section 12.3.1.2. These include new measurements in the NC-EWDP Phase II wells and updated water levels for Phase I wells. Lithologic descriptions and stratigraphic correlations have been completed for the Phase I and Phase II wells. Measurements of sorption coefficients in laboratory batch tests have confirmed that iodine-129 and technetium-99 are essentially nonsorbing in the alluvium under oxidizing conditions. New data from column and batch experiments have been used to define the K_d estimate for neptunium-237. Preliminary results indicate significant filtration of colloids at the Alluvium Testing Complex (ATC). In modeling, a preliminary analysis of the ATC single-well tracer test data has corroborated a continuum porous-media conceptual model for the alluvium hydrogeologic units (Section 12.3.1.2). A complete discussion of new data for flow and transport since the TSPA-SR (CRWMS M&O 2000 [DIRS 153246]) is presented in Sections 12.3.1.2 and 12.3.2.2, respectively.

Uncertainty in flow and transport modeling arises from a number of sources, including the conceptual model of the processes affecting groundwater flow and transport, water-level measurements, simplification of the model geometry, simplification of the boundary conditions, the values of permeability assigned to hydrogeologic units, and simplification of the parameters and geometry of matrix diffusion, dispersion, and sorption models. These various types of uncertainty are accounted for explicitly in the TSPA-SR site-scale SZ flow and transport model through key parameters and conceptual models. Key uncertain SZ parameters are represented stochastically as input to the site-scale SZ model. Examples of some of the important parameters

that are considered stochastically are the specific discharge under Yucca Mountain, the northern and western boundaries of the alluvium, the flowing interval spacing and porosity, sorption coefficients, and dispersivities. Horizontal anisotropy is included as an alternate conceptual flow model by considering an isotropic and an anisotropic case.

An unquantified uncertainty analysis of the site-scale SZ flow and transport model was performed based on results of the TSPA-SR (CRWMS M&O 2000 [DIRS 153246]). The unquantified uncertainty analysis consisted of multiple (100) simulations of radionuclide transport with the site-scale SZ model in which all changes resulting from the unquantified uncertainty analysis were included, as discussed in Section 12.5.1. The resulting SZ radionuclide breakthrough curves for the unquantified uncertainty case are supplied to the total system performance assessment (TSPA) simulator for the SSPA Volume 2 (McNeish 2001 [DIRS 155023]) calculations of simulated dose rates. In general, identification of unquantified uncertainty for the site-scale SZ flow and transport model consisted of re-evaluation of previously quantified uncertainty with focus on the parameters that were most important to performance. Sections 12.3.1.4 and 12.3.2.4 provide the basis for the parameters that were re-evaluated as part of the unquantified uncertainty analysis. A sensitivity analysis based on the TSPA-SR was performed to evaluate the relative importance of the stochastically varied parameters. The results indicated that the median travel time of a conservative species was most sensitive to variations in the groundwater specific discharge beneath Yucca Mountain, with the sorption coefficients, extent of the flow path in the alluvium, and parameters associated with diffusion of solutes into the rock matrix being of secondary importance (Kuzio et al. 2000 [DIRS 154928]) in the TSPA-SR. The groundwater specific discharge parameter was re-evaluated and is discussed in Sections 12.3.1.4.

Parameters affecting transport that were reevaluated as part of the unquantified uncertainty analysis included:

- Distribution of sorption coefficients for neptunium in volcanic rock and alluvium (Sections 12.3.2.4.1 and 12.3.2.4.2)
- Sorption coefficient for Uranium in alluvium (Section 12.3.2.4.3)
- Bulk density of the alluvium (Section 12.3.2.4.4)
- Retardation of radionuclides irreversibly sorbed onto colloids (Section 12.3.2.4.5)
- Distribution of the effective matrix diffusion coefficients and its correlation with the matrix porosity in volcanic rock (Section 12.3.2.4.6)
- Effective porosity of the alluvium (Section 12.3.2.4.7)
- Flowing interval (fracture) porosity in the volcanic rock (Section 12.3.2.4.8).

The bulk density in the alluvium was the only parameter that was a constant value in the TSPA-SR, and as a result of the unquantified uncertainty analyses, it was changed from a constant to a stochastic variable.

Various sensitivity analyses were conducted with the site-scale SZ flow and transport model in support of the SSPA Volume 2 calculations (McNeish 2001 [DIRS 155023]), as discussed in Section 12.5.2. The sensitivity analyses resulted in SZ radionuclide breakthrough curves that are being supplied to the TSPA simulator for the calculation of simulated dose rates in the SSPA Volume 2 (McNeish 2001 [DIRS 155023]). These analyses are performed to evaluate the sensitivity of the SSPA Volume 2 model results (McNeish 2001 [DIRS 155023]) to different parameters. Results of these sensitivity analyses are presented as histograms of times of median breakthrough curves in Section 12.5.2. The analyses investigate the effect of no matrix diffusion in the volcanic units, enhanced matrix diffusion in the volcanic units, a minimum length of alluvium in the flow path, and increased uncertainty in the reversible colloid model. The results of the sensitivity analyses in the SSPA Volume 2 calculations are discussed in more detail in McNeish (2001 [DIRS 155023], Section 3.2.10).

Additionally, sensitivity analyses and new technical work at the process-model level are described in Sections 12.3.1.3 and 12.3.2.3. These analyses are not carried forward to the SSPA Volume 2 calculations (McNeish 2001 [DIRS 155023]). The analyses include discussion of different conceptual models of the large hydraulic gradient, alternative conceptualizations of the Solitario Canyon fault, flexible repository design, new dispersion tensor, effective longitudinal dispersivity in the site-scale SZ flow and transport model, and matrix diffusion sensitivity analyses.

Section 12.4 describes the multiple lines of evidence in support of flow and transport parameter estimation and modeling at Yucca Mountain. The following areas are discussed: evidence for flow paths based on groundwater hydrochemical and isotopic data, uranium mill tailing analogues, preliminary tracer testing results in the alluvial testing complex, Electric Power Research Institute flow and transport modeling, and data transport studies on blocks of intact tuff. The primary goal of this portion of the work is to develop additional confidence in the models and parameters used for the TSPA.

12.2 REVIEW OF TOTAL SYSTEM PERFORMANCE ASSESSMENT-SITE RECOMMENDATION TREATMENT OF RADIONUCLIDE FLOW AND TRANSPORT IN THE SATURATED ZONE

The objective of the SZ flow and transport modeling effort is to provide breakthrough curves for individual radionuclides for input to performance assessment calculations. A breakthrough curve is the variation with time of the mass flux of an individual radionuclide at a distance of 20 km from the potential repository. Developing this input to performance assessment calculations has three steps: (1) hydrogeologic characterization, (2) generation of the site-scale calibrated flow field, and (3) abstraction of SZ flow and radionuclide transport modeling for performance assessment analyses. The first step provides the conceptual basis for developing numerical models used in the second and third steps. The calibrated flow field generated by the second step is used in radionuclide transport calculations performed during the third (abstraction) step.

Section 12.2 provides a summary of the process used to develop SZ input to the TSPA-SR (CRWMS M&O 2000 [DIRS 153246]). A more detailed discussion of this process is presented in the SZ PMR (CRWMS M&O 2000 [DIRS 153168], Section 3.6). An important aspect of this process is that it is periodically updated to include revised interpretations of hydrogeologic data,

new results from field and laboratory experiments, model developments, and quantification of uncertainty. A discussion of changes in these areas since the TSPA-SR is provided in Section 12.3.

12.2.1 Hydrogeologic Characterization

A large amount of information about the regional-scale hydrogeology has been learned from activities of the Yucca Mountain Site Characterization Project and from numerous hydrogeologic studies conducted in the vicinity of the Nevada Test Site (NTS). Specifically, sufficient information is available to describe the stratigraphy, structure, and hydraulic properties of rocks in this region, the recharge and discharge regions, and the groundwater flow paths.

As part of an ongoing effort, the USGS is conducting regional-scale simulations of groundwater flow in a hydrologic basin known as the Death Valley regional groundwater flow system. This model region includes the SZ flow paths from the repository to their discharge areas. This modeling effort, including data synthesis, geologic interpretation, and analysis of model results, provides an essential contribution to understanding of the hydrogeology in the vicinity of Yucca Mountain.

A detailed description of what is known about the hydrogeology of the Yucca Mountain region is contained in the SZ PMR (CRWMS M&O 2000 [DIRS 153168], Section 3.2). The following three paragraphs are abstracted from that document.

Natural recharge to the SZ is from precipitation that infiltrates at the land surface and percolates through the unsaturated zone. Recharge occurs primarily in mountainous areas where relatively large amounts of snow and rainfall occur. Areas of recharge include Yucca Mountain and other regions of higher elevation to the north and northeast. Natural discharge from the Death Valley flow system is from evapotranspiration and springs at low elevations, mainly in Death Valley, Ash Meadows, and Franklin Lake Playa. Groundwater flows from regions of recharge to regions of discharge. Flow paths in the SZ at the regional scale are inferred from a large number of measurements of water levels in boreholes and numerical modeling (D'Agnese et al. 1997 [DIRS 100131]). Taken together, information about recharge, discharge, and measured water levels provides a sound understanding of groundwater flow paths in the SZ in the vicinity of Yucca Mountain.

As groundwater moves from recharge to discharge areas, flow rates and paths depend largely on the hydraulic properties of the rocks and materials along the flow paths. Geologic studies provide a sufficient understanding to identify the important rock types and their spatial distribution. The rock types that play the largest role in regional hydrogeology are Paleozoic carbonates, Quaternary-Tertiary volcanic rocks, and Quaternary-Tertiary sediments and volcanic tuffs that fill structural depressions (referred to as valley-fill material in portions of this report). The valley fill is primarily alluvium. Relatively shallow flow occurs in the volcanic rocks and valley fill; deeper flow occurs in the regionally extensive carbonate aquifer. Along the inferred shallow flow path in the SZ from Yucca Mountain, groundwater flow occurs in volcanic rocks near the potential repository site and in younger valley-fill deposits at greater distances from the potential repository.

The permeability of the volcanic rocks in the vicinity of Yucca Mountain typically is increased by the presence of fractures. An extensive suite of field observations, interpretations of borehole logs, hydrologic tests in boreholes, lab-scale tests, and field tracer tests confirmed that fractures enhance groundwater flow in the volcanic rocks. However, flow in the alluvium occurs through the primary porosity (intergranular porosity) of these sediments.

12.2.2 Site-Scale Calibrated Flow Field

The purpose of the site-scale SZ flow and transport model is to provide a calibrated flow field as input to the step of abstracting SZ flow and radionuclide transport modeling for TSPA analyses. The flow field is three-dimensional and steady-state, and it assumes horizontally isotropic permeability within units and present-day climatic conditions. A detailed description of how this flow field was calculated is provided in the *Calibration of the Site-Scale Saturated Zone Flow Model* report (CRWMS M&O 2000 [DIRS 139582], Section 6). A brief summary is presented here.

A governing equation for mass conservation for flow described by Darcy's Law is solved numerically using the control-volume finite element method. The FEHM code (V2.00) is used to calculate a steady-state flow field. Zyvoloski et al. (1997 [DIRS 110491]) provide a description of the theoretical basis and capabilities of the code. The footprint of the site-scale SZ flow and transport model is a 30- by 45-km rectangle shown in Figure 12.2-1. The water table forms the upper surface of the model. The base of the model is a surface approximately 3,000 m below the water table. A structured grid of orthogonal hexahedral elements is used to discretize the model domain. Horizontal grid spacing is uniform (500 m), and vertical spacing ranges from 10 m near the water table to 550 m at depth.

Various aspects of the hydrogeology within the domain of the site-scale flow and transport model are being investigated as part of ongoing characterization of the region surrounding Yucca Mountain. These include the hydrostratigraphic framework, estimates of recharge rates, position of the water table, rates of groundwater flow at the model boundaries as provided by the USGS regional-scale flow model, and estimates of rock permeability. The site-scale flow and transport model used for input to the TSPA-SR used the most up-to-date information available to represent these aspects of hydrogeology, as described below.

Position of the Water Table–The position of the water table is shown in Figure 12.2-2. As noted above, this interpretation of the water table is used to define the upper surface of the site-scale flow and transport model. Also, the elevation of the water table along the model boundaries is applied as a constant-head boundary condition on the sides of the model. This interpretation of the water-level data assumes that several of the water levels measured north of Yucca Mountain represent the regional potentiometric surface rather than the top of zones of perched water. Consequently, this interpretation maximizes the gradient of the potentiometric surface north of Yucca Mountain. This region of steep gradient is referred to as the large hydraulic gradient. Analysis and interpretation of water-level data are discussed in detail in USGS (2001 [DIRS 154625], Section 6).

Hydrogeologic Framework Model–The geometry of regions with uniform permeability within the model domain is based on geometric modeling of the hydrostratigraphy and geologic

structure of the area. The result is referred to as the hydrogeologic framework model. The version of the hydrogeologic framework model used to support the TSPA-SR is documented in USGS (2000 [DIRS 146835], Section 6).

Treatment of Discrete Faults–One way in which alternative conceptual models are considered in the site-scale model is by representing faults that are believed to be hydrologically important as discrete features. Using this approach, various assumptions about the permeability, and anisotropy in permeability, of the individual faults can be tested. The fault properties assumed to calculate the calibrated flow field for the TSPA-SR are summarized in CRWMS M&O (2000 [DIRS 139582], Table 6).

Permeability Features Related to the Large Hydraulic Gradient–Some adjustments to the permeability distribution are required to better simulate the water levels that define the upgradient portions of the large hydraulic gradient. For the calculations used to generate input to the TSPA-SR, a planar east-west trending zone of low permeability (CRWMS M&O 2000 [DIRS 139582], Table 6) was positioned into the model domain to better match the observed water-level elevations. Alternative adjustments to the permeability distribution to better simulate the large hydraulic gradient are discussed in Section 12.3.1.3.

Recharge Estimates–Recharge is applied as a specified flux on the upper surface of the site-scale model. There are three components of the recharge distribution assumed for the site-scale model: distributed recharge used for the 1997 version of the USGS regional-scale model (D'Agnese et al. 1997 [DIRS 100131]), recharge calculated as the flux at the base of the UZ site-scale model, and focused recharge along Fortymile Wash. A detailed discussion of the assumed distribution of recharge is provided in CRWMS M&O (1999 [DIRS 130979], Section 6.1.1).

Calibration is the process by which values of important model parameters are estimated and optimized to produce the best fit of model output to observed data. For the site-scale flow and transport model, permeability values were optimized to minimize the sum of the squared differences between observed hydraulic conditions and those simulated by the site-scale SZ flow and transport model. Hydraulic conditions included water levels (hydraulic heads) at selected locations and lateral fluxes at selected model boundaries. The specific water levels and boundary fluxes are referred to as calibration targets. Water levels used as calibration targets are documented in USGS (2001 [DIRS 154625], Table I-1), and boundary fluxes used are documented in CRWMS M&O (1999 [DIRS 130979], Section 7.2).

Additional confidence in the results of the site-scale flow and transport model was obtained by comparing estimated to measured permeabilities and calculated flow paths to flow paths inferred from water chemistry data (CRWMS M&O 2000 [DIRS 139582], Section 6.7.8 and 6.7.6, respectively).

12.2.3 Abstraction of Saturated Zone Flow and Radionuclide Transport Modeling for Total System Performance Assessment Analyses

It is desirable to integrate detailed process-level modeling into performance assessment analyses to incorporate site-specific information about the system represented by the process-level model.

This may be accomplished by explicitly coupling the process-level computational model into the performance assessment simulator or by abstracting the process-level model results for incorporation into the performance assessment analyses. An abstraction approach was used to integrate SZ flow and transport modeling into TSPA-SR analyses primarily because of the size and complexity of the site-scale SZ flow and transport model. In addition, an abstraction approach that largely captures the information that is provided by the site-scale SZ flow and transport model about system behavior is possible. Details and results of the abstraction process, as applied to TSPA-SR, are provided in the *Input and Results of the Base Case Saturated Zone Flow and Transport Model for TSPA* report (CRWMS M&O 2000 [DIRS 139440], Section 6) and in the SZ PMR (CRWMS M&O 2000 [DIRS 153168], Section 3.7).

The site-scale SZ flow and transport model results are abstracted by performing radionuclide transport simulations that assume a constant, normalized radionuclide mass flux at the "upstream" end of the SZ. The resulting radionuclide mass breakthrough curves at the "downstream" end of the SZ basically contain all of the information about the model behavior for those source and receptor locations, assuming steady groundwater flow. Breakthrough curves for eight species or classes of species (CRWMS M&O 2000 [DIRS 139440], Section 6.3) are obtained for 100 stochastic realizations of the SZ system (the nominal case) and for one additional case using the median values for all stochastic parameters.

These results are obtained by running the site-scale SZ flow and transport model for each stochastic realization and saving the results for later use by the TSPA simulator. Radionuclide transport is simulated directly for those radionuclides that are not the product of radioactive decay and ingrowth using the FEHM V2.10 software code streamline particle-tracking algorithm. Radioactive ingrowth is the generation of radionuclide mass from the decay of a parent radionuclide.

Stochastic parameters are used to quantify uncertainty in radionuclide transport characteristics of the SZ system. Key parameters include those that describe sorption coefficients for sorbing radionuclides, flowing interval spacing, porosity, matrix porosity in fractured volcanic units, effective porosity in alluvial units, dispersivity, and effective diffusion coefficient. Parameter distributions and rationale are provided in CRWMS M&O (2000 [DIRS 147972]) and CRWMS M&O (2000 [DIRS 154927]). Additional data and inferences regarding colloid-facilitated transport of radionuclides are used (CRWMS M&O 2000 [DIRS 154927]) in the site-scale SZ flow and transport model to simulate this process (CRWMS M&O 2000 [DIRS 129286]; CRWMS M&O 2000 [DIRS 147972]). For the TSPA-SR, the stochastic parameters were sampled to generate the 100 random realizations of the SZ system.

In addition to the relatively high degree of uncertainty in the radionuclide transport characteristics of the SZ system, there is uncertainty in the groundwater flow in the system. Uncertainties exist in the SZ groundwater flux and in the direction of groundwater flow downgradient from the potential repository. To evaluate the uncertainty in groundwater flux, three discrete cases were examined. These consist of the mean case (corresponding to the mean flux of the calibrated site-scale SZ flow and transport model), the low case (mean flux times 0.1), and the high case (mean flux times 10). The flux multipliers and the corresponding probabilities for these cases are quantified based on the uncertainty distribution for specific discharge in the volcanic aquifer from the SZ expert elicitation (CRWMS M&O 1998 [DIRS 100353], p. 3-20).

The analysis is provided in CRWMS M&O (2000 [DIRS 139440], Section 6.2.5). Uncertainty in the direction of groundwater flow along the flow path from the potential repository is incorporated as alternative groundwater flow fields with and without horizontal anisotropy in permeability (CRWMS M&O 2000 [DIRS 147972]). The result of considering both types of uncertainty is six alternative groundwater flow fields (three flux cases times two anisotropy cases).

12.3 ACCOUNT FOR UNCERTAINTIES AND VARIABILITIES IN PARAMETER VALUES

This section provides supplemental information to the TSPA-SR (CRWMS M&O 2000 [DIRS 153246]) and reflects the current understanding of the flow of groundwater and transport of radionuclides through groundwater from beneath the potential repository to the accessible environment at the point of compliance per proposed NRC regulation 10 CFR Part 63 (64 FR 8640, Section 63.115(b) [DIRS 101680].

This section is subdivided into two subsections:

- Flow modeling and associated data and analyses (Section 12.3.1)
- Transport modeling and associated data and analyses (Section 12.3.2).

12.3.1 Groundwater Flow Modeling

This section covers new water-level, hydrostratigraphy, hydrochemistry, and testing data acquired in cooperation with Nye County; analyses using the flow model; and sensitivity analyses on the specific discharge and other flow parameters that affect the specific discharge.

12.3.1.1 Introduction and Goal of the Site-Scale Saturated Zone Flow Model

The purpose of the site-scale SZ flow model is to provide a calibrated flow field that is to be used for calculating radionuclide transport in the SZ. The same calibrated flow field was used for TSPA-SR and SSPA calculations. However, the site-scale model is in the process of being updated to include pertinent geologic and hydrologic information that has become available since the TSPA-SR (CRWMS M&O 2000 [DIRS 153246]) was published. An overview of this information is provided in Section 12.3.1.2. Also section 12.3.1.3 includes a discussion of developments in the numerical model and a model analysis that has been completed since the TSPA-SR was published. Revisions to the site-scale SZ flow model, discussed in Section 12.3.1.3, were not used in SSPA calculations. Unquantified uncertainty addressed in the SSPA Volume 2 (McNeish 2001 [DIRS 155023]) that pertains to the site-scale SZ flow and transport model is discussed in Section 12.3.1.4.

12.3.1.2 New Data and Analysis

The site-scale SZ flow model is being updated to include new data and geologic interpretations. New data and interpretations might require changes in the geometry of hydrostratigraphic units within the model domain, permeability values assigned to hydrostratigraphic units, hydraulic head values used as calibration targets, and boundary fluxes used as calibration targets. New

data and interpretations also help constrain conceptual models and, in some cases, are independent information that build confidence in the current model.

The new data and analysis described in this section will help future versions of the site-scale SZ flow and transport model to represent actual flow conditions in the vicinity of Yucca Mountain more accurately. The new information is not expected to result in significant changes at the TSPA level (CRWMS M&O 2000 [DIRS 139440]).

12.3.1.2.1 Hydraulic Head Data and Potentiometric Surface Map

New measurements of hydraulic head have been obtained as part of the Nye County cooperative program. These include new measurements in the NC-EWDP Phase II wells and updated water levels for Phase I wells (Figure 12.3.1.2-1). These new measurements will be used in calibrating future versions of the site-scale SZ flow model.

A revised potentiometric surface map covering the area of the site-scale SZ flow model (Figure 12.3.1.2.2) is being developed for use in future versions of the site-scale SZ flow model. This map will include data for well USW WT-24 and new data from the Nye County wells. In addition, the new map will present an alternative concept for water levels north of Yucca Mountain in the "large hydraulic gradient area." This concept assumes that water levels reported for wells USW G-2 and UE-25 WT#6 represent perched conditions and are not representative of regional potentiometric levels. Water levels at well USW WT-24, which are significantly lower than those reported for USW G-2 and UE-25 WT#6, are believed to represent the regional potentiometric level. These wells are located within several km of Yucca Mountain. Wells USW G-2 and UE-25 WT#6 are located 3 to 4 km north-northeast of Yucca Mountain. Well USW WT-24 is located about 1 km east of the crest of Yucca Mountain. The impact of this alternative conceptual model is that the large hydraulic gradient, although still present north of Yucca Mountain, is slightly more than half of the previously reported gradient. Tucci and Burkhardt (1995 [DIRS 101060], p. 9) report a value of 0.11 m/m for the large hydraulic gradient area; the gradient based on the revised potentiometric surface map ranges from 0.06 to 0.07 m/m.

Water-level measurements in the recently drilled NC-EWDP-2DB well also add information about differences in hydraulic head between the volcanic rocks and the underlying Paleozoic carbonate rocks. Previous to the drilling of NC-EWDP-2DB, there was only one other measurement of hydraulic head in the carbonate rocks at UE-25 p#1 within the domain of the site-scale SZ flow and transport model. Head measurements in that borehole, located about 4 km east of Yucca Mountain, indicated that the head in the carbonate rocks is about 20 m higher than the head in the overlying volcanic rocks (Craig and Johnson 1984 [DIRS 101039], p. 12). This difference in head is of interest because higher heads in the carbonate unit along flow pathways from the potential repository would prevent a contaminant plume from entering the regional-scale carbonate aquifer.

Water-level measurements in NC-EWDP-2DB, representing the head in the Paleozoic carbonate, indicate that the head in the carbonate rocks is about 714 m above mean sea level (NWPRO 1999 [DIRS 119607]). The head in the overlying volcanic rocks in a borehole drilled at the same site, NC-EWDP-2D, is about 706 m (NWPRO 1999 [DIRS 119607]). Therefore, the new data from

NC-EWDP-2DB support the concept that the head in the Paleozoic carbonates is higher than the head in the volcanic rocks, where flow from the potential repository is expected to occur.

The new and updated water levels for the Nye County wells will not significantly change the potentiometric surface contours south of Yucca Mountain from the contours presented in *Water-Level Data Analysis for the Saturated Zone Site-Scale Flow and Transport Model* (USGS 2001 [DIRS 154625], Section 6). These data will further constrain a moderate to steep hydraulic gradient (0.01 to 0.05 m/m) that roughly parallels U.S. Highway 95 south of Crater Flat and refine the shape of the contours in the Lathrop Wells area. The shape of the contours in the vicinity of Yucca Mountain will not change significantly.

Recent water-level measurements at the Nye County boreholes located at the northern edge of the Amargosa Desert also provide some insight into how the groundwater flow system might respond to future changes in climate. Water levels in these boreholes, located at the Lathrop Wells diatomite deposit (boreholes NC-EWDP-1S (MO0004NC99WL1S.000 [DIRS 149258]) and NC-EWDP-1D (MO0004NC99WL1D.000 [DIRS 149257])) and along Crater Flat Wash (borehole NC-EWDP-9S (MO0004NC99WL9S.000 [DIRS 149263])), show that the regional water table is at an altitude of about 800 m. These data show that 17 to 30 m of water table rise would be sufficient to reach the land surface at these sites.

12.3.1.2.2 Stratigraphy of Nye County Early Warning Drilling Program Boreholes

Lithologic descriptions and stratigraphic correlations have been completed for the Phase I and Phase II boreholes drilled under the NC-EWDP. Alluvium, tuffs, tuffaceous sedimentary rocks, and the Paleozoic rocks that comprise part of the lower carbonate aquifer have been identified. The subsurface geologic data are being compiled, together with surface-based geophysical and geologic-mapping results, to prepare (1) a generally east-west cross section aligned approximately along U.S. Highway 95, near the downgradient boundary of the site-scale SZ flow and transport model, and (2) a north-south cross section generally parallel to Fortymile Wash.

The location where flow paths from the potential repository pass from volcanic rock to alluvium is a specific stratigraphic issue that some of the new data address. Information from boreholes NC-EWDP-2D and NC-EWDP-19D1 is relevant because of the location of these wells along the inferred SZ flow path from Yucca Mountain. Data from borehole NC-EWDP-2D, located approximately 19 km from the potential repository, indicate greater than 800 ft of saturated alluvium beginning at the water table (DTN: GS000808314211.005 [DIRS 154685]; DTN: MO0004NC99WL2D.000 [DIRS 149259]). Data from borehole NC-EWDP-19D1, located approximately 18 km from the repository, show greater than 400 ft of saturated alluvium underlain by a significant section of volcanic rocks (DTN: MO0007NYE02565.024 [DIRS 154686]; Black 2000 [DIRS 154704]).

These observations indicate that groundwater flow in the SZ originating from Yucca Mountain includes flow through a portion of the porous alluvium in the area near the 20-km compliance boundary. Information from borehole NC-EWDP-19D1 is somewhat ambiguous with regard to the groundwater flow path in the alluvium because it has not been established whether greater groundwater flow would be expected in the alluvium or in the underlying volcanic unit. Further to the north of boreholes NC-EWDP-19D1, the question of whether the flow path encounters

alluvium or volcanic rocks is generally open to geologic and hydrologic interpretation. Additional drilling in this area by the Nye County drilling program will further reduce the uncertainty associated with this question. In the meantime, uncertainty about the length of the flow path through the alluvium is included in numerical simulations (CRWMS M&O 2000 [DIRS 139440], Section 6) of site-scale SZ flow and transport for the TSPA-SR.

The cross sections and associated geologic interpretations will be adapted as refinements of the hydrogeologic framework for the site-scale SZ flow and transport model are developed.

12.3.1.2.3 New Regional Flow Model

The steady-state version of the new USGS Death Valley regional flow system model is nearing completion. Stakeholders include the National Park Service, the U.S. Fish and Wildlife Service, and state and county offices in Nevada and California. Some modifications to the hydrogeologic framework and hydrologic parameters are being made as additional data are compiled and in response to calibration results. The importance of structural features, particularly faults, to groundwater flow in this region is emphasized in a new hydrostructural map. These and other geologic data are being processed for application in the next modeling phase, which is the development of a transient model.

The new regional-scale model will provide estimates of groundwater flux along the lateral boundaries of the site-scale SZ flow and transport model. It is anticipated that these new flux estimates will be used as calibration targets in future revisions of the site-scale SZ flow and transport model. Development of the regional-scale model grid and representation of hydrogeologic and hydrologic parameters are being coordinated with the site-scale SZ flow and transport model to assure compatibility at the boundaries of the site-scale model.

12.3.1.2.4 Alluvial Testing Complex

From July 2000 through November 2000, pumping tests were conducted in borehole NC-EWDP-19D1 at the ATC, and data from these tests are being evaluated. There are four screened intervals in the alluvium at this borehole; tests that pump from the four screened intervals combined, as well as from each interval individually, have been performed. These tests will provide estimates of the permeability of the alluvium at this site, including the degree to which the alluvium is heterogeneous and anisotropic with respect to permeability. Information from these tests will be used to update the conceptual understanding of the hydraulic behavior of the alluvium and to constrain the values of permeability of alluvium used in the site-scale flow model. Tracer tests are also being performed at the ATC to estimate transport properties of the alluvium (i.e., effective porosity, dispersivity, and the degree of dual-porosity behavior). Implications of the new information about transport properties are discussed in Sections 12.3.2.2 and 12.3.2.4. Isotopic data are discussed in Section 12.4.

12.3.1.3 New Model Development and Analysis Since Completion of the Total System Performance Assessment-Site Recommendation

This section discusses new model development and new analysis performed since the completion of the TSPA-SR (CRWMS M&O 2000 [DIRS 153246]). One result of the new analysis, as described in Section 12.3.1.3.1, is that different conceptual models of the origin of the large hydraulic gradient north of Yucca Mountain can result in flow paths away from the potential repository that are noticeably different from the flow paths predicted by the flow model used for the TSPA-SR. However, all flow paths are mainly in the same units, i.e., the Bullfrog Tuff and the alluvial units, regardless of the model. The net result of the newer flow paths is a relatively shorter traverse through the alluvial units compared to the paths for the original model.

12.3.1.3.1 Different Conceptual Models of the Large Hydraulic Gradient and Their Effect on the Flow Path and Specific Discharge

An area of large hydraulic gradient north of the potential high-level radioactive waste repository at Yucca Mountain has been inferred from hydraulic head measurements. This area has been a source of controversy and discussion for many years, and the cause of the gradient is unknown. An east-west trending strip with low permeability was incorporated into the SZ site-scale flow model to simulate this steep gradient in the flow field used for the TSPA-SR (CRWMS M&O 2000 [DIRS 153246]). The actual presence of such a feature has not been confirmed by field investigations. Consequently, investigation of additional conceptual models concerning the origin of the large hydraulic gradient has been initiated since the completion of the TSPA-SR.

Two additional conceptual models have been investigated to date. The first of these attributes the apparent large hydraulic gradient to the occurrence of low-permeability hydrothermally altered rock north of Yucca Mountain (DTN: LA0105GZ12213S.002 [DIRS 154888]). The second new conceptual model, in addition to incorporating the hypothesized hydrothermally altered rock north of Yucca Mountain, also attributes hydraulic importance to the faults in the northwest-southeast trending washes in northern Yucca Mountain. The sensitivity of the estimated groundwater flow paths and specific discharge to each of the conceptual models of the large hydraulic gradient has been investigated by recalibrating the numerical model to fit conditions appropriate to each conceptual model, and the input and output files for computer calculations have been recorded (DTN: LA0105GZ12213S.001 [DIRS 154887]).

Subregions within the model domain in which a geologic process is thought to have altered hydraulic properties are referred to as features in constructing and calibrating the site-scale SZ flow and transport model. The new conceptualizations of the large hydraulic gradient reduce the number of features used north of Yucca Mountain (Figure 12.3.1.3-1). To incorporate the area of extensive hydrothermal alteration in the Claim Canyon Caldera north of Yucca Mountain, the hydrogeologic units have been divided into distinct northern and southern calibration zones. Because the northern zones are represented by additional independent calibration parameters, these zones replace the complex feature set in the northern part of the original model. The two newer models differ from each other only by the inclusion of a zone that represents the northwest-southeast trending fault zone north of Yucca Mountain (Figure 12.3.1.3-1, Feature 2).

In general, the simulations of the newer conceptual models better match observations in the low-gradient region southeast of Yucca Mountain than the previous conceptual model. This is important because flow paths leaving the repository pass through this region. However, inclusion of the additional northwest-southeast trending fault zone in the second of the newer conceptual models does not seem to help the calibration.

The flow paths resulting from the simulation of the original and newer conceptual models are shown in Figures 12.3.1.3-2, 12.3.1.3-3, and 12.3.1.3-4. Although the flow paths predicted by the simulation of the newer conceptual models are similar, they differ from the flow paths predicted by simulations of the original conceptual model. The original model produces flow paths that trend in a southeasterly direction from the potential repository site (Figure 12.3.1.3-2). This result is consistent with the inferred geochemical pathlines (CRWMS M&O 2000 [DIRS 139582], Figure 9). The newer models produce pathlines leaving the potential repository that are more southerly in direction than those of the original model (Figures 12.3.1.3-3 and 12.3.1.3-4). Groundwater travels mainly in the same units, the Bullfrog Tuff and the alluvial units, regardless of the model. The net result of the newer flow paths is a relatively shorter traverse through the alluvial units compared to the paths for the original model. The more southeasterly component of the original model is due to the east-west barrier feature that is not present in the newer models. This feature acts as a dam to keep the head elevated in the north and blocks water from the north, thus allowing water from Crater Flat to enter the repository area. The newer models lack this feature and allow the water to flow directly south. This analysis demonstrates that the flow path from the repository can be sensitive to the conceptual model of the large hydraulic gradient.

12.3.1.3.2 Alternative Conceptualizations of the Solitario Canyon Fault

The parameterization of the Solitario Canyon fault is an important part of the site-scale SZ flow and transport model because it can potentially control flow from Crater Flat to Fortymile Wash. This flow, in turn, is important in determining the amount of alluvial material that groundwater flowing from beneath the potential repository region passes through en route to the accessible environment. Investigations of alternative treatments of the Solitario Canyon fault have been recently initiated. Input and output files for these computer calculations can be found in DTN: LA0105GZ12213S.004 ([DIRS 154993]). One aspect of this fault that has been investigated is its effective depth. This fault is included as a discrete feature in the site-scale SZ flow and transport model. Simulations performed for the TSPA-SR included this fault as a feature that extended from the bottom of the model to the top of the water table. The fault is modeled as an anisotropic feature with larger permeability along the plane of the fault than across it. It is possible that this treatment of anisotropy is inappropriate where it cuts the carbonate aquifer deep in the model domain. Consequently, an alternative treatment was simulated in which the fault extends from the water table only to the top of the carbonate aquifer. This simulation produced essentially the same result as the original site-scale SZ flow and transport model with the deeper fault zone, but the calibrated permeability for the fault was approximately 25 percent lower than the original.

12.3.1.4 Quantification of Groundwater Specific Discharge Uncertainty

This section summarizes unquantified uncertainty for the site-scale SZ flow model based on the TSPA-SR (CRWMS M&O 2000 [DIRS 153246]). Uncertainty in flow modeling arises from a number of sources, including the conceptual model of the processes affecting groundwater flow, water-level measurements, simplification of the model geometry, simplification of the boundary conditions, and the values of permeability assigned to hydrogeologic units. These types of uncertainty are accounted for explicitly through key parameters and conceptual models in the site-scale SZ flow and transport model for the updated TSPA-SR. Key SZ input parameters that are uncertain are represented stochastically in the site-scale SZ flow and transport model, and parameter distributions are based on site data, laboratory data, literature data, and expert elicitation. The *Uncertainty Distribution for Stochastic Parameters Report* (CRWMS M&O 2000 [DIRS 147972], Section 6) documents the uncertainties quantified for input to the site-scale SZ flow and transport model for the updated TSPA-SR.

A review was conducted on how uncertainty was treated in the site-scale SZ flow and transport model. The probability distribution for the parameter specific discharge was reevaluated as part of the unquantified uncertainty analysis. This parameter is important because the results of TSPA calculations are sensitive to it at long time periods (i.e., hundreds of thousands of years). Uncertainty in specific discharge was reevaluated because the previous range of values for this parameter is thought to be too large to represent what is reasonably known. Specifically, the principal investigators developing the site-scale SZ flow and transport model concluded that the range for specific discharge used for the TSPA-SR is overly conservative; in particular, the maximum value of the parameter range is unreasonably large.

In the TSPA-SR, specific discharge in the site-scale SZ flow and transport model is represented as three discrete cases: high, medium, and low (CRWMS M&O 2000 [DIRS 139440], Section 6.2.5.1). The medium value was obtained from the calibration effort described in the *Calibration of the Site-Scale Saturated Zone Flow Model* report (CRWMS M&O 2000 [DIRS 139582], Section 6). The low- and high-value cases were calculated by scaling values of flux, recharge, and permeability by the same amount. Calibration is preserved by this scaling process because of the linearity of the numerical model. The value for the low case was one-tenth of the value for the medium case, and the value for the high case was 10 times that of the medium case. This range of values was based primarily on the SZ expert elicitation (CRWMS M&O 2000 [DIRS 147972], Section 6.1; CRWMS M&O 1998 [DIRS 100353], p. 3-20). In sensitivity studies performed as part of the SZ unquantified uncertainty analysis, the range of specific discharge was reduced such that the low- and high-value cases were one-third and three times the medium value, respectively.

Four lines of reasoning are presented in the following paragraphs to support decreasing the range of values used for specific discharge. Specific discharge is the product of rock permeability and hydraulic gradient, and the hydraulic gradient is sufficiently characterized that most of the uncertainty in specific discharge is due to uncertainty in permeability. Consequently, the following lines of reasoning are posed in terms of rock permeability. For comparison, the value of permeability used for the Bullfrog Tuff for the medium case is $15.7 \times 10^{-12}\ m^2$ (CRWMS M&O 2000 [DIRS 139582], Table 16). The values used for the SZ unquantified uncertainty

analysis for the low- and high value cases are 5.2×10^{-12} m^2 and 47.1×10^{-12} m^2, respectively, based on analysis discussed in Section 12.3.1.4.1.

First, the 95 percent confidence interval on mean permeability, calculated from cross-hole tests in the Bullfrog Tuff at the C-wells Complex, has endpoints that are approximately one-third (5.6×10^{-12} m^2) and three times (33.6×10^{-12} m^2) the geometric mean (13.7×10^{-12} m^2) of the interval (CRWMS M&O 2000 [DIRS 139582], Table 9). The mean value, in turn, is close to the nominal calibration value of permeability for the Bullfrog Tuff (15.4×10^{-12} m^2) that was obtained for the site-scale SZ flow and transport model (CRWMS M&O 2000 [DIRS 139582], Table 8). Permeability of the Bullfrog Tuff is important for all reasonable scenarios because it is the highest permeability path for fluid leaving the repository before entering the alluvium (DTN: LA0105G2122135.001 [DIRS 154887]; DTN: LA0105G2122135.002 [DIRS 154888]; DTN: LA0105G2122135.003 [DIRS 154889]).

Second, the value for Bullfrog Tuff permeability used in the model represents the combined values of Bullfrog Tuff permeability where it is far from faults and where it is near faults that are not represented explicitly in the model. The larger values of permeability, measured in the vicinity of known faults, are thought to represent only the latter (near faults) portion of the Bullfrog Tuff. Permeability values representing the averaged Bullfrog Tuff should not exceed values representing the faulted portions. The fact that the values of permeability for the Bullfrog Tuff used for the high specific discharge case in the unquantified uncertainty analysis are close to the upper end of the range measured in the vicinity of known faults is in agreement with this line of reasoning. The values of permeability thought to represent faulted regions were calculated from saturated tests at the C-wells Complex near the Midway Valley fault (54.0×10^{-12} m^2) (Geldon et al. 1998 [DIRS 129721], Figure 3) and from air-injection tests in the UZ adjacent to the Ghost Dance fault (14.6×10^{-12} m^2) (LeCain et al. 2000 [DIRS 144612]). Applicability of air-injection tests of the Ghost Dance fault is discussed in Section 12.3.1.4.1.

Third, single-hole hydraulic tests in the vicinity of Yucca Mountain provide an estimate of the average permeability of volcanic tuffs in unfaulted regions. Using reasoning similar to that presented in the previous paragraph, a value representing the average of faulted and unfaulted regions should be larger than the value for unfaulted regions. The largest value from single-hole tests of the Bullfrog Tuff is 1.7×10^{-12} m^2 (CRWMS M&O 2000 [DIRS 139582], Table 9). This value is smaller than the value used for the low specific discharge case for the unquantified uncertainty analysis. The argument that scale effects do not cause single-hole tests to underestimate the permeability of unfaulted regions is presented in Section 12.3.1.4.1.

Fourth, calibrations of the site-scale SZ flow and transport model that are constrained by all available information about SZ flow in the vicinity of Yucca Mountain, and that consider alternative conceptual models, can only be done for a range of specific discharge values similar to those used in the unquantified uncertainty analysis.

12.3.1.4.1 Evaluation of Permeability Data

Uncertainty in specific discharge is due mainly to uncertainty in permeability. This section discusses permeability data for the volcanic rocks at Yucca Mountain and elsewhere, and it applies these data to calculations of specific discharge. Two main points are made. First, the

maximum permeability values that have been estimated from air-injection tests near the Ghost Dance fault provide an additional estimate of the permeability of faulted tuffs (14.6×10^{-12} m^2) (LeCain et al. 2000 [DIRS 144612], Table 13). Second, the expected values of permeability for unfaulted tuffs are provided by the geometric means calculated from single-hole tests. These values (CRWMS M&O 2000 [DIRS 139582] Table 9) are one to several orders of magnitude less than the values estimated for faulted tuffs.

12.3.1.4.1.1 Evaluation of Permeability in Faulted Regions

Fractured welded tuffs and relatively unfractured nonwelded tuffs occur above and below the water table. Permeabilities measured in the UZ at Yucca Mountain using air may, therefore, have some relevance to the permeability values of similar rocks located below the water table. In the UZ, air-injection tests have been conducted from surface-based boreholes in welded and nonwelded tuffs (LeCain 1997 [DIRS 100153]), and from test alcoves in and adjacent to the Ghost Dance fault zone in the densely welded Topopah Spring Tuff (LeCain et al. 2000 [DIRS 144612]). At Yucca Mountain, no water-injection tests were done in these intervals to compare with the results of the air-injection tests. However, some understanding of the probable relation between permeabilities estimated from air- and water-injection tests at Yucca Mountain can be reached based on tests in non- to partially-welded tuff at the Apache Leap experimental site near Globe, Arizona, where borehole air- and water-injection tests were made at ambient moisture conditions in the same depth intervals (Rasmussen et al. 1993 [DIRS 154688]). The relationship of permeability values estimated using these two methods at Apache Leap suggests that permeability values calculated from air-injection tests in the UZ at Yucca Mountain could provide good approximations to water-permeability values, particularly in the densely welded tuff. It is therefore assumed that air-injection values provide good estimates of water-injection values in Section 12.3.1.4 where an average of the air-injection permeability values (14.6×10^{-12} m^2) is said to represent faulted regions.

Cross-hole air-injection tests conducted in and adjacent to the Ghost Dance fault resulted in geometric mean permeability values of 4.1×10^{-12} m^2 for the hanging wall of the fault, 14.6×10^{-12} m^2 for the main fault zone (defined by a zone of significantly higher fracture density), and 7.8×10^{-12} m^2 for the footwall (LeCain et al. 2000 [DIRS 144612], Table 13). These permeabilities were higher than the permeabilities measured elsewhere in the same units from the surface-based boreholes, and 2 to 10 times higher than the permeabilities estimated for the Ghost Dance fault and adjacent rock from single-hole tests conducted from an exploratory borehole drilled before alcove excavation (LeCain et al. 2000 [DIRS 144612], p. 26).

12.3.1.4.1.2 Scale Effects

In addition to actual variations in permeability, the scale of measurement may influence the permeability value determined by a test. This effect is most often observed when the results of permeability tests conducted on cores that do not incorporate fractures are compared to the results of tests conducted in boreholes that contain fractured intervals. At Yucca Mountain, the relatively high permeabilities estimated from cross-hole tests compared to single-hole tests in the same rock unit have also been attributed to the effects of scale (Geldon 1996 [DIRS 100396], p. 69). According to this interpretation, the cause of the permeability increase in the cross-hole tests is attributed to the greater likelihood of including relatively rare but highly transmissive and

continuous features in the larger rock volume sampled by the cross-hole tests. However, recent work by Vesselinov et al. (2001 [DIRS 154706]) at the Apache Leap test site demonstrated that permeabilities determined from multiple single-well air-injection tests and simultaneous numerical inversion of multiple cross-hole air-injection tests provide comparable estimates of the mean permeability of the test volume. However, when the cross-hole tests were analyzed individually using an approach equivalent to type-curve analyses that requires the assumption of a uniform permeability field and a particular flow geometry (spherical), the resulting mean permeability estimated for the test volume was several orders of magnitude higher than the mean permeability estimated from the single-hole analyses or from more detailed simultaneous numerical inversion of the cross-hole tests. The simultaneous numerical inversion of the cross-hole tests resulted in a larger variance in permeabilities than was estimated from the multiple single-hole tests, which is a result that may have been caused by rounding errors associated with the numerical inversion. The conclusions of this work relevant to the present analysis are that the mean permeabilities would not be a function of test methodology (single-hole or cross-hole analyses) except for the inability of standard cross-hole type-curve methods to account for heterogeneity and departures of the actual flow field from the assumed flow geometry. Therefore, single-hole permeabilities reflect the true permeabilities of the hydrogeologic units in unfaulted areas and can be used to represent the hydrogeologic-unit permeabilities in numerical models, provided the effects of faults are accounted for in some manner.

12.3.2 Transport Modeling

This section covers the site-scale SZ transport model and the introduction of new data, new model development, and new analyses since the completion of the TSPA-SR (CRWMS M&O 2000 [DIRS 153246]). New data, new analyses and new model development, with the exception of that described in Sections 12.3.2.3.3 and 12.3.2.4, are not included in the Volume 2 analyses. The new data and analyses described in this section will facilitate the development of a more representative future versions of the SZ site-scale transport model. This section also discusses quantification of previously unquantified uncertainties for the site-scale SZ transport model and is included in the analyses presented in Volume 2 (McNeish 2001 [DIRS 155023]).

12.3.2.1 Introduction and Goal of Model

Predicting the migration of radionuclides through the SZ to proposed compliance boundaries is important for assessing the overall containment strategy for safely storing radioactive materials at the potential Yucca Mountain repository. The SZ is an important barrier for delaying the movement of radionuclides and potentially reducing the concentrations via the process of retardation. Radionuclides that escape the engineered barrier and near-field environment and migrate to the water table must still travel some 20 km in the aquifer. Only then, as water is being pumped from the aquifer and used for irrigation or domestic consumption, will the radionuclides present a health and safety issue.

12.3.2.1.1 Purpose of the Model

The purpose of the site-scale SZ transport model (CRWMS M&O 2000 [DIRS 151948]), which is used to perform the SZ simulations for the TSPA-SR (CRWMS M&O 2000 [DIRS 153246]),

is to predict the spatial and temporal distribution of any radionuclides that may reach the water table beneath the potential repository. Because fluid flow is the means of transport through the SZ, the site-scale SZ flow model is the basis for the transport model in terms of the potential directions and transport velocities. The transport model builds on the flow model by incorporating mechanisms specific to the migration of contaminants. These mechanisms include:

- Advection (governed solely by the flow model and the effective porosity)
- Dispersion of radionuclides during transport
- Radionuclide sorption on the solid surfaces in the aquifer
- Diffusion from the flowing fractures in the volcanic tuffs into the relatively stagnant fluid in the rock matrix
- Transport through the alluvium
- Colloid-facilitated transport
- Capture at pumping wells.

Using accepted hydrologic principles and data available from the site, the major transport processes listed above were incorporated into a particle-tracking-based transport model that predicts the velocity (migration rate and direction) of radionuclide migration under present and presumed future climatic conditions. Transport data from a variety of sources are used to constrain the model. At the field scale, tracer test results in the fractured volcanic tuffs and preliminary data from the alluvium are used to justify the conceptual models used for transport in these two media. At the laboratory scale, batch and column sorption and diffusion data are cited to define the parameters for the models. Although a large amount of site-specific data exists, there is still uncertainty in the conceptual models and in the parameters used in the models.

A major goal in developing the site-scale transport model was to capture the uncertainties in the model and how they influence the uncertainty in the transport predictions. This goal requires that the model be run for a large variety of transport parameters. Therefore, a computationally efficient model was developed that incorporates the key elements of the conceptual model in a manner that allows multiple simulations to be performed rapidly. The particle-tracking methods developed are suitable for this purpose, and the sensitivity analyses performed often used multiple realizations to characterize the uncertainties.

12.3.2.1.2 Identification of Unquantified Uncertainty from the Total System Performance Assessment for the Site Recommendation

This section summarizes the identification of unquantified uncertainty for the SZ transport model based on the TSPA-SR (CRWMS M&O 2000 [DIRS 153246]). Uncertainty in transport modeling arises from a number of sources including, but not limited to, the conceptual model, assumptions regarding matrix diffusion processes, implementation of colloid-facilitated

transport, assumptions regarding sorption of radionuclides, and the extent the flow path encounters volcanic hydrogeologic units compared to alluvial hydrogeological units. These various types of uncertainties are accounted for explicitly in the site-scale SZ transport model through key parameters and conceptual models as described in the SZ PMR (CRWMS M&O 2000 [DIRS 153168], Sections 3.6 and 3.7). The uncertainty in key SZ parameters are represented stochastically as input to the site-scale SZ model. Parameter distributions are based on a combination of site data, laboratory data, literature data, and expert elicitation. The AMR, *Uncertainty Distribution for Stochastic Parameters* (CRWMS M&O 2000 [DIRS 147972], Table 15), documents the uncertainties quantified for input to the SZ -scale model for TSPA-SR.

In general, identification of unquantified uncertainty for the site-scale SZ transport model consisted of re-evaluation of previously quantified uncertainty with focus on the parameters that were most important to performance of the SZ as a barrier to radionuclide migration. One exception is the bulk density parameter. The value of this parameter was constant in the TSPA-SR analysis (CRWMS M&O 2000 [DIRS 153246]; CRWMS M&O 2000 [DIRS 147972], Section 6.9), but it is treated stochastically in the unquantified uncertainty analysis. New data (Section 12.3.2.2) were used to develop a probability distribution for bulk density (Section 12.3.2.4). For other parameters, distributions were changed from those used for the TSPA-SR based on incorporation of new data and the reevaluation of probability distributions. The technical basis for the reevaluation of the uncertainty quantification is described in Section 12.3.2.4. Table 12.3.2.1.1-1 summarizes the results of the SZ transport unquantified uncertainty analysis.

12.3.2.2 New Data and Analyses Since Completion of Models in the Total System Performance Assessment for the Site Recommendation

The following new information has been obtained since completion of the TSPA-SR (CRWMS M&O 2000 [DIRS 153246]), the SZ PMR (CRWMS M&O 2000 [DIRS 153168]), and their supporting AMRs.

12.3.2.2.1 Bulk Density and Porosity

The average alluvium dry bulk density is 1.91 g/cm^3 based on saturated bulk density estimated from a borehole gravimetry survey in well NC-EWDP-19D1 (Black 2000 [DIRS 154704], p. 18). The corresponding average bulk porosity was calculated to be about 0.24 from the saturated bulk density, the average grain density of 2.52 g/cm^3 (USGS n.d. [DIRS 154495], pp. 3 to 4), and Equation 12.3-5. Point estimates of alluvium dry bulk density computed using the porosity, a grain density of 2.52 g/cm^3, and Equation 12.3-6 ranged from about 1.79 to 2.05 g/cm^3, and point estimates of bulk porosity ranged from 0.185 to 0.291 g/cm^3 from computations using the dry bulk density, the grain density, and Equation 12.3-5.

12.3.2.2.2 Sorption Measurement

Further analysis of batch sorption data of technetium-99 and iodine-129 (as TcO_4^- and I^-) onto alluvium samples, as well as recent technetium-99 and iodine-129 column test results, indicate that sorption distribution (K_d) values for technetium-99 and iodine-129 sorbing onto the alluvium

are zero under oxidizing (ambient) conditions (Reimus 2001 [DIRS 154994], Filename "Tc and I Alluvium Sorption").

New results from two column experiments for K_d values for neptunium-237 in the alluvium have been performed in which the effective K_d values of neptunium-237 were significantly lower than values measured in batch sorption experiments with the same material used to pack the columns as discussed in Section 12.3.2.4.2 (Reimus 2001 [DIRS 154994], Filename "Np Alluvium Sorption"). The differences between the column and batch experiments are explained in Section 12.3.2.4.2.2.

12.3.2.2.3 Conceptualization of Matrix Diffusion in the Alluvium

Preliminary single-well tracer test data at well NC-EWDP-19D1 support the use of a single-porosity flow and transport conceptual model in the alluvium. The normalized concentration responses of conservative tracers with different diffusion coefficients were identical in the tests (Reimus 2001 [DIRS 155251], Filename "ATC Tracers – 1st Test," "ATC Tracers – 2nd Test," and "ATC Tracers – 3rd Test"), indicating little or no diffusion of tracers from flowing water to stagnant water (secondary porosity) in the flow system.

12.3.2.2.4 Matrix Diffusion in the Volcanic Tuffs

Laboratory data from diffusion-cell experiments are being used to establish a correlation between matrix diffusion coefficients and matrix porosities in volcanic rocks. This correlation has been used to adjust effective matrix diffusion coefficients as a function of matrix porosity in transport simulations as described in Section 12.3.2.4.6. That is, for a given sampled value of the effective matrix diffusion coefficient, the value is adjusted upward or downward depending on the sampled value of the matrix porosity.

12.3.2.2.5 Colloid Transport in the Alluvium

Alluvium grain size distributions from well NC-EWDP-19P (Reimus 2001 [DIRS 154994], Filename "EWDP 19P Grain Sizes"), which was drilled using an air-hammer method that preserved smaller and larger grain sizes much better than rotary drilling methods, were used to refine estimates of colloid filtration rate constants in the alluvium.

Preliminary estimates of colloid detachment rate constants in the alluvium have been obtained from microsphere responses in single-well tracer tests at well NC-EWDP-19D1 (Reimus 2001 [DIRS 155251], ATC Detachment 040101). These detachment rate constants fall within the range of detachment rate constants assumed in the colloid retardation factor analysis (see Section 12.3.2.4.5).

Measurements of natural colloid concentrations in the alluvium (Nye County wells) have been consistently higher than those in the volcanics (DTN: LA0002SK831352.002 [DIRS 149194]; DTN: LA0002SK831352.001 [DIRS 149232], Filename "19D1 Colloid Concentrations"). In the lower alluvium intervals at well NC-EWDP-19D1, colloid concentrations are almost three orders of magnitude higher than in water from Well J-13 (Reimus 2001 [DIRS 154994]). The highest colloid concentrations could decrease the travel times of radionuclides that are reversibly sorbed to those colloids by a factor of 3 or 4 relative to colloid concentrations in Well J-13 water

(assuming equilibrium sorption of radionuclides to colloids and the alluvium grains). Parameter uncertainty distributions in SZ transport simulations effectively capture this potential decrease in travel times (CRWMS M&O 2000 [DIRS 147972], Figure 6), although future performance assessments will account for the greater colloid concentrations more explicitly.

12.3.2.3 New Model and Analysis Development Since Completion of the Total System Performance Assessment for the Site Recommendation

This section discusses new model development and new analysis performed since the completion of the TSPA-SR (CRWMS M&O 2000 [DIRS 153246]), the SZ PMR (CRWMS M&O 2000 [DIRS 153168]), and their supporting AMRs. New development and analysis covered in this section include analyses to support the flexible thermal design, a new dispersion tensor, effective dispersivity in the site-scale SZ model, and studies investigating the influence of matrix diffusion.

12.3.2.3.1 Flexible Design

The impact of a lower-temperature repository design for the potential repository on the site-scale SZ flow and transport model is expected to be minor because the pathways in the SZ are separated by a significant distance from the waste canisters. In the SZ PMR, it is demonstrated that the influence of heat on the SZ flow system is minor (CRWMS M&O 2000 [DIRS 153168], p. 3-94). Lower areal heat loads that may arise due to the flexible repository design approach will make this assumption even more appropriate, as the temperatures at the top of the SZ will be perturbed less than was the case in the initial revision of the SZ PMR (CRWMS M&O 2000 [DIRS 153168]). Therefore, heat effects of a lower-temperature repository design do not need to be analyzed. However, because the flexible design approach may require that waste be emplaced over a larger area, radionuclides may reach the water table over a wider area. Other techniques for reducing the temperature, such as surface aging and ventilation, are not considered here because they are expected to have even lower thermal impact on the SZ system than the designs studied to date. Typically, to examine plume size and potential flow paths from the repository to the point of compliance, particles are released from an area derived by projecting the footprint of the repository on the water table. For this sensitivity analysis, a similar analysis was performed with a larger repository footprint to determine if the results change significantly from the past simulations (radionuclides released were simulated to occur from the larger footprint). This analysis does not simulate actual release rates of radionuclides; simply the pathlines predicted for radionuclides initiated beneath the larger footprint.

Figure 12.3.2.3-1 illustrates the preliminary layout for a lower-temperature repository design that would accommodate 70,000 metric tons of heavy metal. This layout, which is preliminary in nature, was obtained from BSC (2001 [DIRS 154548], Section I, p. 2, Figure 1). To determine the particle release locations for this analysis, a software routine (add_repo_nodes.f V1.0) was used to interpolate between the western and eastern ends of each emplacement drift (the values reproduced in Table 12.3.2.3-1). The program linearly interpolates between the coordinate locations of the ends of the drift at a prescribed length spacing along the drift. To maintain an integer number of points along each drift and to include the end points, the actual spacing between points along the drift is typically larger than the input value. The code writes out the coordinates of each point with options to either interpolate to obtain the repository-level

elevation or to write out a user-defined value. For this study, an elevation of 719 m is written for all points because a series of points just below the water table are required as the starting locations in the particle-tracking simulation. The easting and northing coordinates are approximately converted from the given coordinate system (Nevada State Plane meters) to the Universal Transverse Mercator (UTM) geographic coordinate system used for the site-scale SZ model. To do this, the software routine add_repo_nodes.f V1.0 performs a simple linear transformation after using the U.S. Army Corps of Engineers code CORPSCON V5.11.08 to obtain the UTM coordinates for a single translation point in the northern end of the repository. A hand check of the linear transformation method for a point in the far southern point of the repository (farthest from the translation point) revealed that this method produced coordinate locations within about 20 m of the more accurate CORPSCON code. This error is well within the accuracy required to locate approximately the potential repository footprint in the SZ model.

Figure 12.3.2.3-2 shows the locations of the particle tracking points computed using FEHM V2.11 in the new analysis compared to the distribution of points for the original potential repository. The latter was used in previous SZ pathline studies of the SZ PMR (CRWMS M&O 2000 [DIRS 153168]). This footprint is similar to that used in the thermal analysis (Figure 2.3.4-2, Case 3). The lower-temperature, expanded repository design extends farther north, but the primary difference is the extension into a second lobe to the south. To examine the influence of this design on the results, a comparison of pathlines issuing from the previous and lower-temperature repository point distributions was performed. Pathlines are generated using the base-case SZ flow field assuming no dispersion or sorption, and the results are examined visually and in the form of breakthrough curves at the 20-km point of compliance. The results of the particle-tracking pathway analysis for the two designs are compared with the pathlines for the original repository in Figure 12.3.2.3-3a and the pathlines for the lower-temperature repository in Figure 12.3.2.3-3b. Figure 12.3.2.3-3c shows only those pathlines issuing from the southern lobe of the lower-temperature repository. The overall outline of the pathlines for Figures 12.3.2.3-3a and 12.3.2.3-3b are quite similar, suggesting that the flow paths from the lower-temperature repository footprint are quite similar to those from the earlier repository design. This result is due to the predominantly southerly flow paths issuing from nearly all locations in the repository: release locations farther south than previously assumed follow essentially those same southerly flow lines. This conclusion is confirmed in Figure 12.3.2.3-3c, which illustrates that the new pathways follow the same tracks as those from the original repository.

The final analysis is a comparison of the transport times from the repository to the 20-km point of compliance. To compare the original and lower-temperature repository design, breakthrough curves were generated for conservative particles (such as carbon-14) released from each repository footprint, assuming no diffusion or dispersion. Thus, the distribution of transport times is due only to the location of the release and the differences in flow velocities as a function of starting location. Figure 12.3.2.3-4 shows that the two repository designs yield similar breakthrough curves.

Thus, the direction of the flow paths and the transport times are all similar for the lower-temperature repository design. Therefore, the impact on radionuclide transport in the SZ is minor. It should be noted that this conclusion relates only to the performance assuming the base case model and assuming the repository footprint currently envisioned. If a future design specifies waste emplacement in another location, the analysis would need to be repeated.

Furthermore, the potential for additional site characterization, depending on the design, is perhaps more important than the performance assuming the current model. For example, waste emplaced to the west of the Solitario Canyon fault would involve portions of the SZ that are relatively less well characterized. Also, any new data that changes our current understanding of flow through the fractured volcanic tuffs, either in the unsaturated or saturated zone, might create the need to reevaluate these results. For the current designs, further characterization in that location is a relatively low priority because of the lack of sensitivity demonstrated in Figure 12.3.2.3-4. Future designs will have to be assessed with respect to the impact on site characterization needs and schedule in addition to predicted performance.

12.3.2.3.2 New Dispersion Tensor

In the *Saturated Zone Transport Methodology and Transport Component Integration* report (CRWMS M&O 2000 [DIRS 146962], Section 6), a methodology based on particle tracking was developed to simulate transport through the SZ with dispersion incorporated using a random-walk method. For the transport analyses resulting in breakthrough curves at the 20-km point of compliance, the dispersion tensor proposed by Burnett and Frind (1987 [DIRS 130526], pp. 695 to 705) was used to characterize the nature of radionuclide spreading away from the flow streamlines. This tensor, proposed as a simplified form suitable for axisymmetric media, involves the use of three independent parameters, the longitudinal dispersivity α_L, the transverse horizontal dispersivity α^H_T, and the transverse vertical dispersivity α^V_T. This form is generalized from the typical form used for isotropic media to account for the different transverse dispersivities observed in the horizontal and vertical directions of natural stratified media with flow along the bedding plane (e.g., Zheng and Bennett 1995 [DIRS 154702], Section 2.2.4, Equations 2-34 to 2-39).

In simulation models such as the site-scale SZ flow and transport model, this form of the dispersion tensor has drawbacks that make the computation of radionuclide transport difficult for large dispersivity values. Because the longitudinal dispersivity is not a function of either horizontal or vertical direction, the random-walk distance of a particle temporarily traveling vertically is, on average, just as large as for horizontal transport. The grid aspect ratio for the SZ is such that the vertical random walk can result in attempts to jump several grid cells in each random walk unless very small particle time steps are taken. However, there is no experimental basis for applying the same longitudinal dispersivities in the horizontal and vertical directions, and it can be argued that one could expect different dispersivities in the direction of flow depending on these directions. Therefore, a modified form of the Burnett and Frind (1987 [DIRS 130526]) tensor was developed and implemented in FEHM V2.11. This form includes separate longitudinal dispersivities in the horizontal and vertical directions, α^H_L and α^V_L, respectively, to go along with the transverse dispersivity terms α^H_T and α^V_T. This tensor, which we call the modified Burnett and Frind tensor, results in different expressions for the random-walk displacement matrix but reduces to the Burnett and Frind (1987 [DIRS 130526]) form when $\alpha^H_L = \alpha^V_L$.

In this analysis, the breakthrough curves at the 20-km point of compliance for the two tensors are compared. A conservative (carbon-14) and a weakly sorbing radionuclide (neptunium-237) are examined for point releases from source region 1, using the expected values of all dispersion and sorption parameters. To differentiate between the processes of dispersion and matrix diffusion,

this analysis also assumes no matrix diffusion. Figure 12.3.2.3-5 shows the breakthrough curve comparisons. The modified tensor yields a virtually identical breakthrough curve to the original Burnett and Frind tensor for the early and middle portions of the curve, deviating significantly only in the tail. This conclusion is true for carbon-14 and neptunium-237, probably because the flow is primarily horizontal in the site-scale SZ model so that, in most locations, the longitudinal dispersion is identical in the two cases. Therefore, either tensor could be used in the sensitivity analyses and breakthrough curves generated for use in the TSPA.

12.3.2.3.3 Effective Longitudinal Dispersivity in the Site-Scale Saturated Zone Flow and Transport Model

Longitudinal dispersivity for radionuclide transport simulations in the site-scale SZ flow and transport model is specified as a transport parameter (e.g., CRWMS M&O 2000 [DIRS 153168], pp. 3-151). The dispersion process is simulated by the random-walk displacement algorithm on the local scale for each time step in the transport simulation. In addition, the spatial distribution of hydrogeologic units of contrasting permeability within the site-scale SZ flow and transport model imparts additional dispersion to the simulated transport of particles as the flow paths diverge during transport. The effective longitudinal dispersivity simulated by the site-scale SZ model may be significantly larger than the desired specified value due to the additive effects of these two processes.

The effective longitudinal dispersivity in the site-scale SZ flow and transport model is analyzed for a range of values of specified longitudinal dispersivity to evaluate this effect. A point source that is beneath the repository and is located 23.7 km from the 20-km regulatory boundary is used for the analysis. No sorption or matrix diffusion is included in the simulations. Effective longitudinal dispersivity is estimated using the relationship from Kreft and Zuber (1978 [DIRS 107306], Equations 2-34 to 2-39):

$$\alpha_L = \frac{L}{2}\left(\frac{\sigma_t}{m_t}\right)^2 \qquad \text{(Eq. 12.3.2.3-1)}$$

where

α_L = effective longitudinal dispersivity
L = the flow path length
σ_t = the standard deviation in transport time
m_t = the mean transport time

The standard deviation of the dispersivity is estimated from the particle mass breakthrough curve at the 20-km regulatory boundary by taking the difference in time between the arrival of 0.159 fraction of the mass (minus one standard deviation) and the arrival of 0.841 fraction of the mass (plus one standard deviation) and dividing by 2. The mean transport time is estimated using the arrival time of 0.500 fraction of the mass.

The results of the effective longitudinal dispersivity analysis are shown in Figure 12.3.2.3-6 with the plotted open circles. The effective simulated longitudinal dispersivity is consistently about

one order of magnitude higher (bold dashed line) than the specified longitudinal dispersivity when the latter value is less than 1,000 m. These results indicate that the heterogeneous distribution of permeability in the site-scale SZ model in the region along the flow path from repository to the 20-km regulatory boundary is contributing approximately one order of magnitude of dispersivity relative to the specified value. When the specified longitudinal dispersivity is above 1,000 m, the excess longitudinal dispersivity appears to be even greater. However, these large values of longitudinal dispersivity are significantly greater than the geometric mean value of 100 m derived from the uncertainty distribution for this parameter (CRWMS M&O 2000 [DIRS 147972], p. 50).

Based on these results, the value of specified longitudinal dispersivity used in the site-scale SZ flow and transport model for the SSPA abstraction simulations (McNeish 2001 [DIRS 155023]) will be adjusted to yield the appropriate value of effective simulated longitudinal dispersivity. This is accomplished by scaling the specified longitudinal dispersivity down by one order of magnitude in the input files for each realization.

12.3.2.3.4 Matrix Diffusion Sensitivity Analyses

The original conceptual model used in the SZ transport calculations to date consists of individual flowing fractures that transmit fluid and radionuclides as illustrated in Figure 12.3.2.3-7. The surrounding rock matrix contains immobile water, but radionuclides can diffuse into and out of the rock matrix and sorb within the rock matrix. Therefore, radionuclide mass is attenuated with respect to the transport velocities within the fractures. In this section, a variety of model assumptions were explored regarding the process of matrix diffusion, ranging from no diffusion to systems in which matrix diffusion is pervasive within isolated zones of highly fractured tuff. These simulations are presented to provide perspective on the importance of matrix diffusion within the range of uncertainty currently present for this process.

The abstracted model implemented for matrix diffusion is shown in the Figure 12.3.2.3-7. It consists of equally spaced fractures (spacing = $2B$), each carrying fluid at the same velocity. The FEHM particle tracking model employs an analytical solution of Sudicky and Frind (1982 [DIRS 105043]) to impart delays to each particle traveling within the fractured volcanic tuffs so that the diffusion-delayed transport time distribution predicted by the analytical solution is obtained. The fracture aperture ($2b$) represents the mean distance across the fracture, which in reality is a rough-walled discontinuity of variable aperture. The bulk porosity of the medium is, through geometric considerations, b/B. This porosity is to be distinguished from the matrix porosity, which corresponds only to the porosity in the medium surrounding each flowing fracture.

The fracture spacing parameter is obtained from the analysis of field investigations identifying the distance between flowing fractures in boreholes at the site (DTN: SN9907T0571599.001 [DIRS 122261]). This parameter, combined with estimates of the fracture porosity (CRWMS M&O 2000 [DIRS 147972], p. 62), allows the mean fracture to be calculated.

Unfortunately, borehole logs and other data cannot be used to distinguish between single fractures and fracture zones. It is possible that a flowing interval actually represents a zone of fractures rather than an individual fracture. Therefore, an alternate conceptual model that cannot

be ruled out is one in which the flowing intervals depicted as single fractures of aperture $2b$ are actually fractured zones of enhanced permeability through which water and radionuclides transport.

To implement such a model, it is possible to use the same mathematical representation as was employed by Sudicky and Frind (1982 [DIRS 105043]), and therefore, the impact of this conceptualization can be examined using the existing particle tracking model by modifying only the parameterization. To do so, the flowing interval spacing was held constant at a mean value of 21 m (CRWMS M&O 2000 [DIRS 154927], p. 13), while adjusting the fracture porosity and, hence, aperture. The fracture porosity in such a medium is a relatively unconstrained parameter that has been sampled over a wide range. For systems with fracture zones rather than individual fractures, it would seem that the fracture porosity could be larger than assumed in previous calculations, perhaps as large as 1 percent. Keeping $2B = 21$ m, the computed aperture for a fracture porosity of 0.01 would be 0.21 m. Referring to Figure 12.3.2.3-7, fracture aperture is computed using simple geometric considerations such that fracture porosity = b/B. This seemingly large aperture value actually represents all of the pore space within the highly fractured zone, that is, the fracture volume and the intrinsic porosity within the intact rock contained in the fractured zone. By assuming that the concentration profile is constant across this zone, which could perhaps be a meter or two in breadth, a void volume equivalent to an aperture of 21 cm is not unreasonable. This parameter should be thought of as a convenience for setting the spacing and fracture porosity as it no longer has the meaning of an aperture when the model is used to represent a flowing network of fracture zones.

The other element of this alternate description of the fracture transport system is the likelihood of sorption within the fractured zones. As opposed to the individual fracture treatment, in which sorption on the faces of fractures is difficult to justify, the alternate model consists of a porous medium within the fracture zones, and retardation due to sorption is easy to justify. In the matrix diffusion model, this sorption is input as a retardation factor within the fracture zone. To set the retardation factors within the fracture zones, it is assumed that the porosity is essentially that of the intact matrix rock and that the same sorption coefficient K_d applies within the fracture zone. Then, the normal relationship between the sorption coefficient and the retardation factor R_f is assumed to apply:

$$R_f = 1 + \rho_b K_d/\theta \qquad \text{(Eq. 12.3.2.3-2)}$$

where

ρ_b = dry bulk density, including pores
θ = porosity

Two sets of simulations were performed using FEHM V2.11 to examine the impact of this alternate conceptual model. The first considers transport of a conservative species such as carbon-14 to the 20-km boundary. All base case parameters are chosen except the fracture porosity, which is set to 0.01 to capture the effect of transport through fracture zones (spaced 21 m apart) rather than through individual fractures. Figure 12.3.2.3-8 compares the breakthrough curves for a release location in region 1 of the saturated-zone footprint. Also shown in this comparison is the same simulation with no matrix diffusion. The adoption of the

concept of fracture zones results in slightly longer breakthrough times to the 20-km point of compliance compared to the case of individual flowing fractures. Both of these simulations exhibit slight delays of arrival compared to the no-diffusion case, implying that the matrix diffusion process is providing a relatively small improvement to the SZ subsystem performance for conservative radionuclides. The reason for the relatively minor impact in this study is that transport times in the alluvium for the expected case provide several hundred years of transport time delay for all cases, so for matrix diffusion to be important, the amount of delay must approach or exceed this value. With respect to the comparison of the two diffusion conceptual models, there is a tradeoff between the larger fracture porosity, which yields longer transport times within the fracture zones, and the impact of matrix diffusion. The absolute rate of mass diffusion away from the fracture zones are the same as for individual fractures, but the impact is less for fracture zones, which have a large "reservoir" of water containing radionuclide. Thus, the front is not significantly delayed by the presence of the same absolute rate of mass diffusion.

To examine sorption within the fracture zones, neptunium-237 was selected due to its importance in overall radionuclide dose calculations and its propensity to sorb weakly to the rock. This model used the same fracture porosity of 0.01 but included retardation factors within the fractured volcanic tuffs as given by Equation 12.3.2.3-2. A unique value of R_f within each rock type was calculated assuming an average rock bulk density of 2,000 kg/m^3 and the local value of matrix porosity, defined on a node-by-node basis in the site-scale SZ model. Although bulk density and porosity are probably correlated, this approximation will have only a minor affect on the results compared to the inherent uncertainty of the parameters, and therefore, the approximation is valid. The neptunium-237 curves in Figure 12.3.2.3-8 show a minor impact of the type of conceptual model selected, and in fact, the no-diffusion case yields a similar performance as well.

As demonstrated by this sensitivity study, the incorporation of the concept of fracture zones results in little or no improvement in the performance of the SZ as a barrier to radionuclide transport for the expected case. For the purposes of this document, it is concluded that the conceptual model used for the majority of the analyses, namely flow through individual fractures, is bounding in that it provides a lower bound for the transport times through the fractured volcanic tuffs when compared to fracture zone models. However, rather than negating the importance of matrix diffusion as a transport process, this result indicates that other transport barriers within the SZ subsystem can mask the importance of matrix diffusion. In particular, in the expected case, transport through the alluvium adds significant transport time at the end of the pathway to the point of compliance. If this barrier does not perform as currently thought, either because the transport pathways miss the alluvium or because the transport conceptual model for the alluvium is not valid, then matrix diffusion, and differences in the alternate models, would become more important. Therefore, the issue of which matrix diffusion model is appropriate is important despite the apparent lack of sensitivity for the nominal case.

12.3.2.4 Quantification of Previously Unquantified Uncertainty

This section discusses various uncertainty analyses related to transport modeling in the saturated zone. Sections 12.3.2.4.1 and 12.3.2.4.2 deal with sorption of neptunium on volcanic units and in the alluvium, respectively. Section 12.3.2.4.3 deals with sorption of uranium in the alluvium as well as correlation of the sorption coefficients for neptunium and uranium. Section 12.3.2.4.4

treats the bulk density of the alluvium. Section 12.3.2.4.5 discusses irreversible colloidal sorption in the alluvium. Section 12.3.2.4.6 deals with diffusion in the matrix of volcanic tuffs. Section 12.3.2.4.7 handles effective porosity in the alluvium. Finally, Section 12.3.2.4.8 discusses flowing interval porosity (fracture porosity).

12.3.2.4.1 Sorption-Coefficient Distributions for Neptunium in the Volcanic Units

Sorption of neptunium in volcanic units is an important process that contributes to the performance of the SZ as a barrier to radionuclide migration. Neptunium sorption coefficients are important for the nominal scenario results in the TSPA-SR (CRWMS M&O 2000 [DIRS 153246], Section 5.1.2). The sorption coefficient is used to compute retardation as follows Freeze and Cherry (1979 [DIRS 101173], p. 404):

$$R = 1 + \frac{\rho_b}{\theta} K_d \qquad \text{(Eq. 12.3-3)}$$

where

ρ_b = the dry bulk density of the matrix (mass/length^3)
θ = the matrix porosity (dimensionless)
R = the retardation factor in the matrix (dimensionless)
K_d = the sorption coefficient for the matrix (length^3/mass)

12.3.2.4.1.1 Treatment in the Total System Performance Assessment-Site Recommendation

For the TSPA-SR (CRWMS M&O 2000 [DIRS 153246]), the sorption-coefficient probability distribution for neptunium in the matrix was a beta distribution with a mean of 0.5 ml/g, a standard deviation of 0.5, a lower bound of 0, and an upper bound of 2.0 ml/g (CRWMS M&O 2000 [DIRS 147972], p. 62; DTN: LA0003AM831341.001 [DIRS 148751]). Four sorption-coefficient distributions per radionuclide are provided, which are defined as: iron oxides, vitric tuff, devitrified tuff, and zeolitic tuff. The sorption-coefficient distributions used in the SZ site-scale transport calculations correspond to a rock type of vitric tuff, which has the lowest mean value (a conservative approach) that can result in rapid transport through the SZ.

12.3.2.4.1.2 Development of a More Representative Probability Distribution

The main change implemented regarding the neptunium sorption-coefficient probability distribution in the volcanic units for the unquantified uncertainty analysis is that the sorption behavior of zeolitic tuffs is incorporated into the neptunium transport calculation. Because vitric tuffs tend to have the lowest affinity for neptunium (i.e., smallest sorption coefficients) of the three major tuffs (devitrified, vitric, and zeolitic), the use of sorption coefficients for vitric tuffs to represent all three tuff types puts an overly conservative bias on the TSPA-SR transport calculations (CRWMS M&O 2000 [DIRS 147972], Section 6.10). Inclusion of zeolitic tuff sorption coefficients in the transport calculations will result in more representative model simulations and reduce modeling uncertainties.

The integrated site model (V3.1) (CRWMS M&O 2000 [DIRS 146988]) was used to derive the volume of rock (by percent) that is zeolitic within the boundaries of the site-scale SZ flow and transport model and from the water table to 300 m below the water table (Table 12.3.2.4-1) (Kuzio 2001 [DIRS 155004], Filename "Table 12.3.2.4-1.doc"). Rock samples used to derive the neptunium sorption-coefficient distributions typically contained 50 to 60 percent zeolite (CRWMS M&O 2001 [DIRS 154024], Section 6.4.4.1.4.2). However, experiments with pure zeolite yielded lower sorption coefficients than natural rock samples containing 50 to 60 percent zeolite (CRWMS M&O 2001 [DIRS 154024], Section 6.4.4.1.4.2). Therefore, some phase other than zeolite also sorbed neptunium in these samples. To compensate for the sorption by this other phase, it is assumed that a rock must have at least 30 percent zeolite to qualify as a zeolitic tuff. Based on Table 12.3.2.4-1, the volume of zeolitic tuff within the total saturated rock volume with 30 percent or more zeolite is approximately 33 percent. This value is used in the sampling of the neptunium sorption-coefficient probability distributions. That is, the neptunium sorption-coefficient probability distribution for zeolitic tuffs was sampled for 33 percent of the simulations, and the neptunium sorption-coefficient probability distribution for vitric tuffs was sampled for 66 percent of the simulations. The zeolitic probability distribution that was sampled 33 percent of the time is a beta distribution with a mean of 1.0 ml/g, a standard deviation of 0.25, a lower bound of 0, and an upper bound of 5.0 ml/g (DTN: LA0003AM831341.001 [DIRS 148751]).

12.3.2.4.1.3 Summary of the Technical Basis for Uncertainty Analysis

In summary, the probability distribution used for the neptunium sorption coefficient in the matrix was changed from a probability distribution based on a vitric rock type to a probability distribution that is more representative of the rock types that the flow path will encounter. For a given set of realizations (that is, simulations with Monte Carlo sampling) the new probability distribution is determined by sampling the vitric distribution 66 percent of the time and the zeolitic distribution 33 percent of the time.

12.3.2.4.2 Sorption-Coefficient Distributions for Neptunium in the Alluvium

Sorption of neptunium in alluvial material is an important process that contributes to the performance of the SZ as a barrier to radionuclide migration. Neptunium sorption coefficients are important for the nominal scenario results in the TSPA-SR (CRWMS M&O 2000 [DIRS 153246], Section 5.1.2). In general, alluvium has a greater potential for retardation than the tuff matrix (the sorption coefficients are typically larger) due to factors such as mineralogy, reaction kinetics, and water chemistry (CRWMS M&O 2001 [DIRS 154024], Section 6.4.5.2). In addition, sorption in the alluvium is a relatively certain process in that it occurs independent of other processes. By contrast, matrix diffusion must occur in the volcanic units for sorption to become active. No such dependence exists for sorption in the alluvium. Retardation in the alluvium is computed from the sorption coefficient of neptunium using Equation 12.3-3.

12.3.2.4.2.1 Treatment in the Total System Performance Assessment-Site Recommendation

For the TSPA-SR (CRWMS M&O 2000 [DIRS 153246]), the sorption coefficient for neptunium in the alluvium was represented as a beta distribution with a mean of 18.2, a standard deviation

of 18.8, a lower bound of 0, and an upper bound of 100 (CRWMS M&O 2000 [DIRS 147972], p. 63) The source for this parameter (DTN: LA0003AM831341.001 [DIRS 148751]) was developed from preliminary laboratory batch sorption tests using alluvial material from the site (DTN: LA0003JC831341.001 [DIRS 147176]).

12.3.2.4.2.2 Development of a More Representative Probability Distribution

The probability distribution for the neptunium sorption coefficient in alluvium has been modified on the basis of newly acquired laboratory results. These results include batch sorption experiments and column experiments using alluvium samples and water from a well in the alluvium.

The neptunium K_d values (ml/g) were measured in batch sorption tests using alluvium obtained from NC-EWDP boreholes 2D, 3S, and 9SX and samples that were dry sieved to the 75- to 500-micron size range (Reimus 2001 [DIRS 154994], Filename "Np Alluvium Sorption"; DTN: LA0003JC831341.001 [DIRS 147176]). The water for the experiments was from borehole NC-EWDP-3S. Figure 12.3.2.4-1 shows these neptunium batch-sorption K_d values (ml/g). The sorption coefficients obtained for the NC-EWDP-3S borehole samples tended to be at the high end of the range, possibly because Eh conditions in this borehole were more reducing than in the other boreholes. The NC-EWDP-3S data were not used in constructing the final probability distribution function because these data could represent conditions that may not be representative of the dominant flow paths to the accessible environment. The distribution without the NC-EWDP-3S data is shown in Figure 12.3.2.4-1 with diamonds. The mean of the experimental results is 29 ml/g, and the median is 16 ml/g.

The neptunium K_d value obtained in two column experiments was about 0.5 ml/g, which is lower than any of the batch measurements (Reimus 2001 [DIRS 154994], Filename "Np Alluvium Sorption"). The material used to pack the columns had a batch K_d value of about 6 ml/g. The differences in the batch and column results likely reflect the kinetics of the neptunium sorption reactions or rate limitations imposed by mass-transfer processes (e.g., diffusion of neptunium between flowing water and sorbing mineral phases). If the columns were run at slower flow rates, the retardation factors obtained would likely increase in value.

With this new information, a cumulative distribution function (CDF) for neptunium K_d values was derived (Kuzio 2001 [DIRS 155004]) that gives considerable weight to the column experiments to provide conservatism (Figure 12.3.2.4-2). This distribution uses the result of the column experiment that ranges from 0.0 to 0.5 ml/g 33 percent of the time. The remainder of the distribution is derived (Reimus 2001 [DIRS 154994], Filename "Np Alluvium Sorption") from the batch sorption measurements in Figure 12.3.2.4-1 with a range of K_d values from 0.5 to 10 ml/g 47 percent of the time and from 10 and 95 ml/g 20 percent of the time.

12.3.2.4.2.3 Summary of the Technical Basis for Uncertainty Analysis

In summary, the probability distribution used for the unquantified uncertainty analysis was changed from a probability distribution based on laboratory batch experiments to one that represents batch and column laboratory experiments. The distribution function gives

considerable weight to the column experiments, which gives more weight to the lower sorption-coefficient values.

12.3.2.4.3 Sorption-Coefficient Distributions for Uranium in the Alluvium and Correlation of the Sorption Coefficients for Neptunium and Uranium in the Alluvium

Sorption of radionuclides in alluvial material is an important process that contributes to the performance of the SZ as a barrier to uranium migration. As for the case of neptunium, alluvium has a greater potential for retardation than the tuff matrix (the sorption coefficients are typically larger) (CRWMS M&O 2001 [DIRS 154024], Section 6.4.5.2) due to factors such as mineralogy, reaction kinetics, and water chemistry. In addition, sorption in the alluvium is a relatively certain process in that it occurs independently of other processes. By contrast, matrix diffusion must occur in the volcanic units for sorption to become active. No such dependence exists for sorption in the alluvium. Retardation in the alluvium is computed from the sorption coefficient using Equation 12.3-3.

12.3.2.4.3.1 Treatment in the Total System Performance Assessment-Site Recommendation

For the TSPA-SR (CRWMS M&O 2000 [DIRS 153246]), the sorption coefficient for uranium in the alluvium was represented as a uniform distribution with a lower bound of 0 and an upper bound of 8 (CRWMS M&O 2000 [DIRS 147972], p. 63).

12.3.2.4.3.2 Development of a More Representative Probability Distribution

Although sorption-coefficient data for uranium have not been obtained on alluvium samples taken from potential flow paths, an alternative approach for the derivation of sorption-coefficient data was developed in the absence of experimental data. The approach is based on the recognition that uranium and neptunium have similarly small affinities for sorption onto the tuffs within Yucca Mountain (CRWMS M&O 2001 [DIRS 154024], Sections 6.4.4.1.4.2 and 6.4.4.1.4.4). This observation likely reflects the fact that, under oxidizing conditions, these elements form oxycations (uranyl and neptunyl ions, respectively), which have similar sorption mechanisms. On this basis, the sorption-coefficient probability distribution for neptunium in alluvium is taken to also represent the sorption-coefficient probability distribution of uranium in alluvium.

This approach for the derivation of uranium sorption-coefficient probability distributions in alluvium does not reduce the uncertainty in the calculated transport rates for uranium in alluvium in terms of reducing the range of possible error in the calculated rates. However, as discussed below, it does provide conservative estimates of the transport rates for uranium in alluvium. In this sense, it reduces the likelihood that the calculated uranium transport rates are larger than they will be in the natural environment.

A comparison of sorption coefficients for uranium and neptunium obtained for volcanic tuffs indicates that the uranium sorption coefficients are consistently larger in value than the sorption coefficients for neptunium obtained for similar rock samples under similar conditions (Well J-13

water and oxidizing conditions). Data supporting this conclusion are presented in Table 12.3.2.4-2.

12.3.2.4.3.3 Summary of the Technical Basis for Uncertainty Analysis

On this basis, in the absence of experimental data on uranium sorption coefficients in alluvium, the sorption-coefficient probability distribution for neptunium in the alluvium is taken to also represent the sorption-coefficient probability distribution for uranium in the alluvium.

This use of the neptunium sorption-coefficient probability distribution in alluvium for that of the uranium distribution underestimates the uranium transport rates in alluvium because the sorption coefficients for uranium are generally higher in volcanic tuffs than the corresponding ones for neptunium (Table 12.3.2.4-2). The sampling of uranium and neptunium should be identical for a given realization (Monte Carlo simulation result); therefore, the probability distributions for uranium and neptunium have a one-to-one correlation. If they were not correlated, different values would result from sampling identical distributions.

12.3.2.4.4 Bulk Density of the Alluvium

The dry bulk density of the alluvium is important in the computation of the retardation of sorbing radionuclides. The dry bulk density is related to the matrix retardation coefficient through Equation 12.3-4 (Freeze and Cherry 1979 [DIRS 101173], p. 404), which for alluvium, is:

$$R' = 1 + \frac{\rho_b}{\theta} K_m \qquad \text{(Eq. 12.3-4)}$$

where

R' = the retardation factor in the alluvium (dimensionless)
ρ_b = the dry bulk density of the alluvium (mass/length^3)
θ = the porosity of the alluvium (dimensionless)
K_m = the distribution coefficient in the alluvium (length^3/mass)

As can be seen from the equation, the retardation coefficient is linearly dependent on the dry bulk density.

12.3.2.4.4.1 Treatment in the Total System Performance Assessment-Site Recommendation

For the TSPA-SR (CRWMS M&O 2000 [DIRS 153246]), the dry bulk density was considered to be a constant and set to 1.27 g/cm^3 (CRWMS M&O 2000 [DIRS 147972], Section 6.9). The basis for this parameter value is a set of tests performed on four five-foot alluvial intervals from each of the NC-EWDP boreholes 2D, 9S, and 3S at depths of 395 to 415 feet, 145 to 165 feet, and 60 to 80 feet, respectively (DTN: LA0002JC831341.001 [DIRS 147081]). The range of the dry bulk density values in laboratory columns packed with alluvium from these wells was 1.2 to 1.3 g/cm^3. The data are presented in *Unsaturated Zone and Saturated Zone*

Transport Properties (U0100) (CRWMS M&O 2001 [DIRS 154024], p. 86) with a note stating that densities were measured in the laboratory and do not represent in-situ conditions.

12.3.2.4.4.2 Development of a More Representative Model

The values used in the TSPA-SR (CRWMS M&O 2000 [DIRS 153246]) were low compared to dry bulk densities measured in alluvium at Frenchman Flat and the NTS near Yucca Mountain (Howard 1985 [DIRS 153266], Table 3, p. 81, and Table A-1, p. 38). Similarly, a comparison to the range of dry bulk densities of alluvial material in general (Manger 1963 [DIRS 154474], pp. E41 to E42) led to the conclusion that the values used in the TSPA-SR were likely an underestimate of the true bulk density.

Borehole gravimeter surveys were conducted by EDCON Incorporated (Black 2000 [DIRS 154704], pp. 2 to 18) at well NC-EWDP-19D1 directly south of Yucca Mountain on U.S. Highway 95. A total of 36 values of saturated bulk density were estimated based on the geophysical milligal measurements taken from this well (Black 2000 [DIRS 154704], p. 18). Seventeen measurements were taken from a depth corresponding to the inferred depth of the flow path through the alluvium near Yucca Mountain (401.5 to 776 feet). The wet bulk density computed from gravimeter measurements is presented in Table 12.3.2.4-3 as well as the porosity and dry bulk density computed from Freeze and Cherry (1979 [DIRS 101173], p. 337) and Black (2000 [DIRS 154704], p. 18):

$$\theta = \frac{\rho_{sat} - \rho_{grain}}{\rho_w - \rho_{grain}} \qquad \text{(Eq. 12.3-5)}$$

$$\rho_b = \rho_{grain}(1-\theta) \qquad \text{(Eq. 12.3-6)}$$

where

θ = porosity (dimensionless)
ρ_b = dry bulk density in g/cm^3
ρ_{sat} = saturated bulk density in g/cm^3
ρ_{grain} = the average grain density for these samples (2.52 g/cm^3)
ρ_w = the density of water (1.0 g/cm^3)

The mean dry bulk density for this set of measurements was 1.91 g/cm^3. This value is close to dry bulk density values previously measured at Frenchman Flat and the NTS in similar rock at similar depth, and it is the value used as the mean in the unquantified uncertainty simulations. The computed standard deviation for these measurements is 0.080 g/cm^3.

The average grain density was computed to be 2.52 g/cm^3 from alluvial samples from other boreholes in the vicinity of Yucca Mountain (USGS n.d. [DIRS 154495], pp. 3 to 4). The grain density varied little (2.49 to 2.55 g/cm^3), and so the average was used in the computation of the porosity and dry bulk density. A normal distribution was selected to characterize the uncertainty in the dry bulk density based on frequency plots of that parameter.

12.3.2.4.4.3 Summary of the Technical Basis for Uncertainty Analysis

To summarize, the value for dry bulk density in the alluvium is changed from a constant value of 1.27 g/cm^3 to a stochastic variable that more properly characterizes uncertainty at Yucca Mountain for the unquantified uncertainty computations. The new dry stochastic bulk density is chosen from a normal distribution. The mean dry bulk density, 1.91 g/cm^3, and standard deviation, 0.080 g/cm^3, as well as the distribution form are based on new data taken at well NC-EWDP-19D1. Figure 12.3.2.4-3 gives the distribution of 100 realizations of dry bulk density for the alluvium; the normal distribution was used to characterize the dry bulk density. This distribution was found to give a reasonable fit to the data taken at the NC-EWDP-19D1 well, also shown in Figure 12.3.2.4-3.

12.3.2.4.5 Retardation of Radionuclides Irreversibly Sorbed on Colloids in the Alluvium

Radionuclides that sorb strongly to solid geologic materials are generally considered to be immobile. However, colloid-facilitated transport is the one mechanism that can result in enhanced mobility of these radionuclides (discussed below). For the TSPA-SR (CRWMS M&O 2000 [DIRS 153246]), two conceptual models of colloid-facilitated transport of radionuclides were implemented: the first conceptual model involves radionuclides that are irreversibly or permanently (in the time frame of groundwater transport) sorbed onto colloids; the second deals with radionuclides that are reversibly or temporarily attached to colloids.

This section discusses the retardation of radionuclides irreversibly sorbed on colloids in the alluvium. The available data for colloid filtration are reduced in a manner that provides estimates of the colloid retardation factor. However, the particle tracking code component of FEHM V2.10 calls for a K_d value as input for porous continua such as the alluvium. Therefore, in the site-scale SZ flow and transport model, the estimated colloid retardation factors for the alluvium units are converted to a value of effective sorption coefficient according to a rearranged form of Equation 12.3-3 (Freeze and Cherry 1979 [DIRS 101173], p. 404):

$$K_d^{eff} = \frac{(R_f - 1)\phi_{eff}}{\rho_b} \qquad \text{(Eq. 12.3-7)}$$

where

K_d^{eff} = the effective K_d
R_f = the retardation factor for irreversible colloids
θ_{eff} = effective porosity
ρ_b = bulk density

The units are the same ones as in Equation 12.3-3.

12.3.2.4.5.1 Summary of the Treatment in the Total System Performance Assessment-Site Recommendation

The development in the TSPA-SR (CRWMS M&O 2000 [DIRS 153246]) of the CDF for the retardation factor of radionuclides that are irreversibly sorbed to colloids in the alluvium is described in the *Saturated Zone Colloid-Facilitated Transport* report (CRWMS M&0 2000

[DIRS 129286], Figure 8). This AMR provides a theoretical approach based, in part, on field tests at other alluvial aquifers. At the time of that report, the Yucca Mountain alluvium had not been characterized. The CDF was obtained using the following equation for the retardation factor R:

$$R = 1 + \frac{\rho_a}{\theta}\frac{k_f}{k_r} \qquad \text{(Eq. 12.3-8)}$$

where

ρ_a = the density of the alluvial material in g/cm^3
θ = the alluvium porosity
k_f = the rate of colloid attachment onto the immobile material in 1/hr
k_r = the detachment rate in g/cm^3-hr

The attachment rate k_f is further defined as (Harvey and Garabedian 1991 [DIRS 109256], Equation 2):

$$k_f = v\frac{3}{2}\frac{(1-\theta)}{d}\alpha\eta \qquad \text{(Eq. 12.3-9)}$$

where

v = the fluid velocity
d = the diameter of the porous media grains
α = the collision efficiency factor
η = the single-collector efficiency

The single-collector efficiency η can be estimated from:

$$\eta = \eta_D + \eta_I + \eta_G = 0.9\left[\frac{kT}{\mu d_p dv}\right]^{2/3} + 1.5(d_p/d)^2 + \frac{(\rho_p - \rho)g{d_p}^2}{18\mu v} \qquad \text{(Eq. 12.3-10)}$$

where

η_D = the colloid collector collision caused by Brownian motion
η_I = the colloid collector collision caused by interception
η_G = the colloid collector collision caused by settling
k = the Boltzmann constant
T = the solute temperature (absolute temperature)
μ = the fluid viscosity
d_p = the colloid diameter
d = the diameter of the porous media grains
ρ = the fluid density
ρ_p = the colloid density
g = acceleration due to gravity

For Equations 12.3-8 through 12.3-10, the following parameters were held constant: k (1.38×10^{-16} erg/K), T (25°C), μ (0.01 g/cm-sec), ρ (1.0 g/cm^3), ρ_p (2.6 g/cm^3), ρ_a (1.27 g/cm^3), and g (980 cm/sec^2). Parameters that were varied and their assumed distributions are listed in Table 12.3.2.4-4. Each of the parameter distributions in that table were randomly sampled using the GoldSim V6.04.007 software package, and the resulting parameters were used in Equations 12.3-8 through 12.3-10 to obtain an estimate of the colloid retardation factor, R. A CDF was then constructed from 10,000 such realizations of R.

12.3.2.4.5.2 Development of a More Representative Probability Distribution

The revised CDF for the retardation factor of radionuclides that are irreversibly sorbed to colloids in the alluvium was generated using the same equations and procedure as the CDF in the TSPA-SR (CRWMS M&O 2000 [DIRS 153246]). However, the alluvium grain size distribution was modified to reflect actual grain size data from well NC-EWDP-19P and from other locations at the NTS. Additionally, the grain size distribution was weighted by the permeability associated with the different grain sizes, as calculated using the Carman-Kozeny equation (Dagan 1989 [DIRS 147409], p. 104). Thus, given equal volumes of large and small grain sizes, colloids were more likely to encounter larger grains because significantly more flow is conducted through larger grains.

The procedure for obtaining the grain size distribution used in the generation of the revised retardation factor CDF was:

1. Fifty-one alluvium grain size (diameter) distribution data sets from the NTS were fitted assuming a lognormal distribution. The sampling locations included multiple intervals/locations within boreholes u-3bl-d2, u-3bh, and u-3bh-c2 in Yucca Flat (Bechtel Nevada 1998 [DIRS 149177], Table I-1; McKeown 1992 [DIRS 102330], Appendix 1), and trenches near the current location of the Exploratory Studies Facility (ESF) north portal and well NC-EWDP-19P (Reimus 2001 [DIRS 154994], Filename "EWDP 19P Grain Sizes").

2. Discrete and Gaussian CDFs of the means and standard deviations of the 51 lognormal distributions were obtained by fitting the data.

3. The discrete distributions obtained in Step 2 were randomly sampled and the resulting means and standard deviations were used to generate artificial grain size distributions assuming a lognormal distribution. Effective diameters (d_{eff}) of these distributions were obtained by calculating the surface area to volume ratio (A/V) for the entire distribution and then calculating the effective diameter from $d_{eff} = 6V/A$ (which applies to spherical particles).

4. An unweighted CDF was obtained for effective diameters by repeating Step 3 many times.

5. For each effective diameter in the unweighted CDF, a relative permeability, k, was calculated using the Carman-Kozeny equation (Dagan 1989 [DIRS 147409], p. 104):

$$k = \frac{\theta^3}{180\,(1-\theta^2)}\,d_{\text{eff}}^2 \qquad \text{(Eq. 12.3-11)}$$

6. The contribution of each bin in the unweighted CDF to the overall permeability was determined by multiplying the permeability associated with that bin by the probability of that bin. These products were then summed over all bins, and the probability of a colloid experiencing an effective diameter associated with a given bin was assumed to be the product for that bin divided by the sum of the products for all bins. In effect, this procedure made the effective diameter probabilities proportional to the volumetric flow rates through the different bins. Thus, a new CDF of effective diameters with probabilities weighted by volumetric flow rates was created.

7. The weighted CDF from Step 6 was randomly sampled instead of the original uniform distribution of grain diameters in Table 12.3.2.4-4 to obtain a new CDF of colloid retardation factors.

The new and original CDFs for retardation factors of radionuclides irreversibly sorbed to colloids are plotted in Figure 12.3.2.4-4. It is apparent that the new CDF results in lower retardation factors than the original one used in the TSPA-SR (CRWMS M&O 2000 [DIRS 147972], Figure 6).

12.3.2.4.5.3 Summary of the Technical Basis for Uncertainty Analysis

The new CDF for retardation factors of radionuclides irreversibly sorbed to colloids assumes that most water flow, and therefore colloid migration in the alluvium, will occur in high-permeability regions, which should have larger grain sizes than lower-permeability regions. In sampling the CDF, it is implicitly assumed that colloids will experience the same sampled grain size distribution (effective diameter) throughout the entire alluvium. In reality, individual flow streamlines may experience a variety of grain size distributions through the alluvium. The assumption of a single distribution effectively implies a layered system or the existence of continuous channels of interconnected material of similar grain sizes. Although this assumption has not been proven or tested, any distribution of grain sizes that are linked in series will tend to have a permeability and, presumably, a colloid retardation coefficient that is dominated by the lowest permeability and grain size.

The alluvium bulk density assumed in generating the new CDF of retardation factors was 1.27 g/cm^3; the same value that was assumed in the generation of the original CDF, despite the fact that the bulk density was modified based on the borehole gravimeter data from NC-EWDP-19D1 (see Section 12.3.2.4.4). The new value of bulk density will be incorporated into future calculations of the retardation factor CDF. The use of the old bulk density value yields retardation factors that are about 35 percent lower than values calculated using the new bulk density.

Other assumptions associated with the generation of the colloid retardation factor CDF are described in *Saturated Zone Colloid-Facilitated Transport* (CRWMS M&O 2000 [DIRS 129286], pp. 12 to 14).

12.3.2.4.6 Effective Diffusion Coefficient and Correlation

Matrix diffusion is a key retardation process in the volcanic tuffs. For non-sorbing radionuclides, diffusion into the stagnant fluid in the tuff matrix reduces travel times. For sorbing radionuclides, matrix diffusion also provides the mechanism for contact of the radionuclides with the rock matrix which is a necessary precondition for sorptive retardation.

Section 12.3.2.3.4 describes a modest sensitivity of the model results to uncertainty in the matrix diffusion model. However, these simulations all assumed significant transport pathways through the porous alluvium. The matrix diffusion process is anticipated to be most important in providing an additional transport barrier in the event that the transport times provided by the alluvium are not realized.

12.3.2.4.6.1 Treatment in the Total System Performance Assessment-Site Recommendation

In the TSPA-SR calculations, effective radionuclide diffusion coefficients in volcanic matrices were randomly sampled from a log-uniform distribution having values ranging from 10^{-10} to 10^{-13} m^2/sec (CRWMS M&O 2000 [DIRS 147972], p. 62). The basis for this parameter, for the radionuclides of interest, included an analysis of the ionic radius, charge, and most importantly, the differences in tortuosity. Fracture apertures and matrix porosity also influence matrix diffusion of radionuclides. The former is effectively determined in the preprocessor for the site-scale SZ flow and transport model (CRWMS M&O 2000 [DIRS 139440], Section 6.2.1.3) by the fracture porosity divided by the flowing interval spacing, both of which are randomly sampled from distributions (log uniform with bounds of 10^{-1} to 10^{-5} for fracture porosity and lognormal with a geometric mean of approximately 20 m and a $\log_{10}$ standard deviation of 0.43 for flowing interval spacing). The matrix porosity is a constant value for a given TSPA realization, based on the stratigraphic unit(s) in which the SZ transport is assumed to occur. In the TSPA-SR (CRWMS M&O 2000 [DIRS 153246]), there was no correlation between the sampled matrix diffusion coefficients and the matrix porosities.

12.3.2.4.6.2 Development of a More Representative Probability Distribution

Changes made in the treatment of radionuclide matrix diffusion for the SSPA unquantified uncertainties (McNeish 2001 [DIRS 155023]) calculations include the following:

- The distribution for radionuclide effective matrix diffusion coefficients was modified from log uniform to log triangular probability distribution. The upper and lower bounds are still 10^{-10} and 10^{-13} m^2/sec, but the most probable value is 3.2×10^{-11} m^2/sec. The basis for this is to put more emphasis on the mean value compared to sampling a uniform distribution that results in sampling equally all values in the distribution. The effect of this change is that larger and smaller effective diffusion coefficients are less probable.

- The distribution for fracture porosity in the volcanics was modified from log uniform to log triangular. The upper and lower bounds are still 10^{-1} and 10^{-5}, but the most probable value is now 10^{-3}. The basis for this is to put more emphasis on the mean value compared to sampling a uniform distribution that results in sampling equally all values in the distribution.

- Sampled matrix diffusion coefficients are now correlated with matrix porosities using a relationship developed from laboratory diffusion-cell experiments in which anion diffusion coefficients through tuff matrices from various stratigraphic units from the C-wells Complex (Reimus 2001 [DIRS 154994]) and from Pahute Mesa at the NTS (Reimus et al. 1999 [DIRS 154689], pp. 27 to 29; Reimus 2001 [DIRS 154994], Filename "Diffusion Cell Data") were measured. For a given sampled value of the effective matrix diffusion coefficient, the value is adjusted upward or downward, depending on the sampled value of the matrix porosity relative to the average volcanic matrix porosity from laboratory studies, by a value of 0.15 (CRWMS M&O 2000 [DIRS 147972], Section 6.5). The laboratory-derived relationship between matrix diffusion coefficients and matrix porosity is shown in Figure 12.3.2.4-5.

12.3.2.4.6.3 Summary of the Technical Basis for Uncertainty Analysis

To determine whether the probability distributions described above result in realistic treatment of radionuclide matrix diffusion in volcanic rocks, the distributions of mass transfer coefficients obtained from 300 realizations of the SZ flow and transport model with laboratory- and field-derived mass transfer coefficients were compared, as described in the following sections.

The mass transfer coefficient (MTC) is defined as (Robinson 2001 [DIRS 155060]):

$$\frac{\theta}{b}\sqrt{D_m} \quad (\sec^{-1/2}) \qquad \text{Eq. 12.3-12}$$

where

θ = matrix porosity
b = the fracture half-aperture (m)
D_m = the matrix diffusion coefficient (m^2/sec)

Figure 12.3.2.4-6 shows mass transfer coefficients (for halides) as a function of tracer residence time derived from laboratory transport experiments conducted using fractured cores from the C-wells or Pahute Mesa (NTS) and field transport experiments conducted either at the C-wells or Pahute Mesa. The MTCs span a range of almost 4 orders of magnitude of mean tracer residence time, with an apparent trend of decreasing MTC as time scale increases. For comparison, Figure 12.3.2.4-7 shows the distribution of MTCs from 300 realizations of the SZ flow and transport model for the modified uncertainty distributions for diffusion coefficient and fracture porosity described here. It is apparent that the distribution of simulated MTCs spans the experimental range with the lower end of the distribution extending to significantly lower values than the experimental range. This result is considered acceptable because the experimental data

suggest a potential decrease in MTC as time scales extend beyond the experimental range to values relevant for performance assessment.

12.3.2.4.7 Effective Porosity in the Alluvium

The effective porosity in the alluvium is an important parameter controlling transport times through the alluvium. For a given groundwater flux, the travel time of a conservative radionuclide is directly proportional to the effective porosity. In addition, for sorbing radionuclides, Equation 12.3-3 shows that the retardation factor is inversely influenced by the porosity.

12.3.2.4.7.1 Treatment in the Total System Performance Assessment-Site Recommendation

For the TSPA-SR (CRWMS 2000 [DIRS 153246]), effective porosity in the alluvium was a truncated normal distribution with a mean of 0.18, a standard deviation of 0.051, a lower bound of 0, and an upper bound of 0.35 (CRWMS M&O 2000 [DIRS 147972], Section 6.3). The basis for this parameter was Bedinger et al. (1989 [DIRS 129676], p. A18, Table 1). There were no site data for effective porosity in the alluvium at the time of the TSPA-SR. Bedinger et al. (1989 [DIRS 129676]) includes a study of hydraulic characteristics of alluvium within the Southwest Basin and Range Province. This study appears relevant to the local basin fill conditions and provides values for effective porosity as a stochastic parameter.

12.3.2.4.7.2 Development of More Representative Probability Distribution

The mean alluvium flow effective porosity was decreased from 0.18 to 0.15, based primarily on the preliminary results of single-well, isolated interval hydraulic tests at well NC-EWDP-19D1. These results, to date, have indicated that there are negligible hydraulic responses in well screens above and below any isolated screened interval that has been pumped in the alluvium (Kuzio 2001 [DIRS 155004], Filename "transducer data.xls"). That is, the pressure transducers above and below the packers used to isolate the pumped intervals have not responded significantly during pumping. These results suggest that there may be considerable vertical anisotropy in hydraulic conductivity in the alluvium, possibly due to subhorizontal layering of varying degrees of grain coarseness and/or cementation.

12.3.2.4.7.3 Summary of the Technical Basis for Uncertainty Analysis

In summary, the probability distribution used for effective porosity in the alluvium changed from a probability distribution based primarily on Bedinger et al. (1989 [DIRS 129676]) to a probability distribution that is more representative of preliminary results from single-well, isolated-interval hydraulic tests at well NC-EWDP-19D1. The distribution used for the SSPA Volume 2 (McNeish 2001 [DIRS 155023]) calculation was changed from a truncated normal distribution with a mean of 0.18, a standard deviation of 0.051, a lower bound of 0, and an upper bound of 0.35, to a normal distribution with a mean of 0.15, a standard deviation of 0.051, a lower bound of 0, and an upper bound of 0.30. The rational for changing the upper bound from 0.35 to 0.30 is Table 12.3.2.4-3, which indicates a maximum total porosity of approximately 0.30.

12.3.2.4.8 Flowing Interval (Fracture) Porosity

Fracture porosity is defined as the proportion of effective porosity of fractures in which fluid flow and advective solute transport occur. At Yucca Mountain, rather than attempt to define the porosity of individual fractures, a flowing interval is defined as the region in which significant groundwater flow occurs at a well. The fracture porosity then characterizes these flowing intervals rather than individual fractures. The advantage to this means of defining fracture porosity is that in-situ well data may be used to characterize the parameter. Fracture porosity is considered a key parameter in the matrix diffusion process.

12.3.2.4.8.1 Treatment in the Total System Performance Assessment-Site Recommendation

For the TSPA-SR (CRWMS M&O 2000 [DIRS 153246]), the flowing interval (fracture) porosity probability distribution was a uniform distribution with an upper bound of $\log_{10}$ of -1.0 and a lower bound of $\log_{10}$ of -5.0 (CRWMS M&O 2000 [DIRS 147972], p. 39). The basis for this parameter were estimates of fracture porosity in intact cores of volcanic rock and the results of pumping tests and tracer tests in the Bullfrog Tuff at the C-wells Complex (CRWMS M&O 2000 [DIRS 129286]).

12.3.2.4.8.2 Development of More Representative Probability Distribution

The probability distribution for the flowing interval porosity has been modified on the basis of two new sources of information about flowing interval porosity. These are tests in unsaturated tuff in the ESF and the results of tracer tests in saturated tuffs at the C-wells Complex.

Fracture porosity has been estimated in unsaturated volcanic tuff in the ESF for the middle nonlithophysal welded tuff (UZ model layer tsw34) by two methods.

The first method is the gas tracer test. The assumptions used in obtaining the fracture porosity from gas tracer tests are that the diffusion of gas into the rock matrix is negligible compared to the flow through the fractures, that the fracture network is well connected, and that the geometry of the network is known.

This calculation of fracture porosity is documented in the *Analysis of Hydrologic Properties Data* AMR (CRWMS M&O 2000 [DIRS 145771], p. 42). The estimated values of fracture porosity range from 0.006 to 0.02.

For the second method, water was pumped into intervals of boreholes UL, UM, and UR with tracers to identify the travel time to a nearby niche. Based on the water seepage rate and the water release fluxes for the intervals, a seepage threshold flux was determined. From this flux and the arrival time, the average volumetric water content may be estimated from the *Analysis of Hydrologic Properties Data* AMR (CRWMS M&O 2000 [DIRS 145771], Equation 34, p. 58). The volumetric water content approximates the fracture porosity under near saturated conditions. The assumptions are that the liquid flow is downward and steady, and the medium is porous and isotropic (it is assumed that the fractured rock behaves as an equivalent porous medium); that flow is infinite, and flow in the upstream direction is spatially uniform; that an exponential relation exists between the unsaturated hydraulic conductivity and the moisture potential; and

that near saturated conditions exist (under these conditions, the water content is a good approximation of the fracture porosity) (Philip et al. 1989 [DIRS 105743], pp. 16 to 23).

From the tests documented in the *Analysis of Hydrologic Properties Data* AMR (CRWMS M&O 2000 [DIRS 145771], p. 60) the estimated water content values were 0.0242, 0.0124, and 0.0024. These values cover a range similar to the gas-tracer test method.

Fracture porosity has also been estimated using the residence time of conservative tracers during cross-hole tracer tests at the C-wells Complex (Robinson 2001 [DIRS 155060]). This method assumes that the mean tracer arrival time is equal to the time required to drain a homogenous, fractured cylinder of rock with a radius equal to the distance between the pumping well and the tracer-injection well. A large range in estimated fracture porosity for the saturated Bullfrog Tuff resulted from this method because the tracers were interpreted to have traveled along two paths with different travel times. The path with the longer travel time resulted in a larger estimate of fracture porosity. The resulting lower and upper bounds of fracture porosity were 0.0037 and 0.12, respectively (Robinson 2001 [DIRS 155060]). Cross-hole tracer testing in a second interval at the C-wells Complex (the Prow Pass Tuff) resulted in fracture porosity estimates ranging from 0.0027 to 0.0062 (Robinson 2001 [DIRS 155060]).

12.3.2.4.8.3 Summary of the Technical Basis for Uncertainty Analysis

The new data from the ESF and the C-wells tracer tests provide estimates of flowing interval porosity that fall in the upper half of the distribution used for this parameter in the TSPA-SR (CRWMS M&O 2000 [DIRS 153246]). For the SSPA Volume 2 (McNeish 2001 [DIRS 155023]) calculations, a new log-triangular distribution with a lower bound of –5.0, a most-likely value of –3.0, and an upper bound of –1.0 was selected for this parameter. This distribution places more weight at the mid-point of the distribution range compared to the TSPA-SR (CRWMS M&O 2000 [DIRS 153246]; CRWMS M&O 2000 [DIRS 147972], Table 15) uniform distribution that results in equal probabilities for the given range. This midpoint value of –3.0 is representative of the smallest values of fracture porosity estimated from the new data from the ESF and all previous field tests.

12.4 MULTIPLE LINES OF EVIDENCE

This section discusses multiple lines of evidence and confidence-building activities that are independent of TSPA.

Groundwater hydrochemical data were interpreted to estimate flow paths in the vicinity of Yucca Mountain (Section 12.4.1). These estimated flow paths are consistent with flow paths predicted by the site-scale SZ flow model.

Ongoing cleanup efforts at 24 inactive uranium ore processing sites will continue to provide independent information about dispersion and retardation of radionuclides in the subsurface (Section 12.4.2). Studies, to date, provide some information about the transport of uranium that is relevant to Yucca Mountain. First, some fraction of the total uranium inventory of mill tailings appears to be transported as a nonsorbing to weakly sorbing contaminant. Second, the TSPA-SR treatment of uranium as weakly sorbing in the model calculations is supported (CRWMS M&O 2000 [DIRS 153246]). However, the TSPA-SR assumes oxidizing conditions.

More strongly retarding conditions will be appropriate in future performance assessment calculations if new data support the existence of reducing conditions along the flow paths away from Yucca Mountain.

Preliminary results from single-well tracer testing at the ATC are available (Section 12.4.3). These tests are being performed in wells drilled by Nye County as part of their Early Warning Drilling Program. The preliminary results for dissolved tracers suggest diffusion into stagnant or slowly moving groundwater is not an important process in retarding transport of dissolved species in the alluvial materials. This conclusion supports the single-porosity model currently used by the TSPA-SR for transport in alluvium (CRWMS M&O 2000 [DIRS 153246]). Transport of colloids was also investigated in the ATC tests. Preliminary analysis of the behavior of synthetic microspheres indicates that colloids attach to mineral surfaces in the alluvium. This attachment is, however, reversible. These results support the conceptual model used as the basis of the TSPA-SR colloid transport model in alluvium, that is, a model in which colloids attach and detach from mineral surfaces.

The Electric Power Research Institute (EPRI) performed independent modeling of flow and transport in the SZ (Section 12.4.4). The EPRI analysis supports the TSPA-SR conceptualization (CRWMS M&O 2000 [DIRS 153246]) that diffusion of solutes into the matrix of fractured tuffs can slow transport of radionuclides away from the repository. In addition, EPRI concurs that use of flowing intervals is a reasonable conceptualization of SZ conditions. However, EPRI argues that the implementation of dual-porosity transport in the TSPA-SR model is overly conservative in that the assumed distance between fractures is too large.

Preliminary results from the testing of transport behavior of selected radionuclides and compounds on a trial block of intact tuff from the Busted Butte Unsaturated Zone Facility (located near Yucca Mountain) are available and employed to corroborate values used in the transport modeling predictions and performance assessment calculations (Section 12.4.5). The preliminary results indicate that they are consistent with the performance assessment calculations. This statement will be further quantified after the full block test of the Busted Butte Tuff has been completed and a larger fraction of the injected neptunium recovered.

Analogue sites provide data on the transport of uranium, in some cases, over millions of years (Section 12.4.6). Although the geology and geochemistry at many of these sites differ from that at Yucca Mountain, they provide data that may be used to calibrate computer codes, and their analysis can yield a picture of the flow and transport of uranium under various conditions. The sites studied range from ore bodies, such as the Alligator Rivers site in Australia, Poços de Caldas in Brazil, the Oklo site in Gabon, and the Cigar Lake site, to U.S. Department of Energy (DOE) facilities, such as the Idaho National Engineering and Environmental Laboratory (INEEL) site and the NTS.

Measurement of chloride concentrations and uranium isotope activity ratios in groundwater in the Yucca Mountain region serve as a self-analogue study of the site (Section 12.4.7). Such data test the reasonableness of the flow path and travel time computed by the TSPA-SR flow and transport model (CRWMS M&O 2000 [DIRS 153246]).

The Center for Nuclear Waste Regulatory Analysis (CNWRA) completed a flow and transport calculation of radionuclides to assist the U.S. Nuclear Regulatory Commission (NRC) in evaluating the potential repository at Yucca Mountain (see Section 12.4.8). The processes simulated are similar to those included in the TSPA SZ model.

12.4.1 Evidence for Flow Paths Based on Groundwater Hydrochemical and Isotopic Data

Groundwater hydrochemical and isotopic data have been examined to provide estimates of groundwater flow directions in the Yucca Mountain area (CRWMS M&O 2001 [DIRS 154795], Sections 6.5.2.1 and 6.5.2.2, Figure 17). In that analysis, similarities and, more importantly, differences in the concentrations of a number of geochemical and isotopic species were used to identify compositionally distinct waters and trace their movement downgradient. The analysis assumed that the species of interest (i.e., oxygen-18, deuterium, chlorine, SO_4, calcium, and sodium) were sufficiently conservative (species that travel at the speed of the groundwater) that any changes in the species along a flow path were minor compared to differences between adjacent flow paths; thus, relative rather than absolute conservatism of individual species is assumed in the analysis. Maps of the hydraulic head gradient constrained the direction of possible flow paths insofar as groundwater is known not to flow upgradient. However, the flow paths traced from groundwater chemical and isotopic data were allowed to be arbitrarily oblique to the hydraulic gradient to allow for the possible effects of anisotropy in permeability due to preferred north-south fault orientations in the Yucca Mountain area. One important aspect of the flow path analysis is that, under the assumption of two-dimensional steady-state groundwater flow, flow paths do not cross in map view. Therefore, after some flow paths are drawn, the locations of subsequent flow paths are constrained by the existing flow paths.

Other limitations of the two-dimensional flow path analysis discussed in *Geochemical and Isotopic Constraints on Groundwater Flow Directions, Mixing, and Recharge at Yucca Mountain, Nevada* (CRWMS M&O 2001 [DIRS 154795]) pertained to possible bias imparted to the inferred flow directions as a result of compositional changes caused by aquifer mixing or recharge. Compositional changes resulting from these three-dimensional processes would cause the flow paths to be artificially diverted around areas where these effects are important. Groundwater at Yucca Mountain itself may include a large component of local recharge, based on the unique uranium-234/uranium-238 activity ratio of Yucca Mountain perched water and underlying groundwater (CRWMS M&O 2001 [DIRS 154795], Section 6.5.3). Thus, Yucca Mountain itself may be one area where upgradient groundwater is artificially diverted around Yucca Mountain in the analysis.

The groundwater flow paths determined from the analysis of groundwater hydrochemical and isotopic data are shown superimposed on a map of groundwater chloride concentrations in Figure 12.4-1. The red pathline (Path #6) in the figure shows a flow path leading from the potential repository area at Yucca Mountain. This pathline traces the movement of groundwater with chloride concentrations less than 6 mg/L found near the Ghost Dance fault southeastward along Dune Wash and then southwestward to well NC-EWDP-2D along the west side of Fortymile Wash. South of Dune Wash, groundwater west of this pathline has higher chloride and sulfate concentrations than groundwater along the pathline; groundwater east of this pathline has oxygen-18 and deuterium compositions that associate the groundwater with Fortymile Wash (CRWMS M&O 2001 [DIRS 154795], Figures 5, 6, 12, 13, and 26). These same chemical and

isotopic relations, and the previously drawn pathlines (Paths #2 and #5), constrain the position of the pathline (Path #6) southward toward the southern boundary of the site model area.

Due to the different starting positions of particles used to trace groundwater flow paths from the potential repository area in the site-scale model, there is some dispersion in the simulated particle pathlines (CRWMS M&O 2000 [DIRS 139582], Figure 7; see also Figure 12.4-2). Particles entering the groundwater in the northern part of the repository area tend to have a stronger eastward component in their trajectory than particles originating in the southern part of the repository area. Overall, however, there is good agreement between the average trend of pathlines from the repository predicted by the site-scale model and the pathline estimated from the groundwater hydrochemical and isotopic data.

12.4.2 Uranium Mill Tailing Analogues

The Uranium Mill Tailings Remedial Action (UMTRA) Project was authorized by Congress in 1978 to clean up 24 inactive uranium ore processing sites. These sites had been operated during the 1950s through the 1970s to produce uranium for defense and other purposes (DOE 1982 [DIRS 154691]; DOE 1996 [DIRS 154693]). The 24 sites are located mainly in the western United States, but also include two sites in Pennsylvania and one in Texas. Many of the sites are located in the Rocky Mountain states of Colorado (8 sites), Utah (3 sites), Wyoming (2 sites), and New Mexico (2 sites). Sites are also located in Arizona (2 sites), Oregon (1 site), Idaho (1 site), and North Dakota (2 sites). Most of the sites consisted of a uranium processing mill with associated tailings piles and other processing waste streams. The tailings piles were generally initiated on bare soil without intervening barriers. The size of the tailings piles at different sites varied greatly, depending on the volume of uranium ore processed at the site. Sites such as Grand Junction, Rifle, and Naturita in Colorado had large tailings piles, whereas piles at sites in other states were generally smaller. The time of operation also varied. The Old Rifle site started as early as 1924, whereas the sites in North Dakota were only operated in the early 1960s. Most of the sites began operation in the mid- to late-1950s and ended operations in the early 1960s to early 1970s. During the 1980s and 1990s, the tailings piles located at the 24 sites were either capped in place or removed to another location and encapsulated. Therefore, most of the tailings piles were sources of contaminants for, at most, 30 to 40 years. Since 1991, the UMTRA Ground Water Project has been monitoring and developing remediation strategies for the contaminant plumes in the ground at the various sites.

The ores processed at the various locations contained other elements besides uranium, such as vanadium, arsenic, selenium, manganese, molybdenum, barium, and other trace metals. In addition, chemicals used in processing the ore also ended up in the tailings piles. Important among these were sulfate, nitrate, ammonium, and hydrogen ions (i.e., acid solutions). Because the tailings piles were not covered, infiltrating rain and snow have leached constituents from the tailings and subsequently percolated into the subsoils beneath the tailings. Studies of the fate and transport of these constituents in the subsurface is the aspect of the UMTRA Project that is of the greatest interest to the DOE. The DOE is particularly interested in the dispersion characteristics of the plumes and in the retardation behavior of constituents such as uranium that also occur in nuclear waste to be emplaced in a repository.

Although some monitoring has been performed at all the UMTRA sites, selected sites have been monitored more extensively than others. This approach largely reflects the perceived risks associated with the various sites. Those sites where the volumes of ore processed were small and/or where the subsurface geology inhibited transport, monitoring was less extensive. At most of the sites, contaminants related to uranium processing are confined to shallow alluvial aquifers and have not penetrated into the bedrock below the sites. For example, at the site in Gunnison, Colorado, the uranium plume is restricted in depth to the Quaternary alluvium deposited by Tomichi Creek. Further, the areal shape of the plume shows only limited lateral dispersion over most of the length (approximately 1 mile) of the plume (DOE 1994 [DIRS 154692], Figure 3.12). Sulfate was also a major site-related contaminant. This constituent is generally thought to behave conservatively (i.e., is not retarded) in oxidizing groundwaters. The fact that the uranium plume is similar in shape and extent to the sulfate plume indicates at least some of the uranium is also transported with little or no retardation at this site (DOE 1994 [DIRS 154692], Figure 3.11).

At Rifle and Naturita, Colorado, extensive monitoring programs have been conducted to characterize more fully the extent of contaminant transport in the subsurface. Some of the results of these monitoring programs have been made public while the work in progress remains to be published. For the Rifle site, the final observational work plan for the UMTRA Project at New Rifle Site (DOE 1999 [DIRS 154687]) contains extensive detail on the hydrology, hydrogeology, and hydrochemistry of the site. The two volumes of this report also contain the results of transport modeling studies. They form the basis for the discussion presented below. For the Naturita site, the published information is more limited, but several important studies on uranium sorption behavior are in progress at the USGS in Menlo Park, California. Summaries of the results available for these two sites will be discussed below.

The Rifle site is located along the Colorado River approximately 90 miles east of Grand Junction, Colorado. The site actually consists of two separate sites known as Old Rifle and New Rifle. The New Rifle site has been studied in the greatest detail and is, for this reason, the subject of this summary. The site is located within the broad alluvial floodplain of the Colorado River with most of the original site on a strip of land within 0.5 miles of the river. The site is underlain by alluvial sediments deposited by the Colorado River. These, in turn, are underlain by sedimentary rocks of the Eocene Wasatch Formation. Monitoring has shown that contaminants originating from the site are found only in the alluvial sediments.

Monitoring at the New Rifle site has shown that the site-related constituents most prevalent in the alluvial aquifer include ammonia, calcium, nitrate, molybdenum, and uranium. Of these constituents, uranium and molybdenum are of interest to the DOE. Molybdenum is of interest because its chemistry is similar to technetium. Although the molybdenum plume (DOE 1999 [DIRS 154687], Figure 5-31) does not extend as far downgradient as the plume for a conservative constituent such as nitrate (DOE 1999 [DIRS 154687], Figure 5-32), this fact most likely reflects differences in source-term concentrations combined with analytical detection limits. The results of batch sorption coefficient determinations (DOE 1999 [DIRS 154687], Table 4-6) suggest that molybdenum retardation would be minimal in the alluvial aquifer.

Measured uranium concentrations at the New Rifle site are above the regulatory limit of 0.044 mg/L up to 3 miles downgradient from the site (DOE 1999 [DIRS 154687], Figure 5-36).

This distribution is similar to the downgradient extent of the plume observed for the conservative constituent nitrate (DOE 1999 [DIRS 154687], Figure 5-32). The similar lengths of the nitrate and uranium plumes suggest that at least some of the uranium is transported as a conservative constituent. Batch sorption coefficient measurements for uranium using alluvial materials and local groundwaters show a range of coefficients from –0.3 to 1.4 ml/g (DOE 1999 [DIRS 154687], Table 4-6). The conclusion that could be drawn from these data is that some fraction of the uranium emanating from the site follows pathways associated with little or no retardation potential. Transport calculations suggest that natural flushing of the aquifer will reduce the uranium concentrations in the alluvial aquifer beneath the site to below the 0.044 mg/L regulatory limit in 40 years.

The Naturita site along the Dolores River in western Colorado is in a hydrogeologic setting similar to the Rifle site. The contaminants associated with uranium ore processing are confined to groundwater in an alluvial aquifer (DOE 1994 [DIRS 154692]). The details of the uranium and other contaminant plumes are also similar to the New Rifle site. Of particular interest to the DOE is the on-going work pursued by the U.S. Geological Survey (J. Davis, USGS, Menlo Park, CA). The objective of the USGS work is to characterize the controls on contaminant transport behavior, particularly of uranium and vanadium. The work to date has included hydrogeologic characterization and modeling, contaminant concentration monitoring, hydrochemical characterization, in-situ leaching studies, and laboratory studies of the sorption behavior of uranium. A main goal of the present laboratory effort is to develop a surface complexation model of uranium adsorption onto natural aquifer materials. The data obtained to date suggest pH and alkalinity have by far the greatest impact on uranium sorption behavior. The sorption model that provides the best fit to the experimental data is the generalized composite model that was developed by Davis et al. (1998 [DIRS 154436]). This result will be of use to the Yucca Mountain Site Characterization Project in modeling the sorption behavior of uranium in the part of the flow path that is in alluvium.

The overall conclusion from this brief summary of the uranium mill tailings analogues is that, in these systems, some fraction of the total uranium inventory appears to transport as a nonsorbing to weakly sorbing contaminant. Although the hydrogeologic settings of these plumes are different than those expected downgradient from Yucca Mountain, several features of the geochemistry of these systems are pertinent to Yucca Mountain: redox state, pH, and alkalinity. The low pH and high alkalinity of the mill tailings systems tend to minimize the retardation of uranium. The redox state of these systems is variable. Where the redox conditions are not oxidizing, uranium is moderately retarded if alkalinity and pH are in the range found in Yucca Mountain groundwaters. To the extent that the transport pathways from Yucca Mountain to the compliance boundaries are oxidizing, the mill tailings results support the treatment of uranium as weakly sorbing in the model calculations. More strongly retarding conditions might be expected for flow paths traveling through reducing portions of the aquifer. If flow models and field data eventually lead to this result, it will be used in the transport calculations. Until then, the sorption coefficients used in the transport models are conservative and supported by these field analogues.

12.4.3 Preliminary Tracer Testing Results in the Alluvial Testing Complex

Tracer testing is ongoing in the wells of the ATC drilled by Nye County as part of their Early Warning Drilling Program. The goals of the tracer testing are to confirm the transport

conceptual models used in the site-scale SZ model for dissolved radionuclides and colloids and to obtain field-scale parameters for use in transport model simulations. This suite of tests will augment the testing carried out in the C-wells Complex (CRWMS M&O 2000 [DIRS 153168], Section 3.1.3.2.1), which examined transport through the fractured volcanic tuffs. The ATC tracer tests will play a similar role for transport in the alluvium and a combination of single-well and multiple-well tracer experiments are planned. Because interwell tests are more suitable for deriving field-scale transport parameters, fulfilling this goal of the testing program awaits the drilling and completion of new wells that are paired with existing wells. To date, single-well tests have been carried out, and a preliminary interpretation of the results has been performed. These tests are more appropriate for discriminating between conceptual models. Therefore, this section qualitatively describes the preliminary results in the context of the conceptual model.

In a single-well test, known masses/concentrations of tracers are injected into the test interval, followed by a large volume of tracer-free chase water that pushes the tracers away from the injection borehole (minimizing the influence of wellbore effects on the tracer responses). The tracer and chase water injection is followed by an optional rest period during which there is no injection or pumping so that the tracers are free to drift with the prevailing groundwater flow and diffuse into stagnant water (nonadvective porosity) in the flow system. After the rest period, well pumping is initiated and samples are collected and analyzed for tracers. Figure 12.4-3 is a plot of tracers versus volume extracted from single-well tracer testing in NC-EWDP-19D1. The tracer response curves were collected during three sets of tracer injections into the uppermost screened interval in the well (a 20-ft interval ranging from approximately 50 to 70 ft below the water table): (1) injection of 2,6-DFBA and iodide, followed by a 2-day rest period before pumping; (2) injection of 2,4-DFBA, chloride, and 640-nm diameter microspheres, followed immediately by pumping (no rest period); and (3) injection of PFBA and bromide, followed by a 30-day rest period before pumping.

Tracer solution and chase water volumes were approximately the same in all three tests. The first and third tests both featured flow interruptions. The responses in all three tests indicate little diffusion into nonflowing porosity (solutes with different diffusion coefficients essentially overlap each other). This result is qualitatively different than transport in the fractured volcanic tuff, for which a matrix diffusion model was determined to be more appropriate.

With respect to colloid transport, the microspheres in the second test (zero rest period) exhibited the most rapid recovery rates in the first samples produced, after which they were recovered at a much lower rate than the dissolved tracers. These results are consistent with the spheres being reversibly filtered very near the wellbore during injection. In addition, the overall microsphere recovery is relatively low compared to the solutes, indicating considerable filtration. Figure 12.4-4 is a plot of total microsphere recovery as a function of volume pumped (the sum of the second and third tests. Note the breaks in slope upon resumption of pumping at the start of the third test and after the flow interruption in the third test. These effects, though masked somewhat when presented as fractional recoveries instead of concentrations, represent significant increases in microsphere concentrations and suggest that flow transients are quite effective in mobilizing a small fraction of the microspheres. This result is consistent with the filtration model used to characterize colloid transport in the alluvium.

In summary, the initial results of the alluvial tracer-testing program, though preliminary, support the single-porosity model for transport of dissolved species in the alluvium, which is in contrast to the dual-porosity model that best explains solute transport in fractured tuffs. In addition, microsphere data are consistent with the filtration model used to simulate colloid transport in the alluvium in the site-scale SZ model.

The first and third tests both featured flow interruptions, which served as additional diagnostic tools for investigating diffusion into stagnant water in the flow system. A significant increase in tracer concentrations upon resumption of pumping would indicate such diffusion, provided the interruption is conducted during the tailing portion of the tracer responses.

The two tracers with different diffusion coefficients used in each of the three single-well tests (iodide and 2,6-DFBA in Test 1, chloride and 2,4-DFBA in Test 2, and bromide and PFBA in Test 3) had essentially identical responses (Figure 12.4-3). There was also little change in the tracer concentrations after flow interruptions. These results are both consistent with little diffusion into nonflowing porosity in the alluvium, and they suggest that a continuum flow and transport model without diffusive mass transfer between flowing and stagnant water (i.e., a single-porosity model) is appropriate for the alluvium. This result is qualitatively different than transport in the fractured volcanic tuff, for which a matrix diffusion model was determined to be more appropriate. The differences in the tracer response curves for different rest periods (Figure 12.4-3) are almost certainly due to varying amounts of drift with the natural gradient. These different responses will be analyzed in an attempt to obtain estimates of drift velocity in the test interval.

With respect to colloid transport, the microspheres in the second test (zero rest period) exhibited the most rapid recovery rates in the first samples produced (Figure 12.4-3), after which they were recovered at a much lower rate than the dissolved tracers. These results are consistent with the spheres being reversibly filtered very near the wellbore during injection. In addition, the overall microsphere recovery is relatively low compared to the solutes, indicating considerable filtration. Figure 12.4-4 is a plot of microsphere normalized concentrations as a function of time (encompassing both the second and third tests). Note the increases in concentrations upon resumption of pumping at the start of the third test and after the flow interruption in the third test. These effects suggest that flow transients are quite effective in mobilizing a small fraction of the microspheres. This result is consistent with the filtration model used to characterize colloid transport in the alluvium.

In summary, the initial results of the alluvial tracer-testing program, though preliminary, support the single-porosity model for transport of dissolved species in the alluvium, which is in contrast to the dual-porosity model that best explains solute transport in fractured tuffs. In addition, microsphere data are consistent with the filtration model used to simulate colloid transport in the alluvium in the site-scale SZ model.

12.4.4 Electric Power Research Institute Flow and Transport Modeling

The EPRI performed flow and transport modeling in both the UZ and SZ (EPRI 2000 [DIRS 154149]). The EPRI SZ flow and transport model incorporates three-dimensional, steady-state flow and transient mass transport in a dual-porosity media. This model represents

only the portion of the SZ close to a contaminant plume. The rectangular domain is 22 km long, 8.5 km wide, and has a vertical thickness of 200 m. Rock stratigraphy is represented in an idealized way. In the EPRI base case, the upstream 18 km of the domain is volcanic rock, and the downstream 4 km of the domain is assumed to be alluvium. The footprint of the repository is represented as a $2{,}500 \times 700$-m rectangular region on the upper surface of the domain. It is located 2 km from the upstream boundary of the model domain. The TSPA-SR model, in contrast, includes a much larger region of the SZ and a more detailed representation of actual geologic complexity (CRWMS M&O 2000 [DIRS 147972], Section 6.6). The results of these two models, therefore, can only be compared in a qualitative sense.

The most significant conceptual difference between the EPRI and TSPA-SR models is treatment of dual-porosity transport in fractured tuff. In the TSPA-SR model, a flowing interval is represented by a single fracture at the center of the interval (CRWMS M&O 2000 [DIRS 154927], p. 7). Diffusion can occur into a single matrix block between each pair of flowing intervals. In the EPRI model, a flowing interval is treated as a region in which multiple fractures exist and solutes diffuse into smaller blocks between the individual fractures. Mass transfer by diffusion into smaller blocks is faster because there is more surface area of the matrix exposed to fractures. With other factors being equal, the EPRI model predicts slower transport of radionuclides toward the accessible environment in fractured tuff than the TSPA-SR model. EPRI (2000 [DIRS 154149], p. 7-26) argues that the implementation of dual-porosity transport in the TSPA-SR model is overly conservative.

The EPRI analysis supports the TSPA-SR conceptualization that diffusion of solutes into the matrix of fractured tuffs can slow transport of radionuclides away from the repository. In addition, EPRI concurs that use of flowing intervals is a reasonable conceptualization of SZ conditions. The main issue is whether or not the use of smaller matrix block sizes in TSPA-SR models can be supported by the available data. To date, the DOE is of the opinion that the data are not sufficient to support the use of smaller block sizes.

12.4.5 Transport Studies on Blocks of Intact Tuff

The transport behavior of selected radionuclides and compounds (tritium, technetium-95m, neptunium-237, cobalt-60, cesium-137, sodium-fluorescein) is being studied in the laboratory using blocks of intact tuff mined from the Busted Butte Unsaturated Zone Facility. The transport behavior of these radionuclides is being studied under both unsaturated and saturated conditions. Initial results for unsaturated flow conditions have been obtained on a trial block (Vandergraaf et al. n.d. [DIRS 154948]). The results indicate that technetium-95m and sodium-fluorescein elute from the block slightly ahead of tritium. Because tritium moves at the rate of the water, this result indicates technetium-95m and sodium-fluorescein are preferentially eluted probably due to exclusion from small pores (e.g., anion exclusion). The total recovery of tritium, technetium-95m, and sodium-fluorescein was in the range of 70 percent to 80 percent. Batch sorption experiments with crushed tuff show slightly negative sorption coefficients confirming the exclusion behavior (DTN: LA0103TV12213U.001 [DIRS 154929]).

The first breakthrough of neptunium was retarded relative to tritium indicating neptunium had sorbed onto the rock matrix. A retardation factor of 3.2 was calculated from the early elution data. However, the fraction of neptunium that was recovered represented only 0.1 percent of the

total neptunium injected into the block. After the initial breakthrough, the neptunium concentration in the eluted water decreased as additional water was eluted from the block. This result indicates that the 0.1 percent fraction represents an early breakthrough fraction and that most of the neptunium was more strongly retarded. Batch sorption experiments on crushed tuff material and simulated Busted Butte water gave sorption coefficients in the range of 0.43 to 1.09 ml/g (DTN: LA0103TV12213U.001 [DIRS 154929]). Assuming a bulk density of 2.0 g/cm^3 and a porosity of 0.35 (for example, CRWMS M&O 2001 [DIRS 154024], Sections 6.8.7.2 and 6.8.7.3, Table 38), these sorption coefficients equate to retardation factors of 3.5 to 7.2. The fact that the bottom end of this range exceeds the measured retardation factor (3.2) is consistent with the fact that only a small fraction of the neptunium was recovered in the block tests. That is, the calculated retardation factors would predict later breakthrough than was observed. However, the observed breakthrough curve was not of the (simple) type that would be expected from a simple retardation calculation. The greater complexity of the observed breakthrough curve explains the lower retardation factor (3.2) observed in the block test.

The range of neptunium sorption coefficient values measured in the batch tests with Busted Butte materials falls within the probability distribution function for neptunium sorption coefficient (0 to 6 ml/g with an expected value of 1.0 ml/g) in vitric tuff as used in performance assessment calculations (CRWMS M&O 2001 [DIRS 154024], Tables 2a and 2b). Thus, the data obtained on the trial block test are consistent with the performance assessment calculations. This statement will be further quantified once the full block test has been completed and a larger fraction of the injected neptunium recovered.

12.4.6 Analogue Studies

Analogue sites such as the Alligator Rivers site in Australia, Poços de Caldas in Brazil, the Oklo site in Gabon, and the Cigar Lake site provide data on the transport of uranium; in some cases, over millions of years. Although the geology and geochemistry at these sites differ from that at Yucca Mountain, they provide data that may be used to calibrate computer codes, and their analysis can give us a picture of the flow and transport of uranium under various conditions. In Sections 12.4.6.1 and 12.4.6.2, a summary of the geohydrological and geochemistry are given for the Alligator Rivers and Poços de Caldas sites. A summary of the Jove-Colon comparison of the transport of uranium at these sites along with that of the Oklo and Cigar Lake sites is given in Section 12.4.6.3. This study notes that uranium often does not migrate a significant distance from the source due to sorption, even over extended time spans. The analogue site data given by the INEEL site in Section 12.4.6.4 and the Beasley et al. (1998 [DIRS 102430]) study at INEEL provides a degree of confirmation of the conservative or retarding nature of a number of the same radionuclides as would be present in a Yucca Mountain repository (e.g., chlorine-36, technetium-99, uranium-236, iodine-129, and neptunium-237). Underground nuclear test data taken at the NTS (see Section 12.4.6.5) provide valuable information about radionuclide transport of chlorine-36, krypton-85, ruthenium-106, plutonium-240, plutonium-239, and iodine-129 through volcanic tuffs and alluvium. These data are important because the geology and the chemistry at the NTS are similar to that at Yucca Mountain.

12.4.6.1 Alligator Rivers, Australia

The Koongarra secondary enriched-uranium deposit is found in the Alligator Rivers region of the Northern Territory of Australia. The Koongarra ore body lies in two distinct parts separated by a barren zone. The two parts are composed of uraninite- and pitchblende-bearing veins within a zone of steeply dipping, sheared quartz-chlorite schists and a fault that brings the ore body in contact with the Kombolgie sandstone (Airey 1986 [DIRS 127680], Figure 4.15). The primary ore at depth is being leached by groundwater to form a secondary uranium mineralization (Isobe et al. 1992 [DIRS 113260], p. 175) that extends from the ground surface to the base of the weathered zone at about 30 m.

Weathering of the quartz-chlorite schist produces different mineral assemblages according to degree of alteration. The migration behavior of nuclides at each depth is thought to be related to the chlorite alteration mineral assemblage (Ohnuki et al. 1990 [DIRS 126172], p. 607). The zone of lowest uranium concentration corresponds to the chlorite-rich zone, that of intermediate uranium concentration to the vermiculate-rich zone, and that of greatest uranium concentration to the kaolinite-rich zone. Although kaolinite is not being considered in the present Yucca Mountain waste package design, it is considered in the design of many high-level nuclear waste sites. The data provided at the Koongarra site could serve as a means of estimating the sorbing effects of kaolinite over a long period of time and might be used to calibrate geochemistry codes.

As a result of the weathering front, a dispersion fan has developed in the weathering zone where uranium has been mobilized. Secondary minerals are found as far as 50 m downstream from the ore body with detectable concentrations of uranium-series nuclides for about 300 m downstream in the dispersion fan. The age of the dispersion fan has been estimated from 0.5 to 3.0 Ma (Golian and Lever 1992 [DIRS 134175], p. ix).

Isobe et al. (1992 [DIRS 113260]) describe uranium redistribution associated with weathering. Uranium activity closely follows oxidation fronts in the slightly weathered zone and advances most readily along cracks and fissures in which percolation of oxidizing groundwater is most enhanced. Significant flow occurs as fracture flow rather than as porous media flow. Uranium distribution in the most strongly weathered rocks depends only on the mineralogy present and is not controlled by the presence of fissures, as is the case for the more moderately weathered rocks. In the dispersion fan, processes that control the amount of radionuclides that are removed from the groundwater include equilibrium sorption, chemical incorporation into iron oxides, uranium minerals or other crystalline phases, and recoil transfer of daughter products caused by alpha-particle decay (Golian and Lever 1992 [DIRS 134175], p. viii). The fact that the uranium distribution depends only on the mineralogy in strongly weathered (fractured) rocks has implications for the Yucca Mountain conceptual model, which assumes the volcanic tuff is sufficiently fractured to act as an equivalent porous medium for radionuclide transport. Data from the less-weathered rocks, where the uranium concentration in fissures differs from that of the "matrix," is important in establishing the amount of fissuring necessary for the equivalent porous media model to be valid.

Groundwaters are slightly acidic to neutral in pH, oxidizing, relatively dilute, with the major ion chemistry dominated by magnesium and bicarbonate. Waters from the weathered zone are undersaturated with respect to a number of uranium-bearing minerals, consistent with the idea

that the present groundwaters may be dissolving and dispersing the uranium in the phosphate zone of the deposit (Sverjensky et al. 1992 [DIRS 134225], p. 40).

Colloids in groundwater samples taken from drill holes were dominated by iron-rich particles, and uranium was only found in iron-rich species (Ivanovich et al. 1987 [DIRS 125227], pp. 300 to 309). Low colloid concentrations (about 10^6 particles/L or less) and the absence of radionuclides in colloids outside the center of the ore body indicated that colloidal transport of radionuclides is minor at Koongarra (Payne et al. 1992 [DIRS 124812], p. 481). Understanding the absence of radionuclide transport in colloids outside the ore body may have implications for colloid transport at Yucca Mountain. Also, the data provided by the Koongarra site is useful because it is a well-studied site and represents transport carried out over an extremely long time period.

12.4.6.2 Poços de Caldas, Brazil

The Poços de Caldas caldera is a ring structure composed of Cretaceous phonolites, carbonatites, and nepheline syenites (Schorscher and Shea 1991 [DIRS 127147]; Miller et al. 1994 [DIRS 126089]). Two major hydrothermal events that affected the caldera led to widespread argillization (alteration to clay minerals) and zeolite formation. During the first event, local magmatic brecciation occurred in association with intense hydrothermal potassium- and sulfur-rich alteration (Schorscher and Shea 1991 [DIRS 127147], p. 25). A second hydrothermal event is believed responsible for formation of the numerous ore bodies within the caldera complex about 76 Ma (Schorscher and Shea 1991 [DIRS 127147], p. 28).

The Osamu Utsumi open-pit mine is a disseminated, low-grade uranium ore body with subsidiary thorium, zirconium, and REE (rare-earth element, or lanthanide) enrichment and a sharp, well-developed redox front. Morro do Ferro, in contrast, is a thorium and REE ore body with subsidiary uranium. The Morro do Ferro hill has been deeply weathered, so that the hill is now composed of gibbsite, kaolinite, and illite, with additional veins of magnetite and manganese hydroxides. The thorium-REE ore occurs as elongated mineralized lenses that extend down the hill slope. Thorium and REE mineralization is very enriched, with up to 3 weight % ThO_2 and up to 20 weight % total REE in some soils and weathered rocks (Waber 1991 [DIRS 126924], p. 120).

Groundwaters in the Poços de Caldas area typically have low concentrations (less than 1 mg/L) of colloids (Miekeley et al. 1989 [DIRS 126083]; Miekeley et al. 1991 [DIRS 127199], p. i). Most of the colloids are composed of iron and organic species. Only minor amounts of uranium are associated with colloids, but greater amounts of thorium and REEs are transported in the colloidal fraction. The suspended particle concentration is 5 to 10 times greater at Morro do Ferro than at Osamu Utsumi, but there appears to be very little thorium transport at Morro do Ferro, either by colloids or true solution. Amorphous phases in suspension or as mineral coatings are the principal reactive surfaces for many trace elements in solution. The presence of amorphous phases tends to reduce the concentration and mobility of trace elements in solution (Chapman et al. 1991 [DIRS 100423], p. 129). Radionuclide and other trace-element transport by colloidal material in deep groundwaters does not play a significant role in the geochemical processes of weathering, dissolution, and erosion of these ore deposits. This observation is

attributed to filtration of particulate material, which seems to be efficient, even in the highly fractured and porous rocks of the Poços de Caldas plateau (Smellie et al. 1989 [DIRS 126636]).

Microbial activity is important for the oxidation of pyrite and may be responsible for the mobilization and reprecipitation of uraninite at the redox front (West et al. 1989 [DIRS 100834]). This mechanism could explain the observation that the redox front is moving faster than would be expected simply on the basis of dissolved oxygen concentration. Flow channeling in fractures and solute transport in the rock matrix are the key controls of the shape and movement of the redox fronts at Poços de Caldas. The front movement appears to be very slow, and solute transport over the front is dominated by diffusion. The front plays a significant role in retarding a wide spectrum of trace elements.

Colloidal transport of uranium was shown to be minimal at Koongarra and Poços de Caldas, where filtration of colloids appears to be effective. The filtration of colloids that have the potential of carrying radionuclides by the highly fractured and porous rocks at this site has important implications in Yucca Mountain colloid transport in the saturated zone because an increase in colloid filtration will result in a reduction of radionuclides reaching the site boundary.

12.4.6.3 Comparison Study

A comparison study was made of plumes from uranium ore bodies and contaminated sites to identify characteristics of uranium plume movement (Jove-Colon et al. 2001 [DIRS 154444], p. 1). The study included uranium mines and natural analogue sites (Koongarra, Oklo, Poços de Caldas, and Cigar Lake) as well as Title I and Title II UMTRA plumes. Despite the uncertainties and variability of the magnitude of the original contaminant source, geologic setting, and hydrologic regime of the sites, as well as age of the plumes and availability of time-series data, the plume dataset provides a relatively consistent picture of uranium plume behavior. Specifically, the uranium plumes appeared to have stopped spreading rapidly within a few years; they exceed approximately 2 km in length only in special cases where in situ leaching has been carried out, and they exhibit very similar uranium chemistry between sites (Jove-Colon et al. 2001 [DIRS 154444], p. 1).

Although the hydrologic conductivity, K_d values, and original contaminant source masses for the various sites varied by orders of magnitude, plume trajectories seemed to cluster and to suggest that the combined effects of dispersion and chemical reaction are sufficient to arrest most uranium plumes before they move more than roughly a kilometer from their source (Jove-Colon et al. 2001 [DIRS 154444], p. 24). The natural life cycle of a uranium plume appears to involve an initial movement away from a source region that takes place within a few years and does not exceed 2 km, followed by a geologically long period of immobile quiescence. Natural plumes from ores that have been weathered and subjected to periodic meteoric inputs for long periods of time do not migrate appreciably beyond their known natural barriers, even during mining. Similarly, the UMTRA sites do not show a significant dispersion of contaminants beyond the limits of the contaminated area, even though these sources are not as deeply buried and are in more porous strata than those found in the natural analogue and uranium mining sites. The plume length and the uranium concentration in monitoring wells remain relatively constant or change insignificantly for periods of time approaching 15 years in many cases. It appears that sorption, dilution, and precipitation are sufficiently effective sinks to limit the advance of

artificial uranium plumes in the short term (years to decades). In long-term situations of thousands to millions of years, weathering processes and secondary precipitation of oxidized uranyl phases appears to limit advance of natural plumes.

Jove-Colon et al. (2001 [DIRS 154444], p. 259) concluded that source-term removal alone can limit plume advance, assuming no change in the geochemical state of the uranium near the source, such as the introduction of chelating agents and/or a deleterious shift in redox conditions. Only two of the few plumes examined for the Title II sites exceed plume lengths of more than 2.5 km (Jove-Colon et al. 2001 [DIRS 154444], p. 29). Title II sites may produce longer plumes than Title I sites because the source term is still in place; however, with the two exceptions, the rest fell well within the plume-length distribution range (less than 2 km) obtained for both UMTRA Title I and Title II sites (Jove-Colon et al. 2001 [DIRS 154444], p. 29). Geochemical factors favor uranium transport over transport of many other cationic metals and radionuclides, such as lead, cadmium, strontium-90, or cesium-137, because uranium is a relatively weak sorber and because the fraction of uranium that sorbs irreversibly in soils is relatively small. For these reasons a plume advance for most other cationic metals and radionuclides should be substantially less than the 2 km observed for uranium.

12.4.6.4 Retardation at Idaho National Engineering and Environmental Laboratory

From 1952 until 1984, low-level radioactive waste was discharged from the Idaho Chemical Processing Plant (ICPP) by means of an injection well and seepage ponds. Over time, a suite of radionuclides has been measured in the Snake River Plain (SRP) aquifer, including tritium, chlorine-36, strontium-90, cesium-137, iodine-129, and plutonium isotopes. Beasley et al. (1998 [DIRS 102430]) reported the first measurement of the long-lived radionuclides technetium-99, uranium-236, and neptunium-237 in the aquifer and their downgradient concentration changes during water transport through fractured basalt. Their study showed that chlorine-36 and technetium-99 behave conservatively during transport whereas iodine-129, uranium-236, and neptunium-237 were retarded.

The calculated residence time of water in the SRP aquifer is 55 to 82 years, although water travel times within different parts of the aquifer, from recharge to discharge points, are estimated between 12 and 350 years (Beasley et al. 1998 [DIRS 102430], p. 3876). Groundwater flow is from the northeast to the southwest, and depth to groundwater varies from about 60 m at the northern site boundary to about 275 m at the southern site boundary. Beasley et al. (1998 [DIRS 102430], p. 3876) report that the average hydraulic gradient across the INEEL is about 2 m/km, and water travel times between the ICPP and the southern site boundary have been estimated at 2 m/day.

Over a period of four years, monitoring wells at INEEL were sampled for radionuclide measurements. Activity concentrations were measured for chlorine-36, technetium-99, uranium-236, iodine-129, and neptunium-237. To determine the relative mobility of these radionuclides, individual radionuclide activities in wells near the ICPP were normalized to those at a distance. The close correspondence in the decrease of chlorine-36 and technetium-99 concentrations with distance from the ICPP suggests that technetium-99, like chlorine-36, behaves conservatively in the fractured basalt and that observed concentration decreases occur only as a result of dilution or dispersion (Beasley et al. 1998 [DIRS 102430], p. 3880).

Iodine-129 is attenuated, and neptunium-237 and uranium-236 are even more attenuated. However, the authors point out that even though the absolute amounts of radioactivity most likely varied over time, the ratios of radionuclides in the discharges probably were consistent in order not to affect the composition of radioactivity in the waste streams.

Although the initial conditions and geologic medium are different at INEEL than at Yucca Mountain, the Beasley et al. (1998 [DIRS 102430]) study at INEEL provides a degree of confirmation of the conservative or retarding nature of a number of the same radionuclides as would be present in a Yucca Mountain repository (e.g., chlorine-36, technetium-99, uranium-236, iodine-129, and neptunium-237). In particular, the INEEL site appears to be much closer in terms of geology to Yucca Mountain than the Koongarra, Oklo, and Poços de Caldas.

12.4.6.5 Colloids at Nevada Test Site

Data taken at the NTS from underground nuclear tests provide valuable information about transport through volcanic tuffs and alluvium. These data are important because the geology and the chemistry at NTS are similar to that at Yucca Mountain due to its proximity. An important consideration in the evaluation of these tests is the distance that radionuclides may transport immediately after the event.

Data from a field experiment initiated in 1974 at the Cambric site have provided direct information on the transport rates of radionuclides through saturated alluvium (Hoffman and Daniels 1981 [DIRS 125168]). The field study began with the completion of a satellite well 91 m from the Cambric cavity, followed by drilling of a reentry well into the cavity itself. Both solid and liquid samples were taken from the reentry well to determine the distribution of radionuclides between the solid material and the groundwater. Water was then pumped from the satellite well to induce an artificial gradient sufficient to draw water from the Cambric cavity through the surrounding rocks.

Approximately two years after pumping began, significant amounts of tritiated water were found in water from the satellite well, signaling the arrival of water from the Cambric cavity region. After almost six years of pumping, the tritium concentration in the pumped water reached a maximum (Hoffman et al. 1977 [DIRS 125087], p. 52). By the end of September 1984, about 60 percent of the initial tritium inventory had been pumped out through the satellite well.

Other radionuclides were also measured in water from the satellite well, including chlorine-36, krypton-85, ruthenium-106, and iodine-129. Strontium-90 and cesium-137 were not detected in the pumped water during the 10-year experiment (Thompson 1986 [DIRS 126796], p. 3). The chlorine-36 pulse and the iodine-129 pulse preceded the tritium pulse. Krypton was correlated with tritium but more strongly sorbed onto alluvium than tritium. Ruthenium-106 was detected in well RNM-2S water and was unretarded in the alluvium (Thompson 1986 [DIRS 126796], p. 3).

The Cheshire event took place in 1976 (Buddemeier and Hunt 1988 [DIRS 100712], p. 537). Detonation occurred at a depth of 1,167 m, approximately 544 m below the water table, in fractured rhyolitic lavas of Paiute Mesa. Water was obtained from two wells, one inside the Cheshire experimental site and the other 300 m away. Tritium, krypton, strontium, cesium,

antimony, cobalt, cerium, and europium were detected in the pumped water. All of the cobalt, cerium, and europium were associated with colloids in samples from both locations. The authors maintained that the presence of colloidal radionuclides outside the cavity indicates radionuclide transport as colloids.

The Benham test was detonated in 1968 at a depth of 1402 m below the water table. In a recent field test, plutonium was measured in groundwater at the NTS ER-20-5 wells at a maximum activity concentration of 0.63 pCi/L (Kersting et al. 1999 [DIRS 103282], p. 57). The ratio of plutonium-240/plutonium-239 indicates that the plutonium originated at the site of the nuclear test Benham, which is a distance of 1.3 km from the wells. The minimum distance for plutonium migration at the NTS is therefore 1.3 km in 28 years. The plutonium detected was associated with colloidal material consisting mainly of clays, zeolites, and silica (Kersting et al. 1999 [DIRS 103282], p. 2). It is not likely that the plutonium was transported by prompt injection or that its soluble fraction migrated along fast flow paths. Colloidal transport is a possible mechanism for plutonium migration because colloidal transport of radionuclides was observed at the Cheshire site. Possible colloid transport of plutonium at the NTS has important implications to Yucca Mountain due to the similar geology at this site.

12.4.7 Yucca Mountain Self-Analogue Using Uranium Isotopes

The flow model for the saturated zone predicts that radionuclides that reach the saturated zone would have a travel time of at least 3,600 years before they could reach the accessible environment, which is defined as being 20 km from the potential repository (CRWMS M&O 2000 [DIRS 153168], Sections 3.6 and 3.7). The model is based on a site conceptual model and discretization with model hydrologic parameters chosen to be consistent with measured hydrologic data. Chemical and isotopic data for groundwater in the Yucca Mountain area can be used to test the reasonableness of the flow path and travel time computed by the TSPA-SR flow and transport model (CRWMS M&O 2000 [DIRS 153246]). As such, the chemical and isotopic data serve as a sort of self-analogue.

Figure 12.4-5 shows a map of the chloride concentrations. The contours, which denote waters of similar composition, clearly show a flow path from north of Yucca Mountain to the Amargosa Desert south of Yucca Mountain, a flow path that is in agreement with that derived from TSPA-SR flow and transport modeling and hydrologic head data (CRWMS M&O 2000 [DIRS 153246]). Within this general flow path, the TSPA-SR flow modeling suggests a short flow eastward from beneath Yucca Mountain towards Fortymile Wash with continued flow to the south. Any radionuclides that reached the saturated zone beneath the potential repository would be expected to follow this flow path.

Naturally occurring radioactive isotopes of uranium can be used to examine what has happened over thousands of years to radioactive atoms that have passed through the unsaturated zone and reached the saturated zone beneath the mountain. There are three radioactive isotopes of uranium. Of interest for this analogue are uranium-238, which has a half-life of 4.468×10^9 years, and one of its daughter products (uranium-234), which has a half-life of 2.446×10^9 years. When the amount of uranium-234 being produced by the decay of uranium-238 is equal to the amount lost by the decay of uranium-234, the two isotopes are in secular equilibrium and, by definition, have an activity ratio of 1.0. The activity ratio for uranium-234/uranium-238 is

generally near 1.0 for most geologic materials, but certain nuclear-chemical processes can cause uranium-234 to become enriched or depleted relative to its parent. This outcome has been documented to occur for groundwater in many arid regions where there is a small volume of water moving through a large volume of rock.

At Yucca Mountain, the uranium dissolved in water has an extremely anomalous activity ratio within the unsaturated zone. Analyses of perched water from two wells within the unsaturated zone yield uranium-234/uranium-238 activity ratios greater than 7.0 (CRWMS M&O 2001 [DIRS 154795], Figure 18). As this water eventually reaches the saturated zone, these anomalous ratios provide a natural analogue to the escape of radioactive materials from a potential repository.

Figure 12.4-6 shows a map of activity ratios for uranium-234/uranium-238 in water from the saturated zone. As expected, the water directly beneath Yucca Mountain has anomalously large activity ratios that have been acquired by the slow percolation of waters from the unsaturated zone above. These anomalous ratios are noted again in well J-13 on the edge of Fortymile Wash, as predicted by the SZ flow model. Although the data do not appear to form a distinct plume southward down gradient of the mountain as would be expected from the flow model, elevated values of the activity ratio (as compared to surrounding area) may be observed in most wells along Fortymile Wash and south of Yucca Mountain along the predicted flow path. Values for uranium-234/uranium-238 are somewhat elevated in well J-12 about 5 km south of J-13 and also on the edge of Fortymile Wash. The anomaly becomes more subdued about 1 km further south in well JF-3. The uranium-234/uranium-238 values decrease to essentially background level in well NC-EWDP-2D within Fortymile Wash about 20 km south of Yucca Mountain.

The lack of a distinct plume could be due to some chemical causes, but it is likely due to mixing with recharge along Fortymile Wash as well as inflow from waters to the east and north of Yucca Mountain. Flow and transport modeling, assuming a high activity source at Yucca Mountain, may help yield understanding of the data. A chemical consideration would be the possible dissolution of uranium from minerals in the aquifer as the water moves south, thereby diluting the signal of the natural radioactive tracer. However, uranium concentrations in groundwater beneath and south of Yucca Mountain are fairly similar, and therefore, a swamping of the signal by dissolved uranium seems unlikely.

Another consideration is the unique hydrology of Yucca Mountain that may create a nearly stagnant pocket of water there. The anomalous uranium activity ratios occur south of the large hydraulic gradient. It may be that a large proportion of the flow from the north is diverted to the east and west of Yucca Mountain or to the carbonate aquifer beneath Yucca Mountain such that there is a small pocket of very slowly moving water beneath the potential repository with only minor flow towards Fortymile Wash.

In summary, the chemical and isotopic data for chloride concentrations confirm the general flow paths of the saturated-zone flow model. The uranium-234/uranium-238 activity ratio data appear to indicate a south to southeast movement of the water beneath Yucca Mountain and, in addition, suggest a significant dilution or dispersion during flow. These data provide an independent confirmation of the flow path direction of the TSPA-SR (CRWMS M&O 2000 [DIRS 153246])

model and, in the future, may help to provide confirming evidence of inflow and recharge in the Yucca Mountain area.

12.4.8 U.S. Nuclear Regulatory Commission Flow and Transport Studies

The CNWRA supports the NRC role of evaluating the potential repository at Yucca Mountain by developing a set of computer codes to simulate the behavior of the repository. The CNWRA calculates transport of radionuclides along one-dimensional streamtubes in the saturated zone (NRC 2001 [DIRS 154949]). The processes simulated by the NRC model include advective transport through tuff and alluvial aquifers, longitudinal dispersion, chemical sorption and retardation in the alluvium and matrix of the tuff, and diffusion of radionuclides from fractures into the matrix of the tuff. The streamtubes are abstracted from results of a detailed two-dimensional flow model. This model provides an opportunity to check results of the SZ site-scale flow and transport model because it is based on the same data set of rock properties and hydraulic head measurements, and because it simulates a similar suite of transport processes.

12.5 SENSITIVITY ANALYSIS

Section 12.5.1 describes the unquantified uncertainty analysis conducted with the site-scale SZ flow and transport model. These analyses were performed to evaluate the sensitivity of the TSPA-SR supplemental analysis (McNeish 2001 [DIRS 155023]) to changes in parameters as a result of the unquantified uncertainty analysis in the model. Section 12.5.2 discusses several additional sensitivity analyses conducted to evaluate the sensitivity of model results to specific critical features or processes in the site-scale SZ model. The FEHM computer code (V2.10) was used to perform transport calculations for all of the analyses discussed in Section 12.5. Additionally, the GoldSim (V6.04.007) computer code was used to sample the parameter distributions for the transport calculations for all of the analyses discussed in Section 12.5. Calculated breakthrough curves are documented in Kuzio (2001 [DIRS 154912], Filename "archive_sspa_v1_data"). The analyses are based on a model that is appropriately conservative for TSPA sensitivity analyses and is not intended to represent expected radionuclide breakthrough or groundwater transport time for the SZ portion of the Yucca Mountain flow system.

12.5.1 Unquantified Uncertainty Sensitivity Analysis for Supplemental Science and Performance Analyses

This section describes the unquantified uncertainty analysis conducted to evaluate the sensitivity of the TSPA-SR supplemental analysis (McNeish 2001 [DIRS 155023]) results to changes in parameters as a result of the unquantified uncertainty analysis in the site-scale SZ model. The unquantified uncertainty analysis consisted of multiple (100) simulations of radionuclide transport with the site-scale SZ model in which all changes resulting from the unquantified uncertainty analysis were included. The resulting SZ radionuclide breakthrough curves for the unquantified uncertainty case are supplied to the TSPA simulator for the Volume 2 calculation of simulated dose rates. The results of the unquantified uncertainty sensitivity analysis from the model are discussed in Section 3 of Volume 2.

The simulated radionuclide breakthrough curves from the unquantified uncertainty analysis (Kuzio 2001 [DIRS 154912], Filename "archive_sspa_v1_data/uu") have shorter transport times for long time periods and longer transport times for early time periods than the TSPA-SR supplemental analysis (McNeish 2001 [DIRS 155023]). As an example, the histograms of times of median breakthrough for neptunium are compared to the unquantified uncertainty case and the TSPA-SR supplemental analysis (Figure 12.5.1-1). Visual comparison of the upper histogram for the TSPA-SR supplemental analysis and the lower histogram for the unquantified uncertainty case shows a reduction in the width of the histogram transport times. The unquantified uncertainty analysis includes changes to many parameters, as indicated in Table 12.5.1-1. Some of the changes to the parameters result in a reduction in transport times; other changes could result in an increase in transport time. The overall uncertainty in the times of median breakthrough, as represented by the reduced width of the histograms, represents primarily the uncertainty associated with the parameter groundwater specific discharge.

12.5.2 Additional Sensitivity Analyses for Supplemental Science and Performance Assessment

Several other sensitivity analyses are conducted with the site-scale SZ flow and transport model (Sections 12.5.2 and 12.5.3) in addition to the unquantified uncertainties analysis. These system analyses were performed to evaluate the sensitivity of the TSPA-SR supplemental analysis results (McNeish 2001 [DIRS 155023]) to specific critical features or processes in the site-scale SZ model. Each sensitivity analysis consisted of multiple (100) simulations of radionuclide transport with the site-scale SZ model in which all stochastic parameters were varied, as in the original model, with the exception of the parameter controlling the process or feature being evaluated. The resulting suite of SZ radionuclide breakthrough curves for each sensitivity case was supplied to the TSPA for the Volume 2 calculation of simulated dose rates (Kuzio 2001 [DIRS 154912], Filename "archive_sspa_v1_data"). Results of the sensitivity analyses from the model are discussed in Section 3 of Volume 2.

12.5.2.1 No Matrix Diffusion in Volcanic Units

Diffusion of radionuclides into the matrix of volcanic units of the SZ is potentially significant to transport in groundwater because of the higher porosity in the matrix and because of the sorptive capacity of the matrix for some radionuclides. Both of these effects tend to delay the migration of radionuclides relative to transport solely in the fractures of the system. The sensitivity case in which no matrix diffusion occurs represents a bounding analysis with respect to the matrix diffusion process.

The sensitivity analysis for no matrix diffusion is implemented in the site-scale SZ flow and transport model by reducing the value of the effective matrix diffusion coefficient by 10 orders of magnitude in all realizations (Kuzio 2001 [DIRS 154912], Filename "archive_sspa_v1_data/high_diff"). This large reduction in the matrix diffusion coefficient effectively renders the simulated radionuclide mass delay to matrix diffusion insignificant. Other stochastic parameters for the SZ have the same values used for the sensitivity analysis as the TSPA-SR supplemental analysis (McNeish 2001 [DIRS 155023]).

The simulated radionuclide breakthrough curves from the no matrix diffusion analysis have somewhat shorter transport times than the breakthrough curves from the TSPA-SR supplemental analysis (McNeish 2001 [DIRS 155023]) on a realization-by-realization basis. The differences in the transport time between the no matrix diffusion case and the TSPA-SR supplemental analysis are greater for those radionuclides that experience significant sorption in the volcanic matrix (Kuzio 2001 [DIRS 154912], Filename "archive_sspa_v1_data/no_diff"). As an example, the histograms of times of median breakthrough (i.e., the time at the midpoint of the breakthrough curve) for uranium are compared for the no matrix diffusion case and the TSPA-SR supplemental analysis in Figure 12.5.2-1. Uranium is used in this example because it experiences moderate sorption in the volcanic rock matrix for most realizations of the TSPA-SR supplemental analysis case, and therefore it should show discernible differences for the no matrix diffusion case. The upper histogram shows the results for the TSPA-SR supplemental analysis case, and the lower histogram shows the results for the no matrix diffusion case. As expected, the distribution of times of median breakthrough for the no matrix diffusion case is shifted toward shorter transport times, with 61 of the realizations having times of median breakthrough less than 10,000 years for the no diffusion case and 54 of the realizations having times of median breakthrough less than 10,000 years for the TSPA-SR supplemental analysis case. However, the overall uncertainty in the times of median breakthrough, as represented by the width of the histograms, is larger than the shift in times of median breakthrough from the TSPA-SR supplemental analysis case to the no matrix diffusion case.

12.5.2.2 Enhanced Matrix Diffusion in Volcanic Units

Another sensitivity analysis is defined for the case in which the effects of matrix diffusion in the volcanic units of the SZ are greatly enhanced. The enhanced matrix diffusion case represents a bounding analysis at the opposite extreme from the no matrix diffusion case. For this case, most of the rock matrix in the volcanic units is available for radionuclide storage and sorption in the transport process in most of the realizations. The sensitivity analysis for the enhanced matrix diffusion case is implemented by reducing the flowing interval spacing by two orders of magnitude for all realizations. This approach reduces the geometric mean of the flowing interval spacing from about 20 to 0.2 m, which is a relatively small distance for matrix diffusion (CRWMS M&O 2000 [DIRS 154927], Section 7). Other stochastic parameters for the SZ have the same values for the sensitivity analysis as the TSPA-SR supplemental analysis (McNeish 2001 [DIRS 155023]).

The simulated radionuclide breakthrough curves from the enhanced matrix diffusion analysis have longer transport times than for the TSPA-SR supplemental analysis (Kuzio 2001 [DIRS 154912], Filename "archive_sspa_v1_data/high_diff"; McNeish 2001 [DIRS 155023]). As an example, the histograms of times of median breakthrough for neptunium are compared for the enhanced matrix diffusion case and the TSPA-SR supplemental analysis case in Figure 12.5.2-2. Neptunium is used in this example because it experiences a small amount of sorption in the volcanic rock matrix for most realizations of the TSPA-SR supplemental analysis and because neptunium-237 is a major contributor to dose in the TSPA analyses. Visual comparison of the upper histogram for the TSPA-SR supplemental analysis and the lower histogram for the enhanced matrix diffusion case shows the generally longer transport times for the enhanced matrix diffusion case, as expected. In the enhanced diffusion case, 25 of the times of median breakthrough are less than 10,000 years, whereas in the TSPA-SR supplemental

analysis, 40 of the times of median breakthrough for neptunium are less than 10,000 years. As in the no matrix diffusion case, the overall uncertainty in the times of median breakthrough, as represented by the width of the histograms, is much larger than the shift in times of median breakthrough from the TSPA-SR supplemental analysis to the enhanced-diffusion case.

12.5.2.3 Minimum Length of Alluvium in the Flow Path

The length of the flow pathway from the repository in the alluvium of the SZ could be significant to radionuclide migration rates because of the relatively high effective porosity in the alluvium and because of the potentially higher sorptive capacity of the alluvium relative to the volcanic rocks, particularly for neptunium. Both of these factors result in longer transport times for radionuclides through the SZ system. The objective of the minimum alluvium analysis is to examine the impact of uncertainty in the location along the flow path from the repository at which groundwater flow transitions from fractured volcanic units to the alluvium in a bounding manner. In addition, the minimum alluvium analysis indirectly examines the potential consequences of an alternative flow path farther to the west of Fortymile Wash that remains in the volcanic units approximately to the location of U.S. Highway 95 (see Figure 12.3.1.3-3 for the location of the predicted flow path from the repository). This sensitivity analysis is bounding in the sense that flow path length in the alluvium is reduced to the minimum reasonable value, based on current geologic data. However, it is not absolutely bounding because it still includes approximately 1 to 2 km of alluvium at the end of the flow path near the 20-km point of compliance as defined per proposed NRC regulation 10 CFR Part 63 (64 FR 8640, Section 63.115(b) [DIRS 101680]).

The minimum-alluvium sensitivity analysis is implemented in the site-scale SZ flow and transport model by reducing the extent of the alluvium uncertainty zone to zero. This reduction has the effect of leaving the default volcanic hydrogeologic units and their associated transport properties in the flow path from the repository up to the approximate location of U.S. Highway 95 (Figure 12.3.1.2-1).

The simulated breakthrough curves for the minimum alluvium case have shorter transport times than those for the TSPA-SR supplemental analysis, as expected (Kuzio 2001 [DIRS 154912], Filename "archive_sspa_v1_data/no_alluv"; McNeish 2001 [DIRS 155023]). Example results for neptunium transport with the site-scale SZ model are shown in Figure 12.5.2-3. The upper histogram shows the distribution of times of median breakthrough for neptunium in the TSPA-SR supplemental analysis, and the lower histogram shows the transport times for the minimum alluvium sensitivity study. The times of median breakthrough are somewhat lower for the minimum alluvium case, with 56 realizations having times of median breakthrough less than 10,000 years, compared to 40 realizations for the TSPA-SR supplemental analysis. As for the no matrix diffusion case, the overall uncertainty in the times of median breakthrough, as represented by the width of the histograms, is larger than the shift in times of median breakthrough from the TSPA-SR supplemental analysis to the minimum alluvium case.

12.5.2.4 Increased Uncertainty in the Reversible Colloid (K_c) Model

The model of colloid-facilitated transport used in the TSPA for radionuclides that are reversibly attached to colloids is implemented within several components of the repository engineered and natural systems. Considerable uncertainty exists in the parameters associated with this model. An integrated re-analysis of uncertainty associated with the parameterization of this model was conducted for all components of the repository system as a sensitivity study for Volume 2 (McNeish 2001 [DIRS 155023]).

The sensitivity analysis for the SZ consists of simulation of radionuclide breakthrough curves for the two classes of radionuclides associated with the reversible colloid model: strongly sorbing radionuclides (americium and thorium) and moderately sorbing radionuclides (strontium, plutonium, cesium, and protactinium) (Kuzio 2001 [DIRS 154912]), Filename "archive_sspa_vl_data/alt_colloids"). These simulations are implemented in the site-scale SZ flow and transport model using resampled values for the K_c parameter and for the K_d of strongly sorbing radionuclides. The values for the K_c parameter used in this analysis are based on sampling of uncertainty distributions for the K_d of americium onto colloids and for the concentration of colloids in the groundwater, as explained in Volume 2 (McNeish 2001 [DIRS 155023], Section 3). The uncertainty distribution for K_d of strongly sorbing radionuclides onto the alluvium material is changed to beta distribution with greater statistical mass near the expected value of 50 ml/g (McNeish 2001 [DIRS 155023], Section 3). Other stochastic parameters for the SZ have the same values for the sensitivity analysis as the TSPA-SR supplemental analysis (McNeish 2001 [DIRS 155023]). Also, the SZ breakthrough curves for other radionuclides are identical to those from the TSPA-SR supplemental analysis case.

The results of the sensitivity analysis for the increased uncertainty in the reversible-colloid model are shown in Figure 12.5.2-4. The upper histogram shows the distribution of times of median breakthrough for the TSPA-SR supplemental analysis case (McNeish 2001 [DIRS 155023]), and the lower histogram shows similar results for the case of increased uncertainty in the K_c model. As illustrated in Figure 12.5.2-4, the case of increased uncertainty in colloid-facilitated transport results in somewhat longer transport times compared to the TSPA-SR supplemental analysis case. There are 13 realizations of times of median breakthrough less than 10,000 years for this case and 16 realizations of transport times less than 10,000 years for the TSPA-SR supplemental analysis case (Kuzio 2001 [DIRS 154912], Filename "archive_sspa_vl_data/alt_colloids"). The distribution of values for the K_c parameter in the case of increased uncertainty in colloid-facilitated transport is significantly broader than in the TSPA-SR supplemental analysis case, containing several values of K_c greater than 1.0 in the 100 realizations. Higher values of K_c result in shorter transport times through the SZ system. The narrower distribution of values for the K_d onto the aquifer medium of the strongly sorbing radionuclides used in the case of increased uncertainty in colloid-facilitated transport tends to reduce the variability in simulated transport times in an opposing fashion.

12.5.3 Evaluation of Boundary to the Accessible Environment

The recently issued EPA regulation, 40 CFR 197.12 (66 FR 32074 [DIRS 155216]), specifies the controlled area boundary as follows:

> Controlled area means:
>
> (1) the surface area, identified by passive institutional controls, that encompasses no more than 300 square kilometers. It must not extend farther:
>
> (a) south than 36° 40' 13.6661" north latitude, in the predominant direction of ground water flow; and
>
> (b) than five kilometers form the repository footprint in any other direction; and
>
> (2) the subsurface underlying the surface area.

The boundary is defined at the point above the highest concentration of radionuclides in the simulated plume of contamination where the plume crosses the southernmost boundary of the controlled area (at a latitude of 36° 40' 13.6661" North) and reaches the accessible environment. This southern boundary is approximately 18 km (11 mi), compared to the original distance of approximately 20 km (12 mi) used in the saturated zone transport modeling for TSPA-SR. To evaluate compliance with the EPA regulation, additional SZ breakthrough curves were calculated for neptunium-237 and carbon-14 to simulate radionuclide transport from the water table beneath the potential repository to a defined downgradient location using the revised definition of the accessible environment. The maximum southerly extent of the controlled area corresponds to a distance of approximately 18 km from the potential higher-temperature operating mode repository.

A sensitivity analysis was performed (using 100 realizations of the site-scale SZ flow and transport model) to compare simulated breakthrough curves at 20-km and 18-km from the site (Kuzio 2001 [DIRS 155244], Appendix 2 and 3). Other stochastic parameters for the SZ simulations use the same values as was used in the breakthrough curves for the SSPA supplemental analysis (McNeish 2001 [DIRS 155023]).

The simulated radionuclide breakthrough curves at 18 km have somewhat shorter transport times (Kuzio 2001 [DIRS 155244], Appendix 2 and 3) than those at 20 km as presented in SSPA supplemental analysis (McNeish 2001 [DIRS 155023]) on a realization-by-realization basis. As examples, the histograms of times of median breakthrough (i.e., the times at the midpoints of the breakthrough curves) for neptunium (a sorbing radionuclide) and carbon (a nonsorbing radionuclide, which acts as a surrogate for other non-retarding radionuclides such as technetium-99 and iodine-129) have been simulated and compared for the 18 km and 20 km distances (Figures 12.5.3-2 and 12.5.3-3). These radionuclides were chosen because they are representative of the solutes that would be most rapidly transported (i.e., nonsorbing carbon-14) or are among the largest contributors to peak dose (i.e., neptunium-237) (CRWMS M&O 2000 [154657]) Page F4-19, Figure 4.1-19a) and together they bound the range of solute transport.

For the neptunium times of median breakthrough at 20 km, 42 of the times of median breakthrough are less than 10,000 years; while at 18 km, 53 times of median breakthrough are less than 10,000 years. For the carbon at 20 km, 19 of the times of median breakthrough are less than 100 years; while at 18 km, 28 times of median breakthrough are less than 100 years. The somewhat shorter times of median breakthrough for carbon are primarily a result of a reduction in the flow path length. The shorter times of median breakthrough for neptunium can be attributed to a reduction in the flow path length and a reduction in the amount of sorption that could occur because the flow path length in alluvium has been reduced. As noted in Section 12.5, the analyses are based on a model that is appropriately conservative for TSPA sensitivity analyses and is not intended to represent expected radionuclide breakthrough or groundwater transport time for the SZ portion of the Yucca Mountain flow system.

Table 12.3.2.1.1-1. Identification and Treatment of Unquantified Uncertainties Based on the Total System Performance Assessment-Site Recommendation

Identification of Unquantified Uncertainties	TSPA-SR Treatment of Uncertainties	Reevaluation of the Quantified Uncertainties
Bulk Density	Constant value of 1.270 kg/m^3, based on a limited data set	Defined as a probability distribution based on site data. Normal distribution E(x): 1910 kg/m^3, SD: 80
Sorption coefficient for neptunium in the alluvium	CDF based on a preliminary data set	Redefined CDF based on complete data set
Sorption coefficient for technetium and iodine in the alluvium	Probability distribution based on a preliminary data set	Final data sets did not show sorption occurring for oxidizing conditions
Sorption coefficient for uranium in the Alluvium	Uniform distribution LB: 0 mL/g; UB: 8.0 mL/g	Redefined to be the same as the CDF for neptunium in the alluvium
Correlation of sorption coefficient in the alluvium for uranium and neptunium	Not correlated	Correlated neptunium and uranium one to one
Fracture porosity	Uniform distribution: Log_{10}(LB): -5.0; Log_{10}(UB): -1.0	Redefined the shape of the probability distribution. Triangular: Log_{10}(LB): -5.0; Log_{10}(UB): -1.0, Most likely value Log_{10}: -3.0
Effective diffusion coefficient	Uniform distribution: Log_{10}(LB): -13.0 m^2/s; Log_{10}(UB): -10.0 m^2/s	Redefined the shape of the probability distribution. Triangular: Log_{10}(LB): -13.0; Log_{10}(UB): -10.0, most likely value Log_{10}: -10.5 (m^2/s)
Effective porosity in the alluvium	Normal distribution, E(x) = 0.18, SD: 0.051; upper bound 0.35	Shifted the E(x) to 0.15 and truncated the upper end at 0.3
Correlation of matrix porosity and effective diffusion coefficient	Not correlated	Matrix porosity was correlated to the effective diffusion coefficient
Neptunium sorption coefficient in the volcanic units	Probability distribution was based on the vitric rock type. Beta distribution: E(x): 0.5 mL/g; SD: 0.5, and LB: 0.0 mL/g, UB: 2.0 mL/g	Sampled the vitric neptunium sorption coefficient 66% of the time and sampled the zeolitic neptunium sorption coefficient distribution 33% of the time
Retardation factor for irreversible colloids in the alluvium	Site grain size data was not available	New probability distribution derived from new grain size data

Source: Information in columns 1 and 2 are from the *Uncertainty Distribution for Stochastic Parameters* report (CRWMS M&O 2000 [DIRS 147972], Section 7, Table 15).

NOTE: UB = Upper bound; LB = Lower bound; E(x) = mean; SD = standard deviation; CDF = cumulative distribution function. Identification and treatment of unquantified uncertainties is based on the TSPA-SR (CRWMS M&O 2000 [DIRS 153246]).

Table 12.3.2.3-1. Bounding Nevada State Plane Coordinates for the Emplacement Area for the Potential Lower-Temperature Operating Mode Repository Footprint

Drift Number	East Side of Emplacement Drift			West Side of Emplacement Drift		
	Northing (m)	Easting (m)	Elevation (m)	Northing (m)	Easting (m)	Elevation (m)
PC1	236,606.073	171,378.875	1,032.437	236,391.550	170,718.641	1,032.437
1	236,521.040	171,379.292	1,033.659	236,292.756	170,676.706	1,033.659
2	236,434.396	171,374.751	1,034.831	236,193.962	170,634.770	1,034.831
3	236,347.752	171,370.210	1,036.002	236,095.168	170,592.834	1,036.002
4	236,261.109	171,365.669	1,037.173	235,996.374	170,550.899	1,037.173
5	236,174.465	171,361.129	1,038.345	235,897.579	170,508.963	1,038.345
6	236,087.821	171,356.588	1,039.516	235,798.785	170,467.027	1,039.516
7	236,001.177	171,352.047	1,040.687	235,699.991	170,425.092	1,040.687
8	235,914.533	171,347.506	1,041.858	235,601.197	170,383.156	1,041.858
9	235,827.889	171,342.965	1,043.030	235,502.403	170,341.221	1,043.030
10	235,741.245	171,338.424	1,044.201	235,403.608	170,299.285	1,044.201
11	235,654.601	171,333.884	1,045.372	235,304.814	170,257.349	1,045.372
12	235,567.957	171,329.343	1,046.544	235,206.020	170,215.414	1,046.544
13	235,481.314	171,324.802	1,047.715	235,102.137	170,157.816	1,047.715
14	235,394.670	171,320.261	1,048.886	235,005.154	170,121.454	1,048.886
15	235,308.026	171,315.720	1,050.058	234,918.510	170,116.913	1,050.058
16	235,221.382	171,311.180	1,051.229	234,831.866	170,112.372	1,051.229
17	235,134.738	171,306.639	1,052.400	234,745.222	170,107.831	1,052.400
18	235,048.094	171,302.098	1,053.571	234,658.578	170,103.290	1,053.571
19	234,961.450	171,297.557	1,054.743	234,571.935	170,098.749	1,054.743
20	234,874.806	171,293.016	1,055.914	234,485.291	170,094.209	1,055.914
21	234,788.163	171,288.475	1,057.085	234,398.647	170,089.668	1,057.085
22	234,701.519	171,283.935	1,058.257	234,312.003	170,085.127	1,058.257
23	234,614.875	171,279.394	1,059.428	234,225.359	170,080.586	1,059.428
24	234,528.231	171,274.853	1,060.599	234,138.715	170,076.045	1,060.599
25	234,441.587	171,270.312	1,061.770	234,052.071	170,071.505	1,061.770
26	234,354.943	171,265.771	1,062.942	233,965.427	170,066.964	1,062.942
27	234,268.299	171,261.231	1,064.113	233,878.784	170,062.423	1,064.113
28	234,181.655	171,256.690	1,065.284	233,792.140	170,057.882	1,065.284

Table 12.3.2.3-1. Bounding Nevada State Plane Coordinates for the Emplacement Area for the Potential Lower-Temperature Operating Mode Repository Footprint (Continued)

Drift Number	East Side of Emplacement Drift			West Side of Emplacement Drift		
	Northing (m)	Easting (m)	Elevation (m)	Northing (m)	Easting (m)	Elevation (m)
29	234,095.012	171,252.149	1,066.456	233,705.496	170,053.341	1,066.456
30	234,008.368	171,247.608	1,067.627	233,618.852	170,048.801	1,067.627
31	233,921.724	171,243.067	1,068.798	233,532.208	170,044.260	1,068.798
32	233,835.080	171,238.527	1,069.969	233,445.564	170,039.719	1,069.969
33	233,748.436	171,233.986	1,071.141	233,358.817	170,034.860	1,071.141
34	233,661.792	171,229.445	1,072.312	233,276.916	170,044.916	1,072.312
35	233,575.148	171,224.904	1,073.483	233,195.015	170,054.972	1,073.483
36	233,488.504	171,220.363	1,074.655	233,113.114	170,065.029	1,074.655
37	233,401.861	171,215.822	1,075.826	233,031.213	170,075.085	1,075.826
38	233,315.217	171,211.282	1,076.997	232,949.312	170,085.141	1,076.997
39	233,228.573	171,206.741	1,078.169	232,867.411	170,095.197	1,078.169
40	233,141.929	171,202.200	1,079.340	232,785.510	170,105.253	1,079.340
41	233,055.285	171,197.659	1,080.511	232,703.609	170,115.309	1,080.511
42	232,968.641	171,193.118	1,081.682	232,621.708	170,125.366	1,081.682
43	232,881.997	171,188.578	1,082.854	232,539.807	170,135.422	1,082.854
44	232,795.353	171,184.037	1,084.025	232,457.906	170,145.478	1,084.025
45	232,708.710	171,179.496	1,085.196	232,376.005	170,155.534	1,085.196
46	232,622.066	171,174.955	1,086.368	232,294.104	170,165.590	1,086.368
47	232,535.422	171,170.414	1,087.539	232,212.203	170,175.647	1,087.539
48	232,448.778	171,165.874	1,088.710	232,130.301	170,185.703	1,088.710
49	232,362.134	171,161.333	1,089.881	232,048.400	170,195.759	1,089.881
50	232,275.490	171,156.792	1,091.053	231,966.499	170,205.815	1,091.053
51	232,188.846	171,152.251	1,092.224	231,884.598	170,215.871	1,092.224
52	232,102.202	171,147.710	1,093.395	231,802.697	170,225.927	1,093.395
53	232,015.558	171,143.169	1,094.567	231,720.796	170,235.984	1,094.567
54	231,928.915	171,138.629	1,095.738	231,638.895	170,246.040	1,095.738
55	231,842.271	171,134.088	1,096.909	231,556.994	170,256.096	1,096.909
56	231,755.627	171,129.547	1,098.081	231,475.093	170,266.152	1,098.081

Table 12.3.2.3-1. Bounding Nevada State Plane Coordinates for the Emplacement Area for the Potential Lower-Temperature Operating Mode Repository Footprint (Continued)

Drift Number	East Side of Emplacement Drift			West Side of Emplacement Drift		
	Northing (m)	Easting (m)	Elevation (m)	Northing (m)	Easting (m)	Elevation (m)
57	231,668.983	171,125.006	1,099.252	231,393.192	170,276.208	1,099.252
58	231,582.339	171,120.465	1,100.423	231,311.291	170,286.265	1,100.423
59	231,495.695	171,115.925	1,101.594	231,229.390	170,296.321	1,101.594
60	231,409.051	171,111.384	1,102.766	231,147.489	170,306.377	1,102.766
61	231,322.407	171,106.843	1,103.937	231,065.588	170,316.433	1,103.937
62	231,228.794	171,080.845	1,105.126	230,983.689	170,326.489	1,105.126
63	231,129.221	171,036.512	1,106.128	230,901.788	170,336.545	1,106.128
64	231,029.648	170,992.179	1,107.130	230,819.887	170,346.601	1,107.130
65	230,161.806	170,680.331	1,112.032	230,059.664	170,365.970	1,112.032
66	230,075.660	170,677.322	1,112.463	229,973.518	170,362.962	1,112.463
67	229,989.514	170,674.314	1,112.894	229,887.373	170,359.954	1,112.894
68	229,903.957	170,673.116	1,113.279	229,801.227	170,356.946	1,113.279
69	229,823.182	170,686.637	1,113.667	229,715.081	170,353.937	1,113.667
70	229,746.888	170,713.951	1,114.115	229,628.935	170,350.929	1,114.115
71	229,671.164	170,743.018	1,114.549	229,543.716	170,350.774	1,114.549
72	229,595.440	170,772.086	1,115.001	229,454.670	170,338.840	1,115.001
73	229,519.716	170,801.154	1,115.479	229,361.994	170,315.734	1,115.479
74	229,443.993	170,830.221	1,115.957	229,269.318	170,292.627	1,115.957
75	229,368.269	170,859.289	1,116.434	229,176.641	170,269.520	1,116.434
76	229,292.545	170,888.357	1,116.912	229,083.965	170,246.413	1,116.912
77	229,216.821	170,917.424	1,117.389	228,991.289	170,223.306	1,117.389
78	229,141.098	170,946.492	1,117.275	228,898.612	170,200.200	1,117.275
79	229,065.285	170,975.285	1,116.251	228,804.965	170,174.104	1,116.251
80	228,986.633	170,995.342	1,115.190	228,721.372	170,178.952	1,115.190
81	228,907.407	171,013.632	1,114.059	228,646.270	170,209.934	1,114.059
82	228,828.182	171,031.923	1,112.851	228,573.648	170,248.548	1,112.851
83	228,748.957	171,050.214	1,111.535	228,501.026	170,287.162	1,111.535
84	228,669.731	171,068.504	1,110.219	228,428.404	170,325.776	1,110.219

Table 12.3.2.3-1. Bounding Nevada State Plane Coordinates for the Emplacement Area for the Potential Lower-Temperature Operating Mode Repository Footprint (Continued)

Drift Number	East Side of Emplacement Drift			West Side of Emplacement Drift		
	Northing (m)	Easting (m)	Elevation (m)	Northing (m)	Easting (m)	Elevation (m)
85	228,590.506	171,086.795	1,108.903	228,355.782	170,364.389	1,108.903
87	228,432.055	171,123.376	1,106.271	228,210.538	170,441.617	1,106.271
88	228,352.829	171,141.667	1,104.955	228,137.916	170,480.231	1,104.955
89	228,273.604	171,159.957	1,103.663	228,065.294	170,518.845	1,103.663
90	228,194.378	171,178.248	1,102.370	227,992.672	170,557.459	1,102.370
91	228,115.153	171,196.539	1,101.078	227,920.050	170,596.072	1,101.078

Source: BSC 2001 [DIRS 154548], Table 1.

Table 12.3.2.4-1. Zeolitic Rock Volume

Zeolitic Percentage	Percentage of Rock Mass Volume with the Zeolitic Percentage or Greater
5	38.4
10	38.2
20	34.9
30	32.1
40	25.4
50	16.2
60	2.2
70	0.07

Source: Kuzio 2001 [DIRS 155004], Filename "Table 12.3.2.4-1.doc".

Table 12.3.2.4-2. Comparison of Sorption Coefficients for Uranium and Neptunium

Solid Phase	pH	Uranium K_d (ml/g)	Neptunium K_d (ml/g)
G4-268 Devitrified Tuff	7	0.2	0.007
	8.5	0.7	(-0.04)[a]
GU3-1405 Vitric tuff	7	(-0.5)[a]	0.2
	8.5	0.6	0.3
G4-1510 Zeolitic Tuff	7	16[b]	3
	8.5	8[b]	1.5

Sources: Data for samples G4-268 and GU3-1405 are from Triay et al. (1997 [DIRS 100422], Table 15). Data for sample G4-1510 are from CRWMS M&O (2001 [DIRS 154024], Section 6.4.4.1.4.2).

NOTES: [a]Negative values most likely reflect analytical artifacts. The magnitude of the negative value provides an indication of the analytical error associated with this type of analysis.

[b]These K_d values are for solution concentrations less than 1 mg/L.

Table 12.3.2.4-3. Measured Saturated Density, Computed Porosity, and Computed Dry Bulk Density for Depths from 402 to 776 Feet Below the Surface at the Nye County EWDP-19D1 Well

Sample Depth (ft)	Drift-Corrected Saturated Bulk Density, ρ_{sat} (g/cm^3)	Computed Porosity, θ	Computed Dry Bulk Density, ρ_b (g/cm^3)
402	2.231	0.190	2.04
422	2.156	0.239	1.92
442	2.180	0.224	1.96
485	2.163	0.235	1.93
505	2.174	0.228	1.95
525	2.214	0.201	2.01
569.95	2.148	0.245	1.90
589.9	2.142	0.249	1.89
610	2.105	0.273	1.83
630	2.079	0.290	1.79
649.95	2.077	0.291	1.79
669.95	2.133	0.255	1.88
690	2.121	0.262	1.86
715.95	2.158	0.238	1.92
736	2.143	0.248	1.90
756	2.105	0.273	1.83
776	2.239	0.185	2.05

Source: Black 2000 [DIRS 154704], p.18.

Table 12.3.2.4-4. Parameters for Retardation Factor Calculations and Uncertainty Range Distributions

Parameter	Min	Max	Distribution
Grain size (d) (cm) [a]	0.02	0.11	Uniform
Colloid Size (d_p) (cm) [b]	6.0E-07	4.5E-05	Uniform
Alpha (α) [c]	.005	.025	Uniform
Porosity (θ) [d]	0 (min limit)	1 (max limit)	Truncated Normal (mean = 0.18, σ = 0.055)
Flux (q) (m/yr) [e]	0.2	20	Discrete (0.2, 24%; 2.0, 52%; 20.0, 24%)
Detachment Rate (k_r) (g/ml-hr) [f]	1.0E-05	3.33	Log-Uniform

Sources: [a] Marshall et al. 1996 [DIRS 144573], Figure 1.2, p. 4; Bechtel Nevada 1998 [DIRS 149177], Table I-1; Bechtel Nevada 1998 [DIRS 149178].

[b] CRWMS M&O 2000 [DIRS 122799], p. 24.

[c] Harvey and Garabedian 1991 [DIRS 109256], pp. 178 to 185.

[d] CRWMS M&O 2000 [DIRS 147972], Section 6.3 (effective porosity of the alluvium).

[e] CRWMS M&O 2000 [DIRS 139440], Section 6.2.5.1 and Section 6.5.1 (flux was approximated from this information).

[f] Bales et al. 1997 [DIRS 144535], Table 3, parameter K2 and CRWMS M&O 2000 [DIRS 129286], Table 6.

Table 12.5.1-1. Identification and Treatment of Unquantified Uncertainties Based on the Total System Performance Assessment-Site Recommendation

Identification of Unquantified Uncertainties	TSPA-SR Treatment of Uncertainties	Reevaluation of the Quantified Uncertainties
Bulk density	Constant value of 1.27 g/cm^3, based on a limited data set	Defined as a probability distribution based on site data. Normal distribution E(x): 1.91 g/cm^3, SD: 0.08
Sorption coefficient for neptunium in the alluvium	CDF based on a preliminary data set	Redefined CDF based on complete data set
Sorption coefficient for technetium and iodine in the alluvium	Probability distribution based on a preliminary data set	Final data sets did not show sorption occurring for oxidizing conditions
Sorption coefficient for uranium in the Alluvium	Uniform distribution LB: 0; UB: 8.0 (ml/g)	Redefined to be the same as the CDF for neptunium in the alluvium
Correlation of sorption coefficient in the alluvium for uranium and neptunium	Not correlated	Correlated neptunium and uranium 1:1
Fracture porosity	Uniform distribution: Log_{10}(LB): -5.0; Log_{10}(UB): -1.0	Redefined the shape of the probability distribution. Triangular: Log_{10}(LB): -5.0; Log_{10}(UB): -1.0, Most likely value Log_{10}: -3.0
Effective diffusion coefficient	Uniform distribution: Log_{10}(LB): -13.0 m^2/s; Log_{10}(UB): -10.0 (m^2/s)	Redefined the shape of the probability distribution. Triangular: Log_{10}(LB): -13.0; Log_{10}(UB): -10.0, most likely value Log_{10}: -10.5 (m^2/s)
Effective porosity in the alluvium	Normal distribution, E(x) = 0.18, SD: 0.051; upper bound 0.35	Shifted the E(x) to 0.15 and truncated the upper end at 0.3
Correlation of matrix porosity and effective diffusion coefficient	Not correlated	Matrix porosity was correlated to the effective diffusion coefficient
Retardation factor for irreversible colloids in the alluvium	Site grain size data was not available	New probability distribution derived from new grain size data
Neptunium sorption coefficient in the volcanic units	Probability distribution was based on the vitric rock type. Beta distribution: E(x): 0.5; SD: 0.5 and LB: 0.0, UB: 2.0 ml/g	Sampled the vitric neptunium sorption coefficient 66% of the time and sampled the zeolitic neptunium sorption coefficient distribution 33% of the time
Groundwater specific discharge	Probability distribution based on SZ Expert Elicitation. Three discrete cases considered (low: 0.06, medium: 0.6, high: 6.0 m/yr	Three discrete cases adjusted to (low: 0.2, medium: 0.6, high 1.8 m/yr)

Source: Information in Columns 1 and 2 is from the *Uncertainty Distribution for Stochastic Parameters* report (CRWMS M&O 2000 [DIRS 147972], Section 7, Table 15).

NOTES: CDF = cumulative distribution function; E(x) = expected value; UB = upper bound; LB = lower bound; SD = standard deviation. Identification and treatment of unquantified uncertainties is based on the TSPA-SR (CRWMS M&O 2000 [DIRS 153246]).

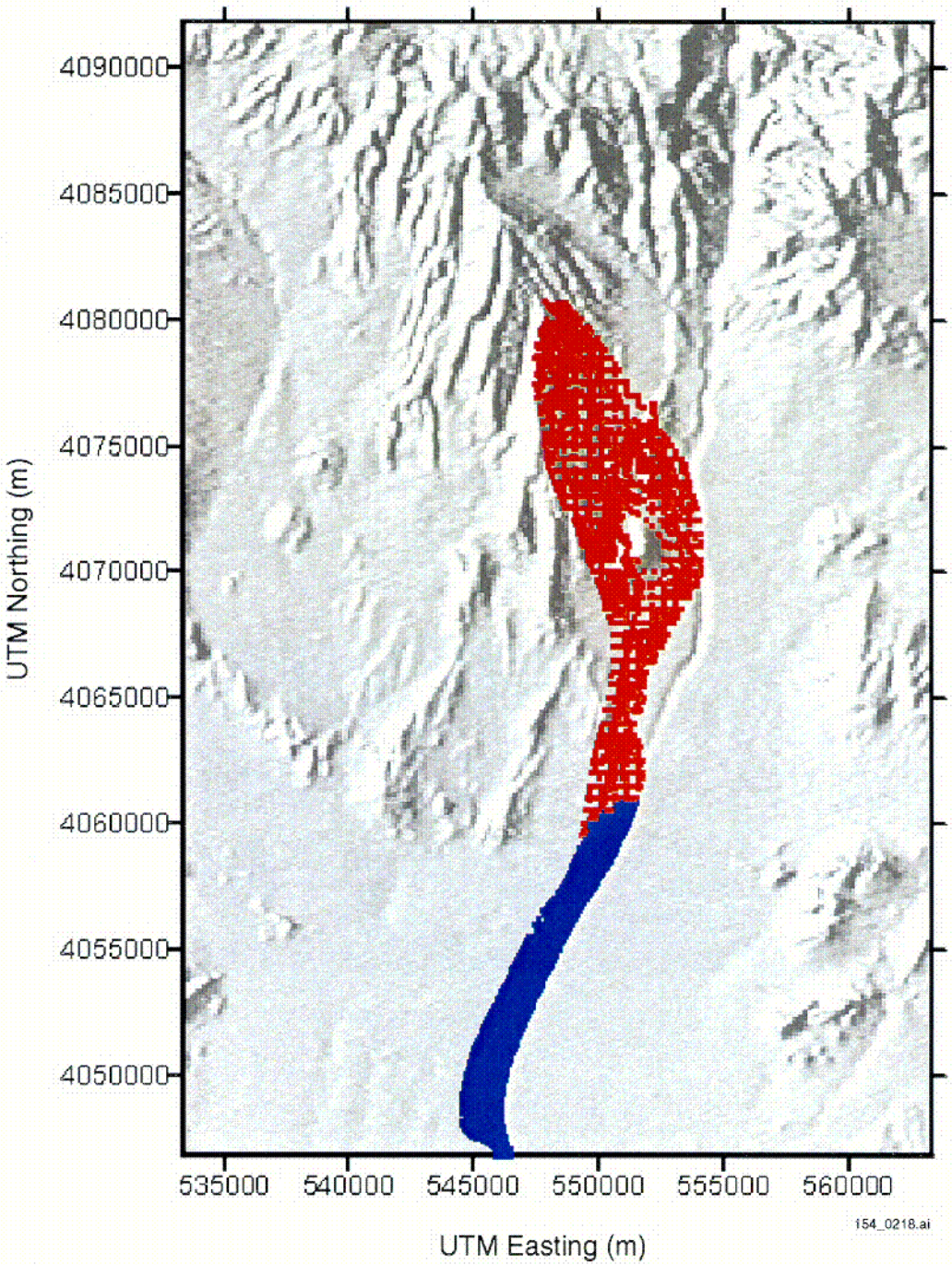

154_0218.ai

Source: Adapted from DOE 2001 [DIRS 153849], Figure 4-129.

NOTE: The potential repository is located in the upper central part of the figure. Released particles move from the upper central area in the figure to the bottom. The red portion of the illustration indicates flow (particle positions) through fractured volcanic tuff, and the blue portion indicates flow through alluvium (modeled as a porous medium). The spatial pattern in the volcanic tuff reflects the numerical algorithm that illustrates particle positions at grid boundaries or at the end of a time step. The location of the contact of tuff and alluvium is uncertain and is treated stochastically, and it is shown here at the expected-value location.

Figure 12.1-1. Flow Paths Predicted by the Site-Scale Saturated Zone Flow and Transport Model

C01

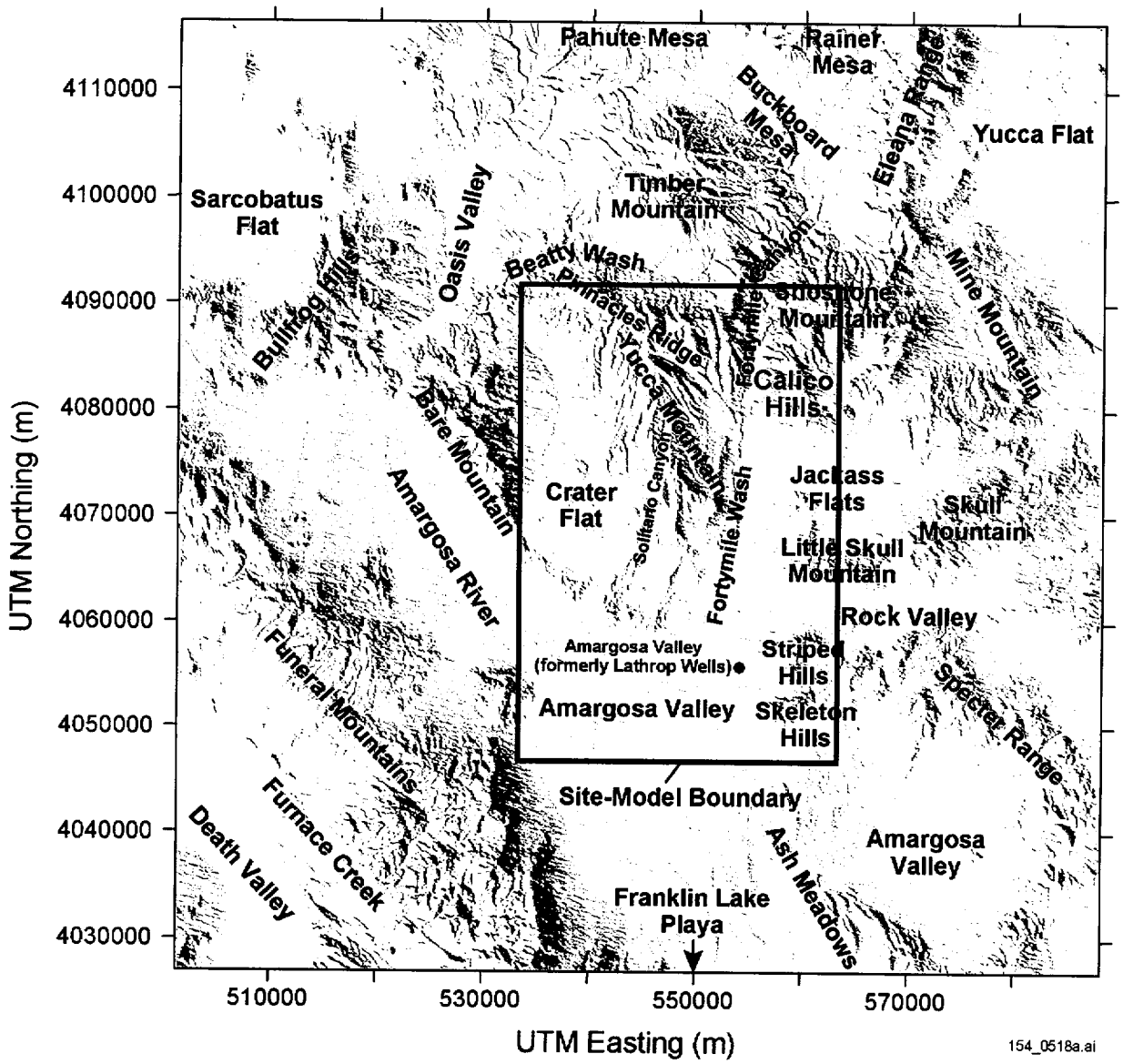

154_0518a.ai

Source: CRWMS M&O 2000 [DIRS 139582], p. 24.

Figure 12.2-1. Boundary of the Numerical Model for the Site-Scale Saturated Zone Flow and Transport Model

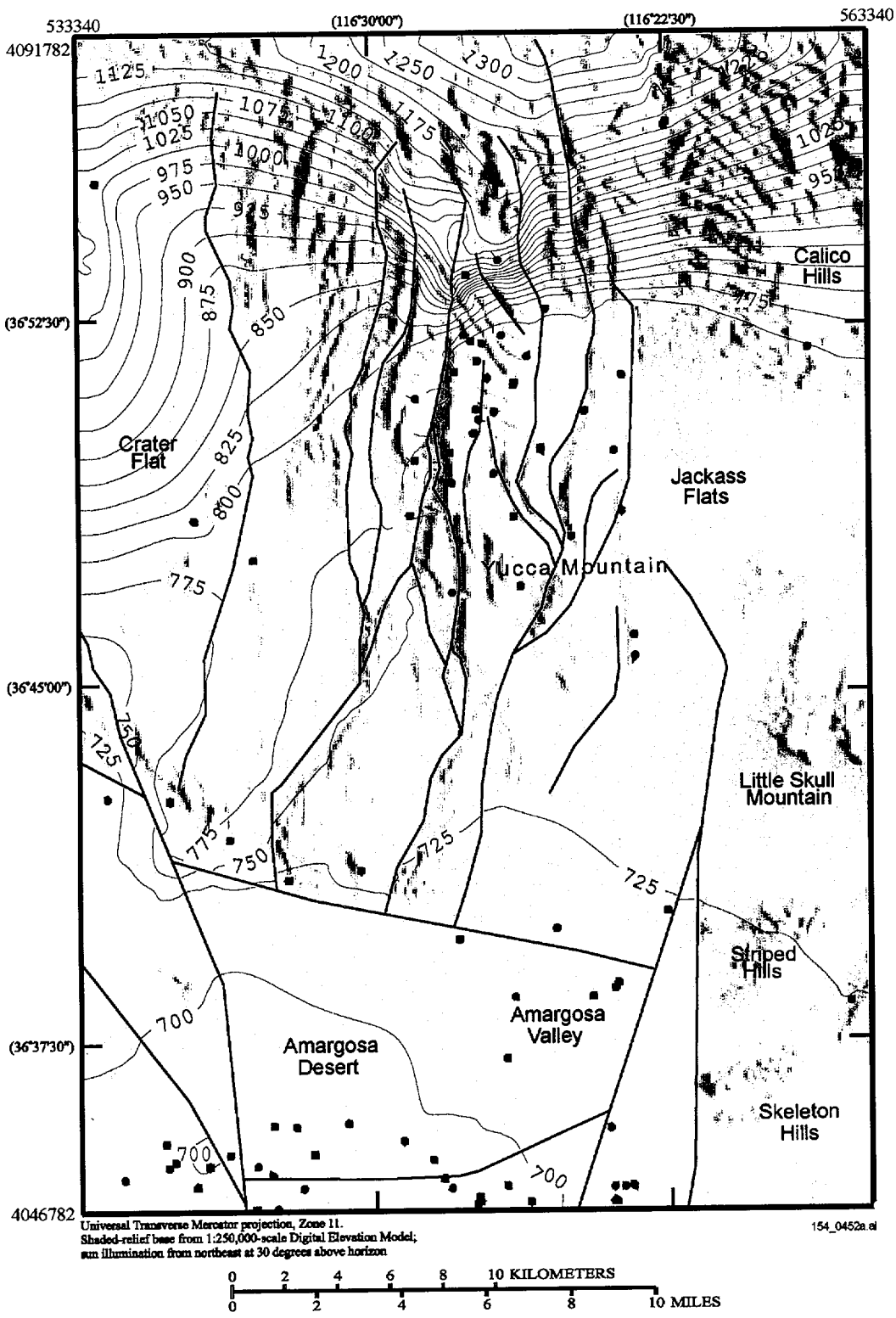

154_0452a.ai

Source: Adapted from USGS 2001 [DIRS 154625], Figure 1-2.

Figure 12.2-2. Borehole Locations, Water-Level Altitudes, Potentiometric Surface Contours, and Location of Tertiary Faults in the Site-Scale Saturated Zone Model Area

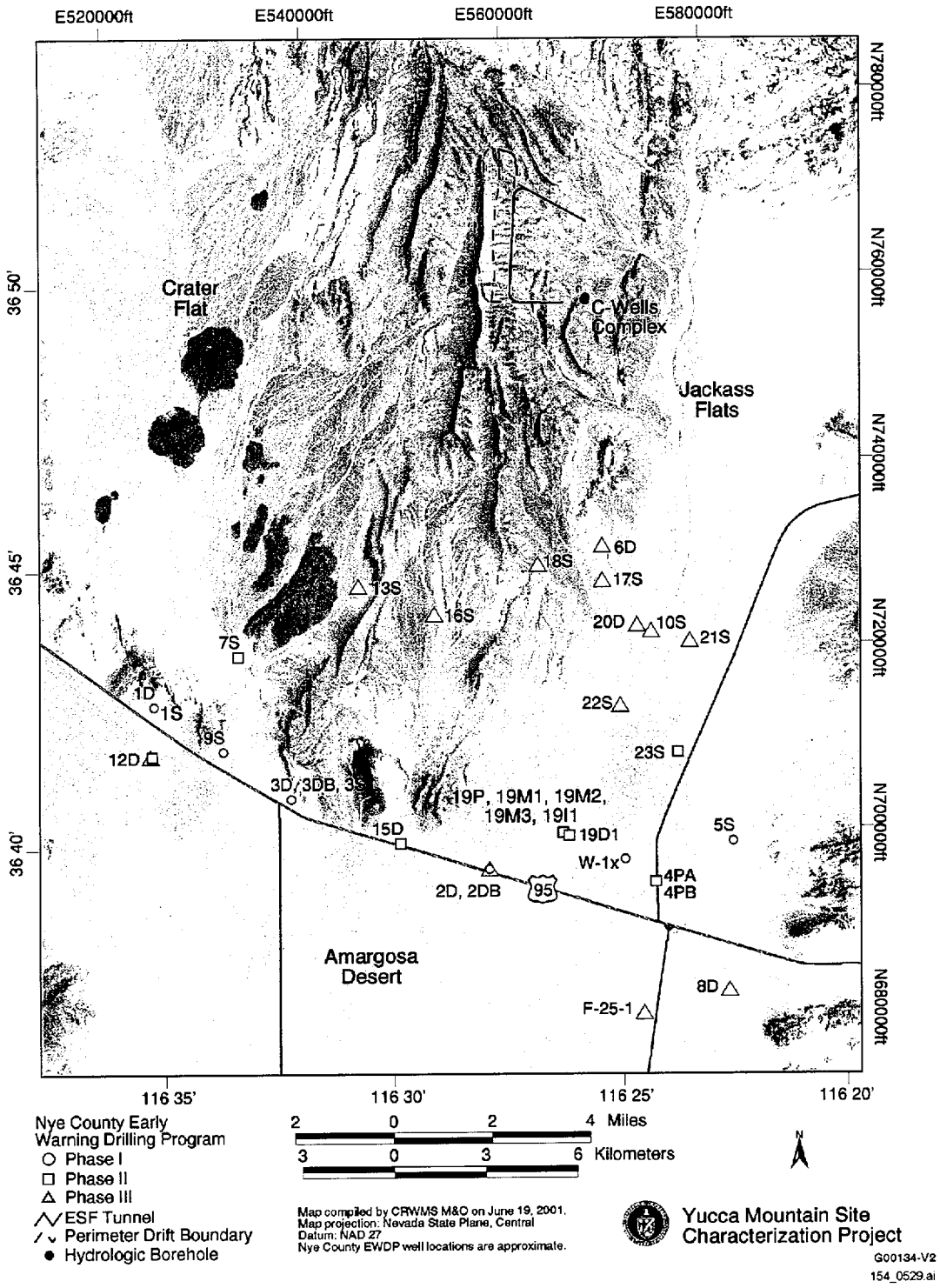

154_0529.ai

Source: CRWMS M&O 2000 [DIRS 153168], Figure 2-3.

NOTE: Borehole NC-EWDP-9SX is located adjacent to Borehole NC-EWDP-9S.

Figure 12.3.1.2-1. Locations of Nye County Early Warning Drilling Program Wells

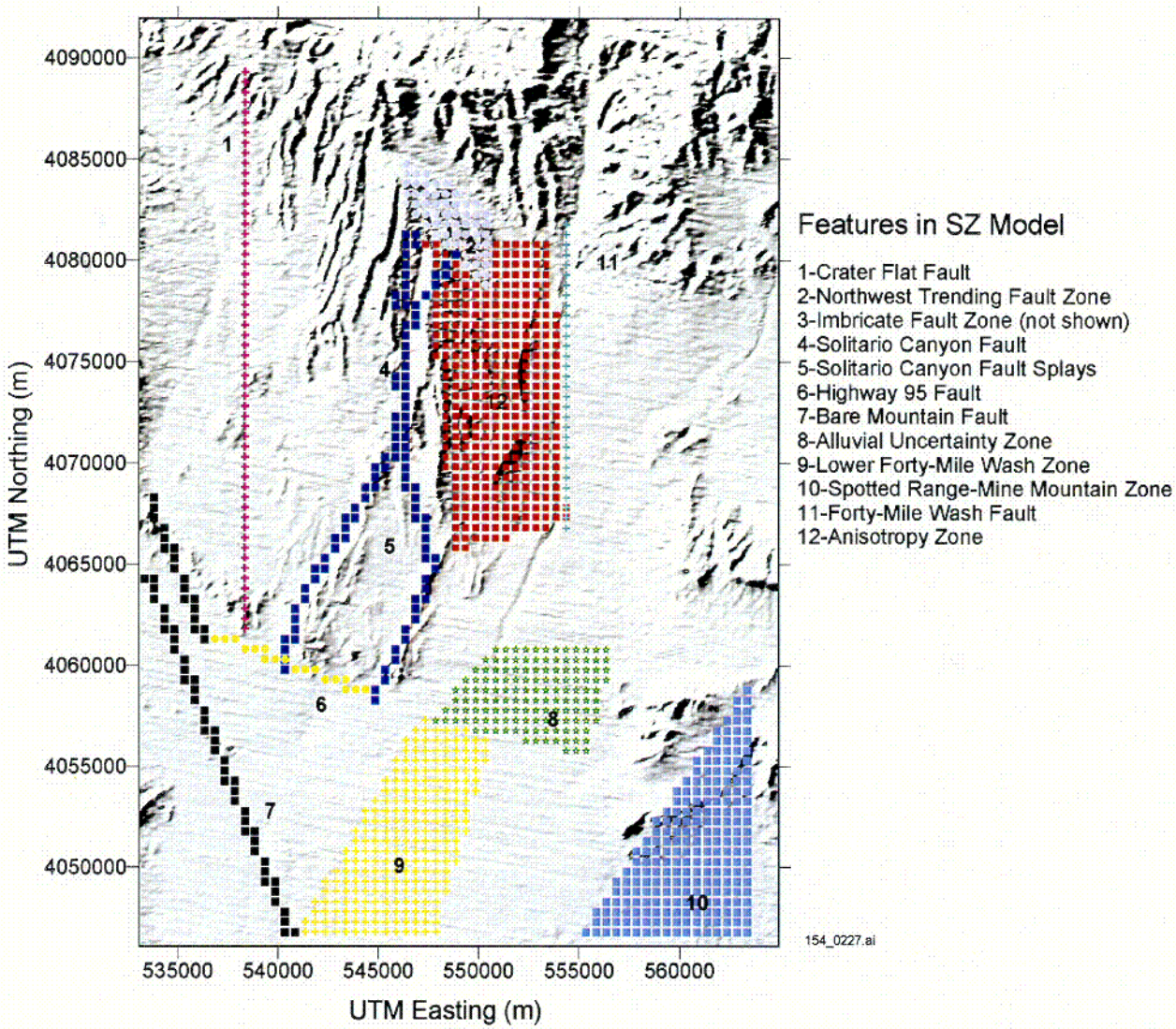

154_0227.ai

Source: DTN: LA0105GZ12213S.001 [DIRS 154887]; DTN: LA0105GZ12213S.002 [DIRS 154888]; DTN: LA0105GZ12213S.003 [DIRS 154889].

NOTE: The east-west barrier of the original model is not included in this newer model.

Figure 12.3.1.3-1. Features in the Newer Saturated Zone Model

C02

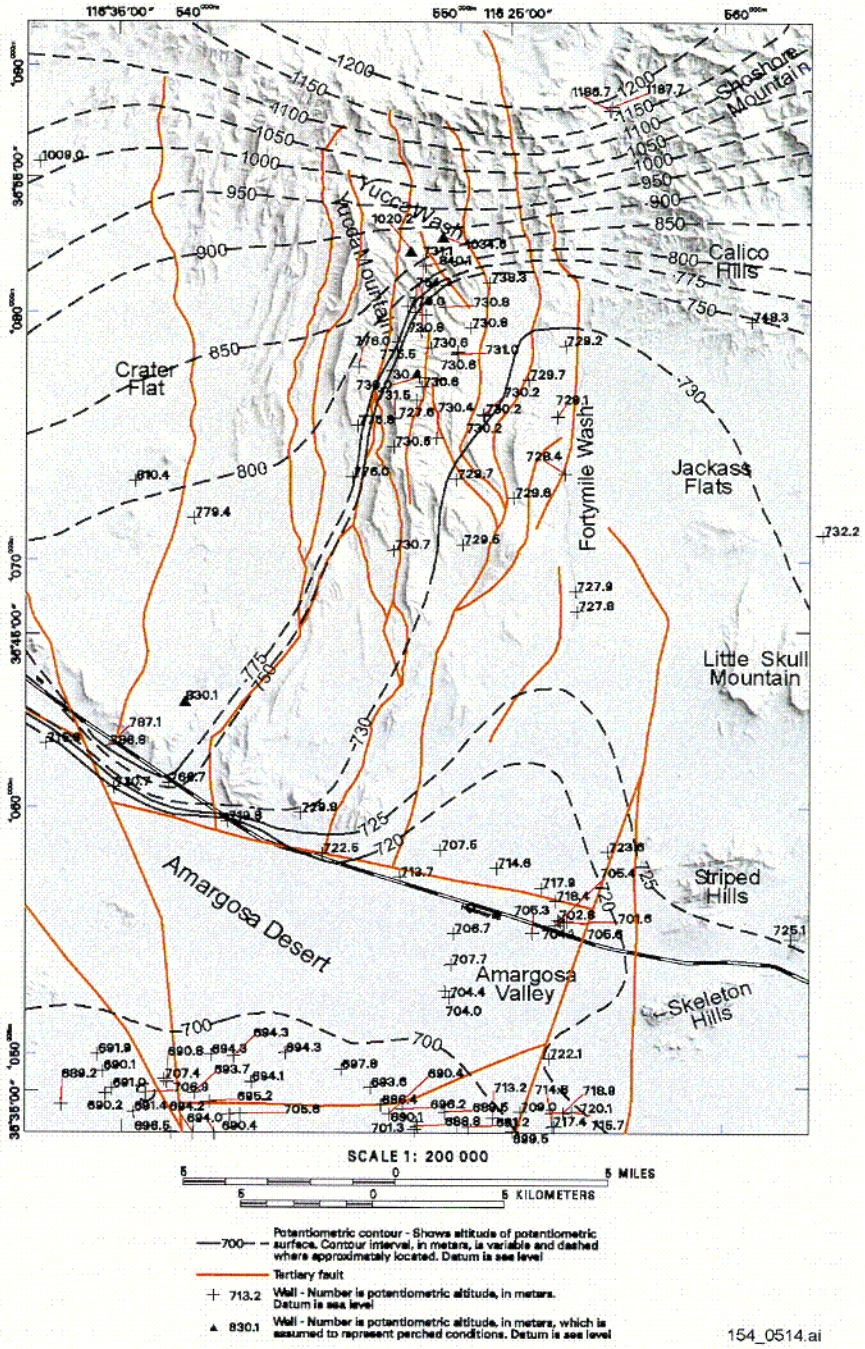

154_0514.ai

Source: BSC 2001 [DIRS 155312].

NOTE: The potentiometric surface map was developed assuming perched conditions north of Yucca Mountain.

Figure 12.3.1.2-2. Potentiometric Surface Map in the Saturated Zone Site-Scale Model Area

C03

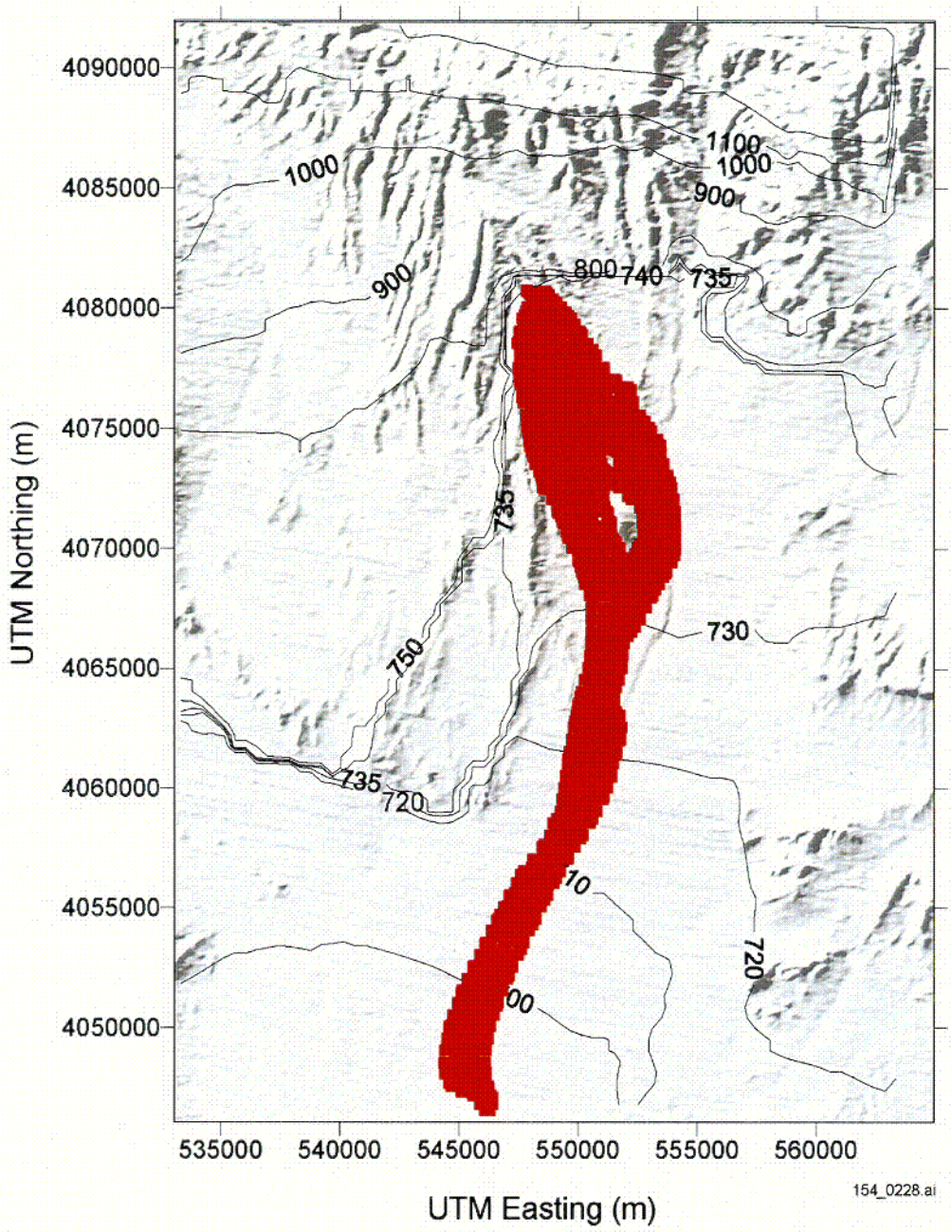

154_0228.ai

Source: Adapted from CRWMS M&O 2000 [DIRS 139582], Figure 8.

NOTE: All features in the original site-scale model, including the east-west barrier, are represented in this simulation.

Figure 12.3.1.3-2. Flow Paths Simulated with the Original Site-Scale Saturated Zone Flow and Transport Model

C04

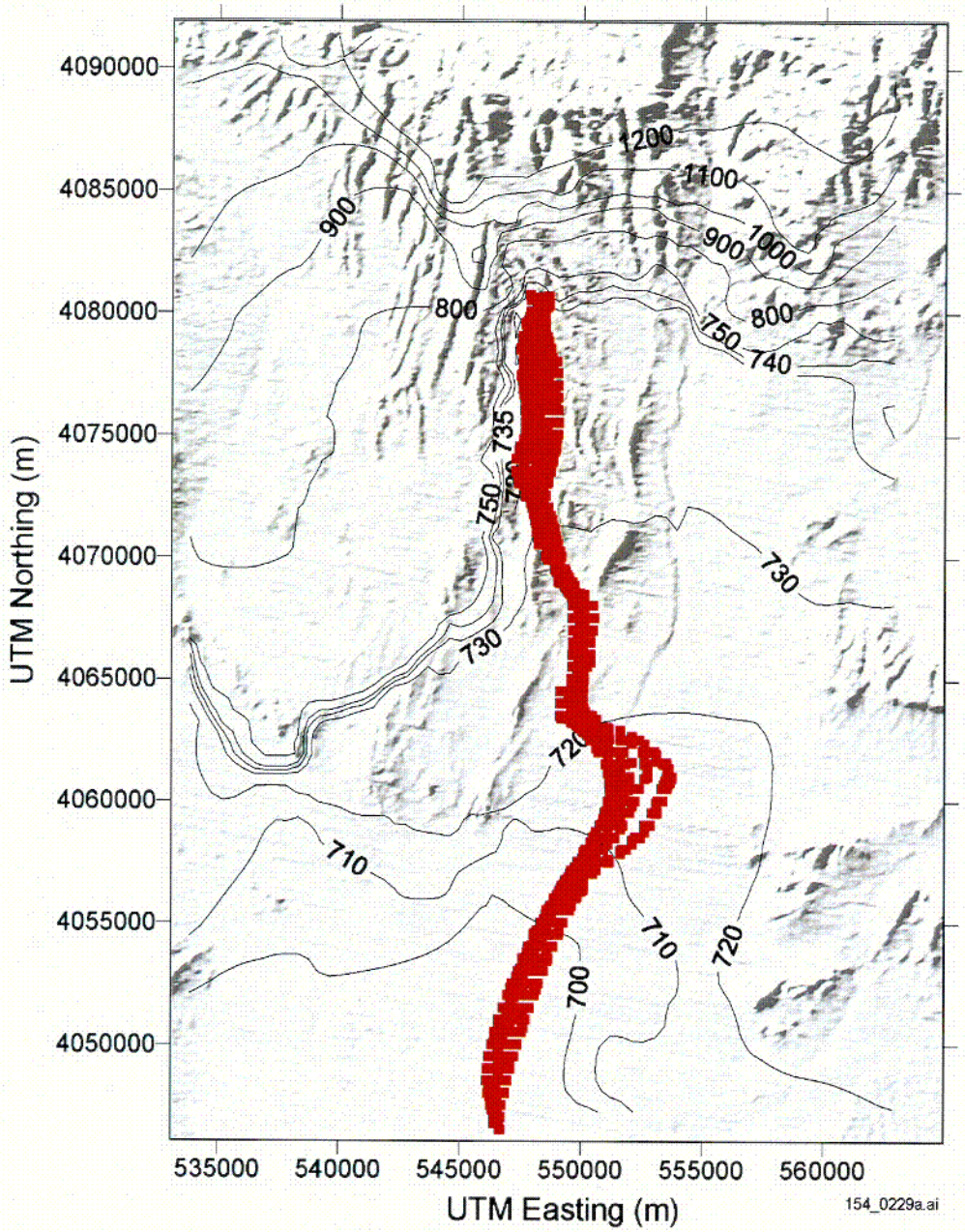

154_0229.ai

Source: DTN: LA0105GZ12213S.002 [DIRS 154888].

NOTE: All features in Figure 12.3.1.3-1, except the northwest trending fault zone (Feature 2), are represented in this simulation.

Figure 12.3.1.3-3. Flow Paths Simulated with the New Saturated Zone Model (Excluding the Northwest Trending Fault Zone)

C05

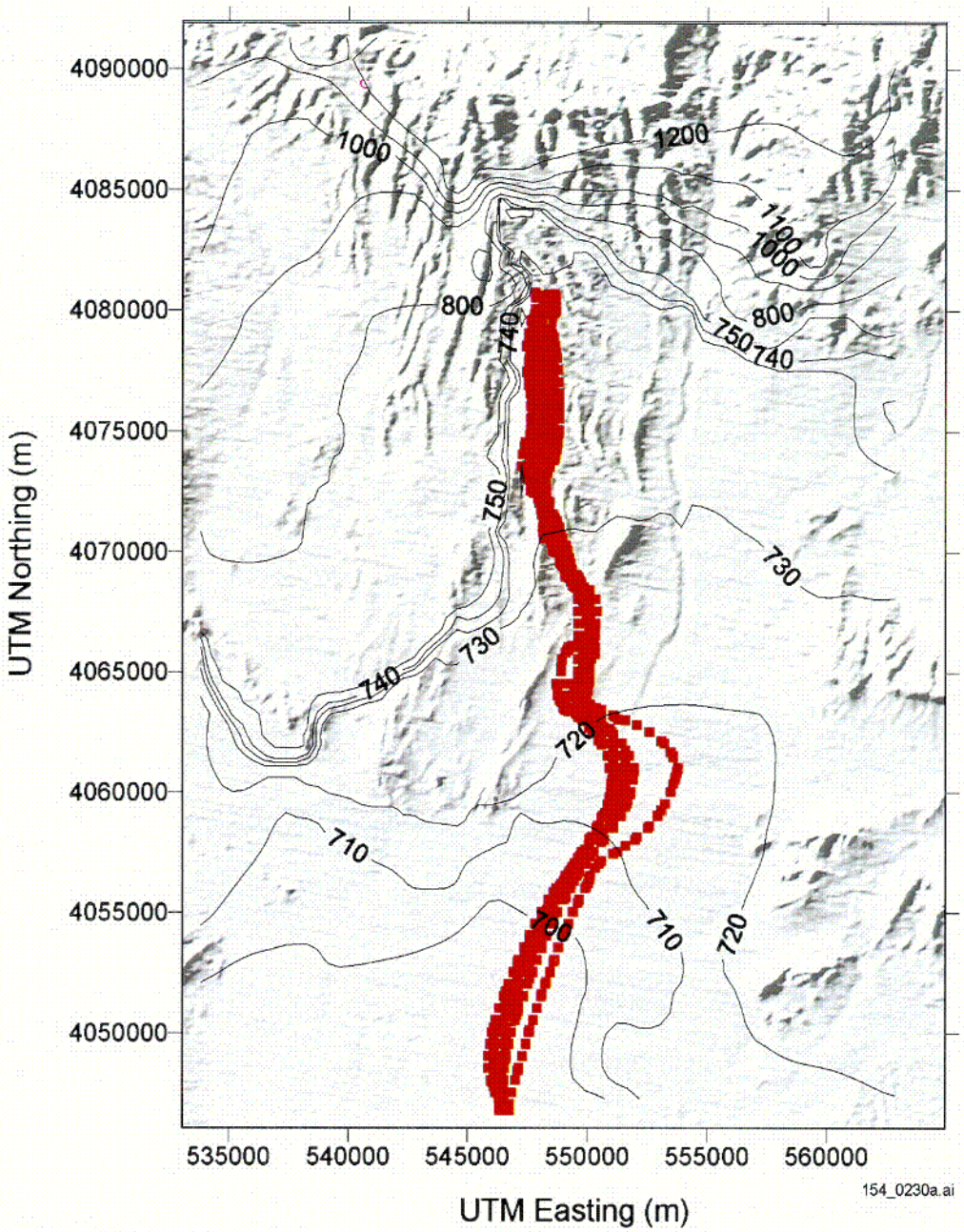

154_0230a.ai

Source: DTN: LA0105GZ12213S.001 [DIRS 154887].

NOTE: All features in Figure 12.3.1.3-1, including the northwest trending fault zone (Feature 2), are represented in this simulation.

Figure 12.3.1.3-4. Flow Paths Simulated with the New Saturated Zone Model (Including the Northwest Trending Fault Zone)

C06

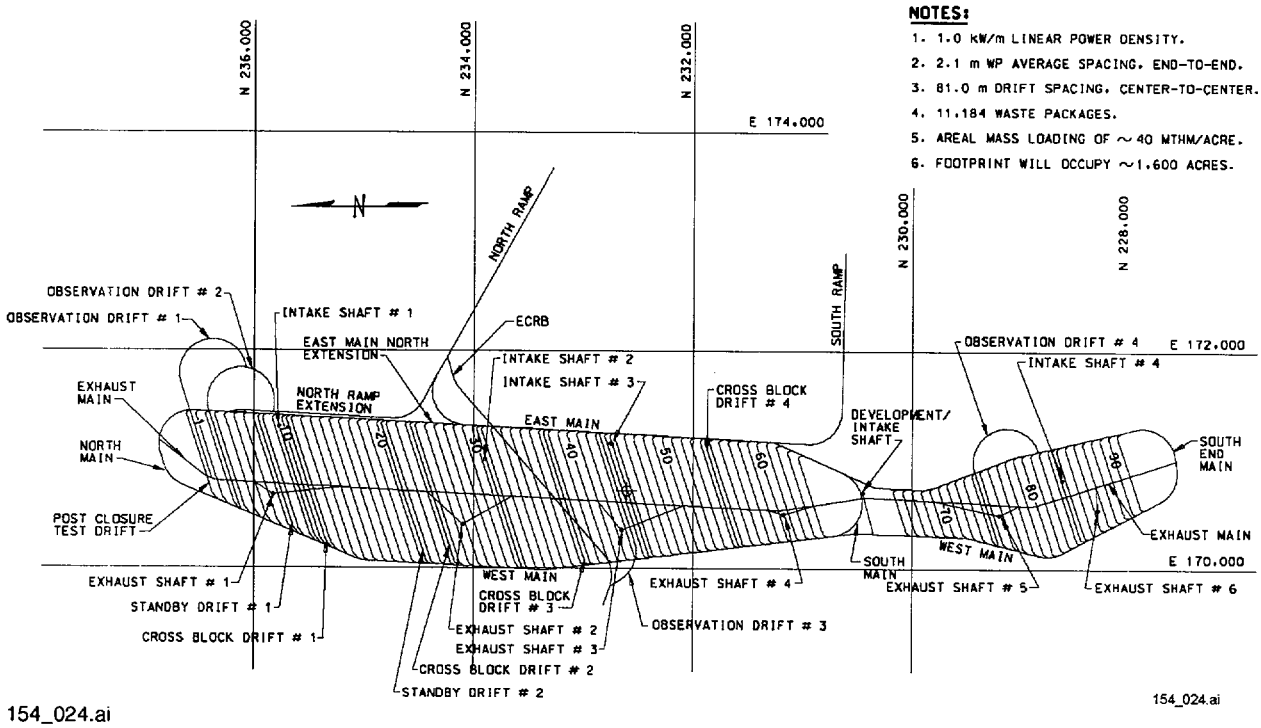

154_024.ai

Source: BSC 2001 [DIRS 154548], Section I, Figure 1, p. 1.

NOTE: MTHM = metric tons of heavy metal.

Figure 12.3.2.3-1. Preliminary 70,000 MTHM Layout for the Lower-Temperature Operating Mode

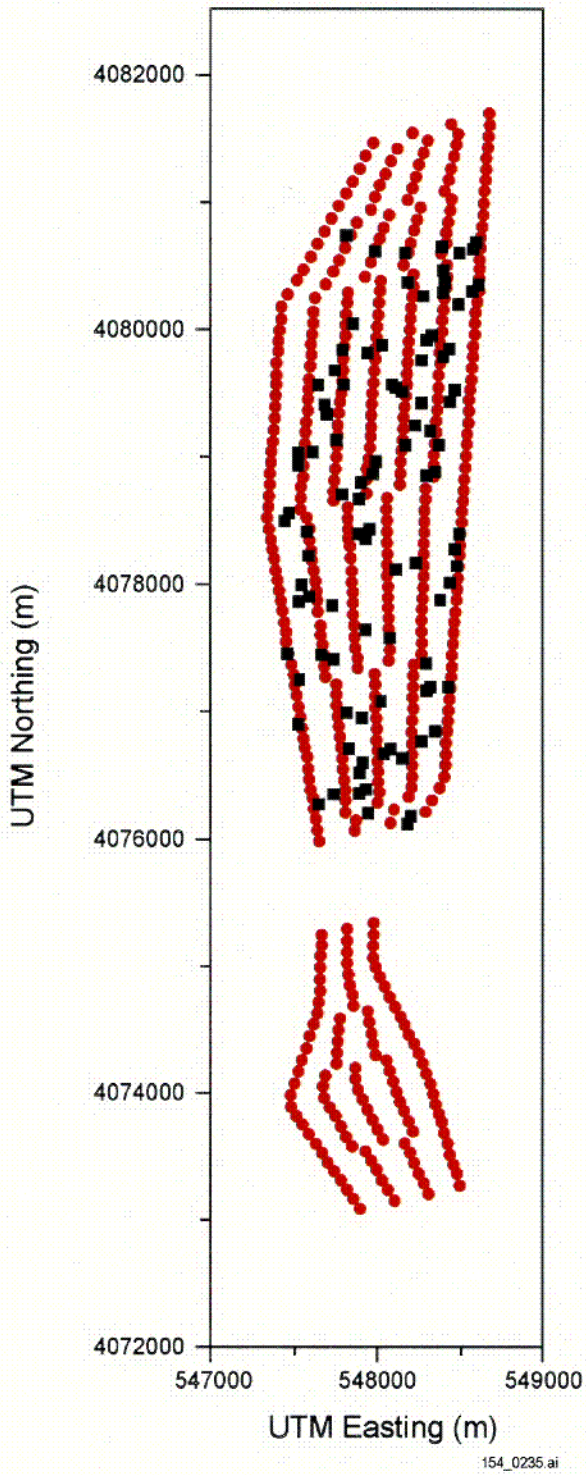

154_0235.ai

Source: Robinson 2001 [DIRS 154995], Filename "original_points.txt" and "out.pts250".

NOTE: Original potential repository footprint (black squares) and the increased footprint (red circles) associated with the flexible design.

Figure 12.3.2.3-2. Locations of Particle Tracking Points Associated with Differing Potential Repository Footprints

C07

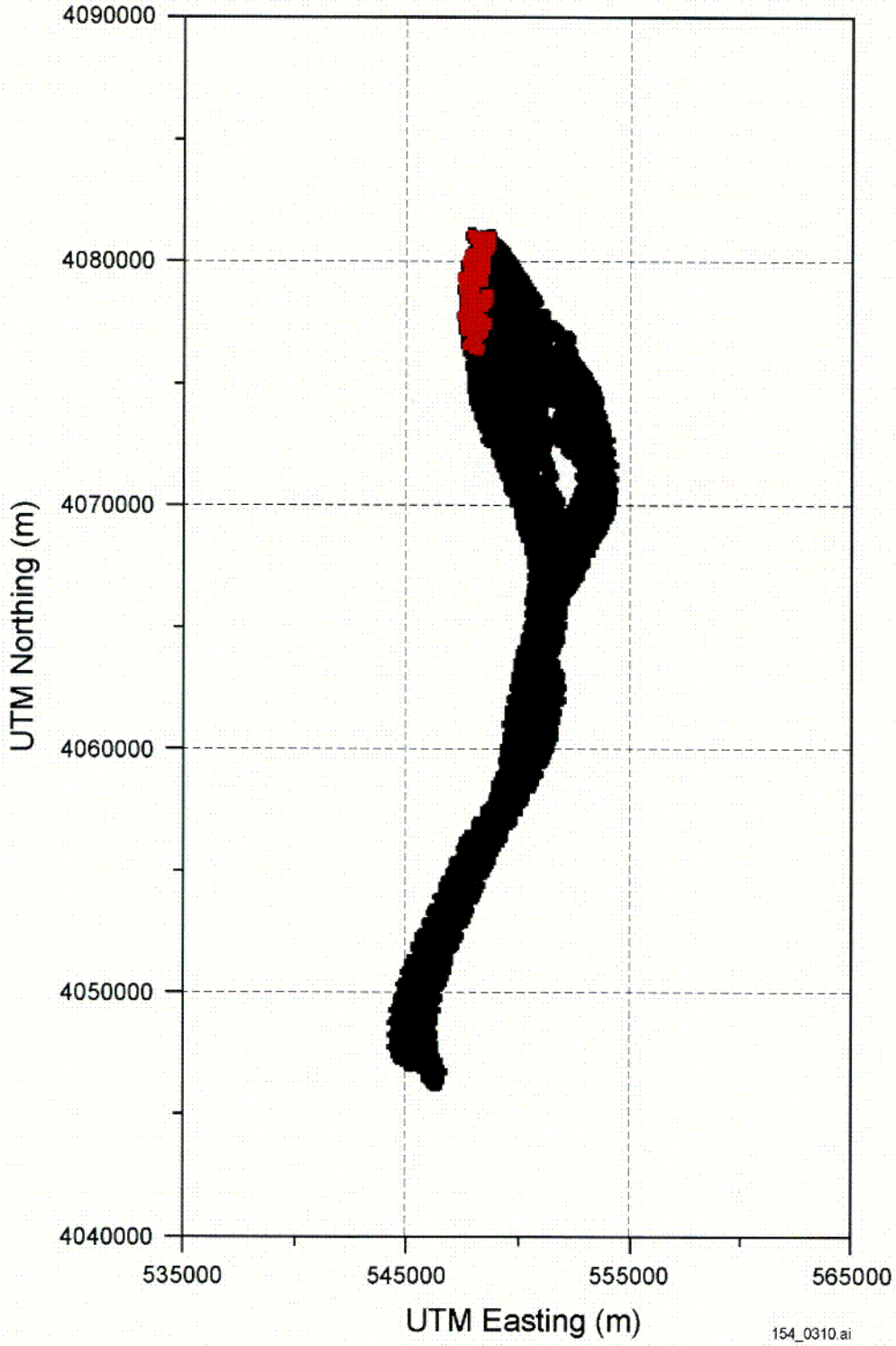

154_0310.ai

Source: Robinson 2001 [DIRS 154995], Filename "02_calib.sptr2.sr".

Figure 12.3.2.3-3a. Plan View of Particle Pathlines the Higher-Temperature Operating Mode for the Potential Repository

108

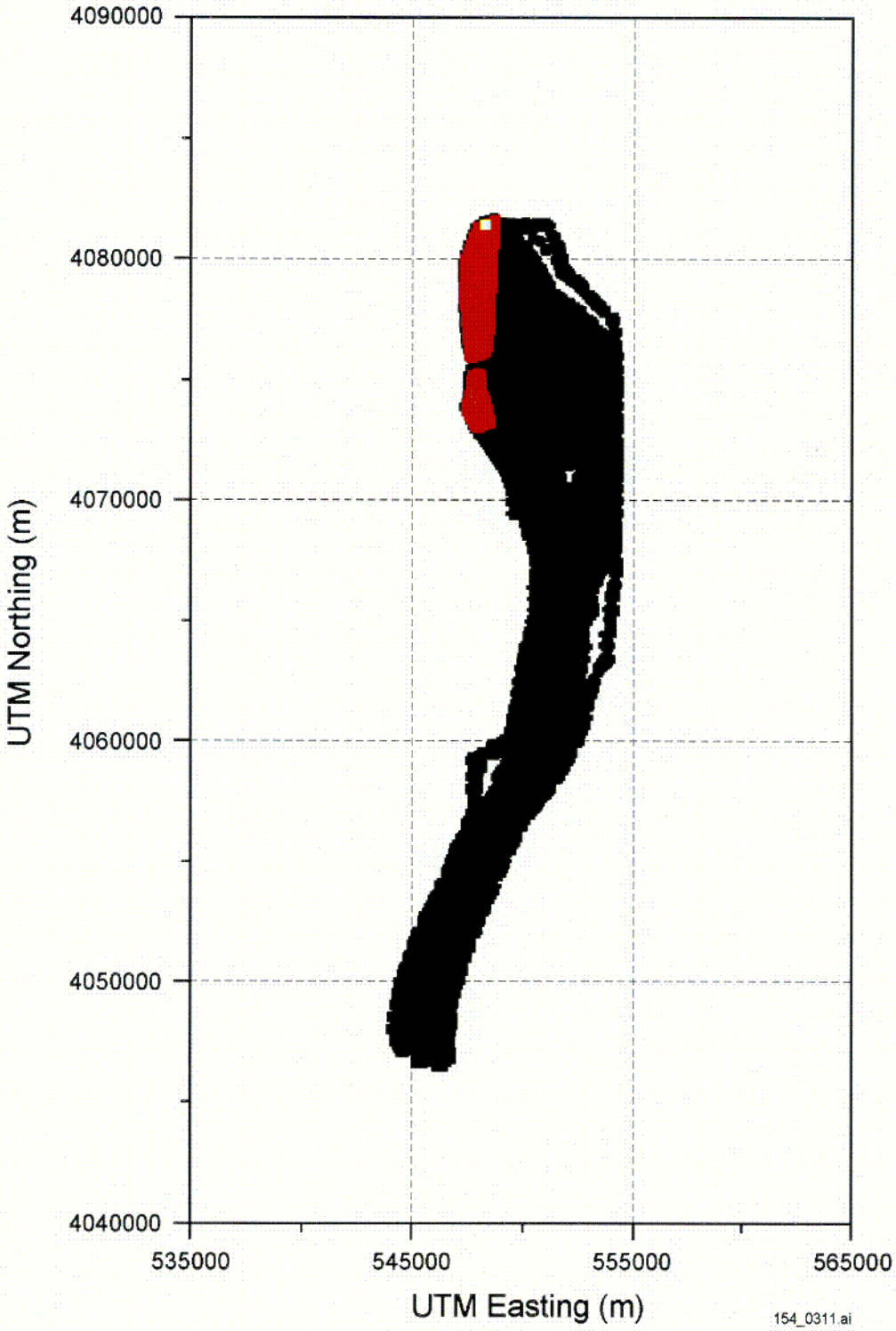

154_0311.ai

Source: Robinson 2001 [DIRS 154995], Filename "02_calib.sptra2.enlarged".

Figure 12.3.2.3-3b. Plan View of Particle Pathlines from the Potential Repository with Pathlines from an Increased Repository Footprint

C09

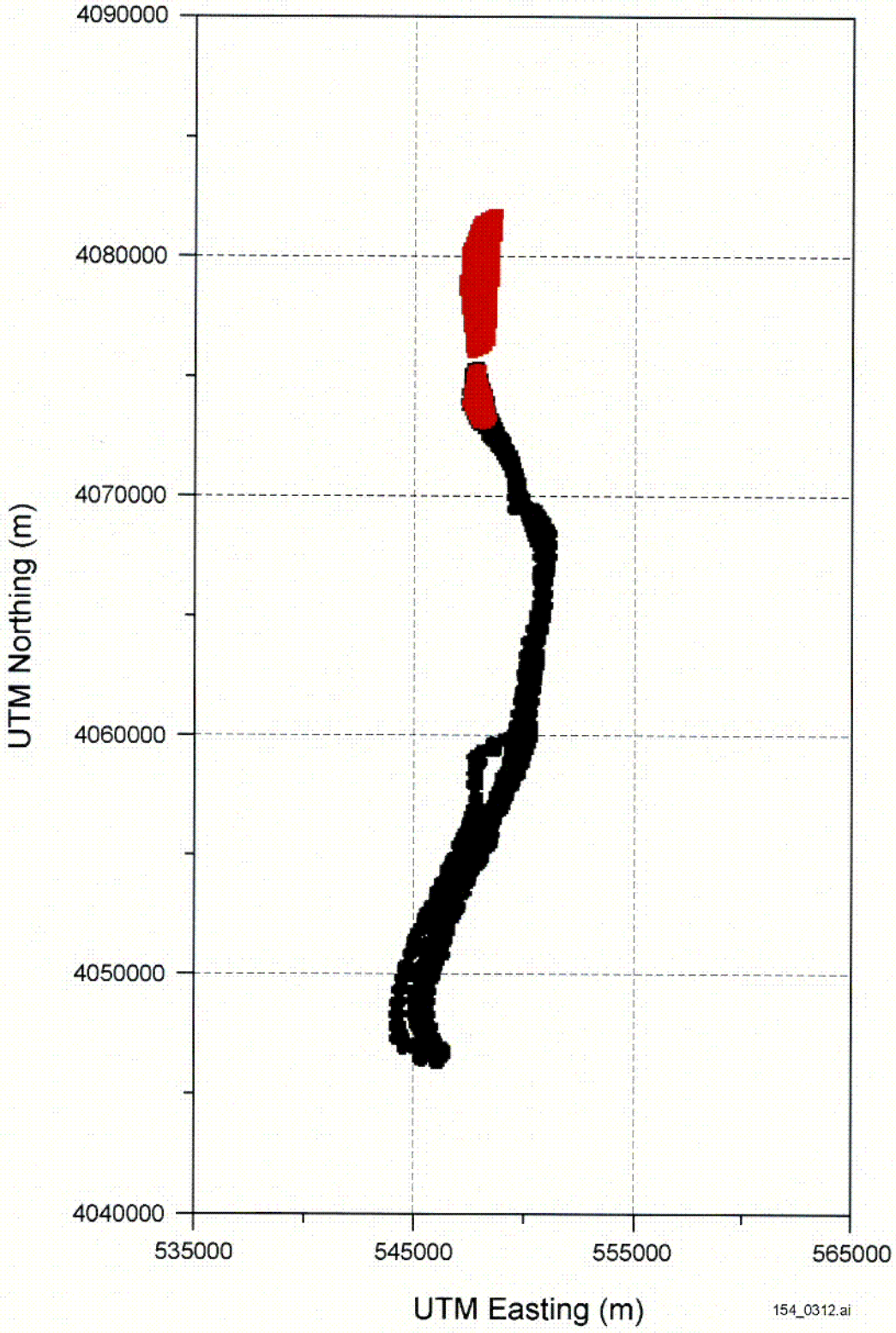

154_0312.ai

Source: Robinson 2001 [DIRS 154995], Filename "02_calib.sptr2".

Figure 12.3.2.3-3c. Plan View of Particle Pathlines from the Potential Repository with Pathlines from the Southern Lobe of an Increased Repository Footprint

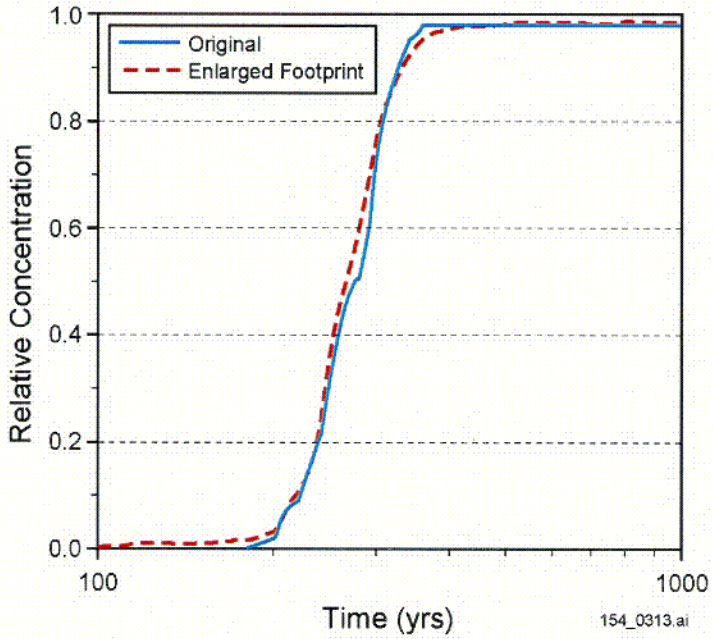

154_0313.ai

Source: Robinson 2001 [DIRS 154995], Filename "fig4.txt".

NOTE: Data for the original potential repository footprint and the increased footprint associated with the flexible design are shown. The model was run using expected values for all parameters and no diffusion. The model used to generate the breakthrough curves is reasonably conservative for TSPA analyses, and furthermore, the resulting times only represent travel in the saturated zone portion of the system. Consequently, the results should not be used to evaluate the expected breakthrough of radionuclides or groundwater travel time at the point of compliance.

Figure 12.3.2.3-4. Breakthrough Curves to the 20-km Compliance Boundary for the Case of No Matrix Diffusion and Distributed Release Over the Entire Potential Repository Footprint

C11

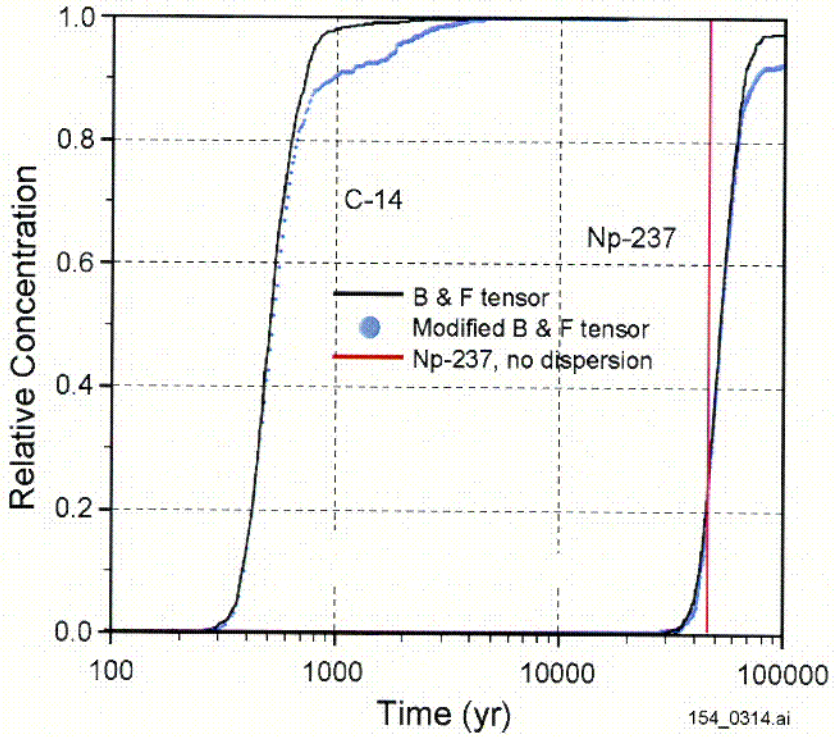

154_0314.ai

Source: Robinson 2001 [DIRS 154995], Filename "fig5c-14.txt" and "fig5np-237.txt".

NOTE: Black curves use the Burnett and Frind (1987 [DIRS 130526]) tensor; blue points use the modified Burnett and Frind tensor. C-14 = carbon-14; Np-237 = neptunium-237. The model was run using expected values for all parameters and no matrix diffusion. The model used to generate the breakthrough curves is reasonably conservative for TSPA analyses, and furthermore, the resulting times only represent travel in the saturated zone portion of the system. Consequently, the results should not be used to evaluate the expected breakthrough of radionuclides or groundwater travel time at the point of compliance.

Figure 12.3.2.3-5. Breakthrough Curves at the 20-km Point of Compliance Using Two Dispersion Coefficient Tensors and Two Radionuclides

C12

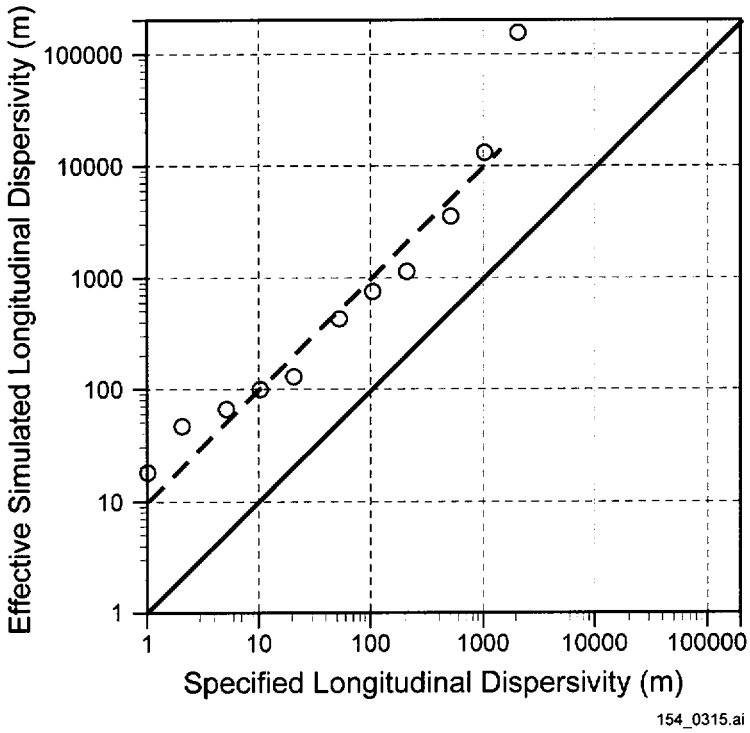

154_0315.ai

Source: Kuzio 2001 [DIRS 154912].

NOTE: Data from the site-scale saturated zone flow and transport model. Open circles are the results of the effective longitudinal dispersivity analysis. The bold line is the specified longitudinal dispersivity.

Figure 12.3.2.3-6. Effective Simulated Longitudinal Dispersivity Versus Specified Longitudinal Dispersivity

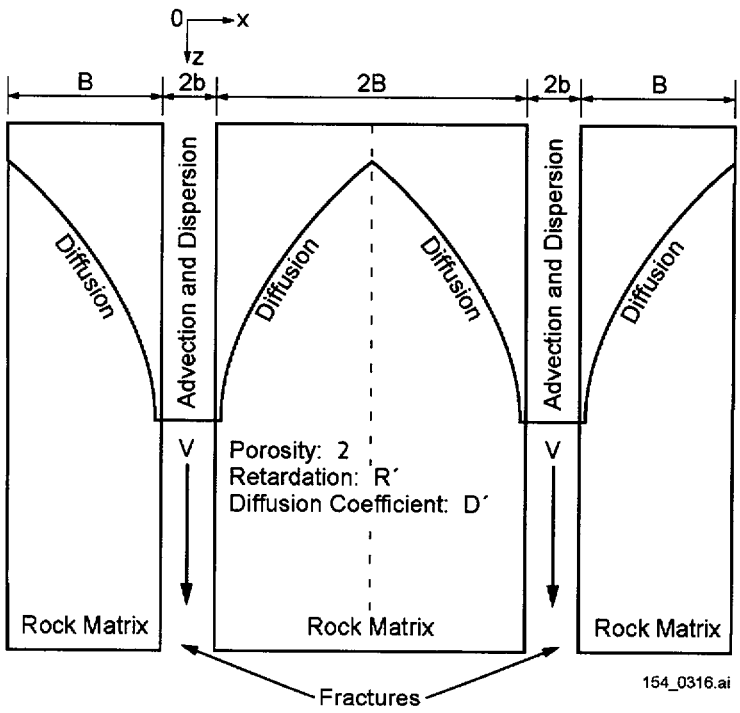

154_0316.ai

Figure 12.3.2.3-7. Schematic Diagram of the Matrix Diffusion Model

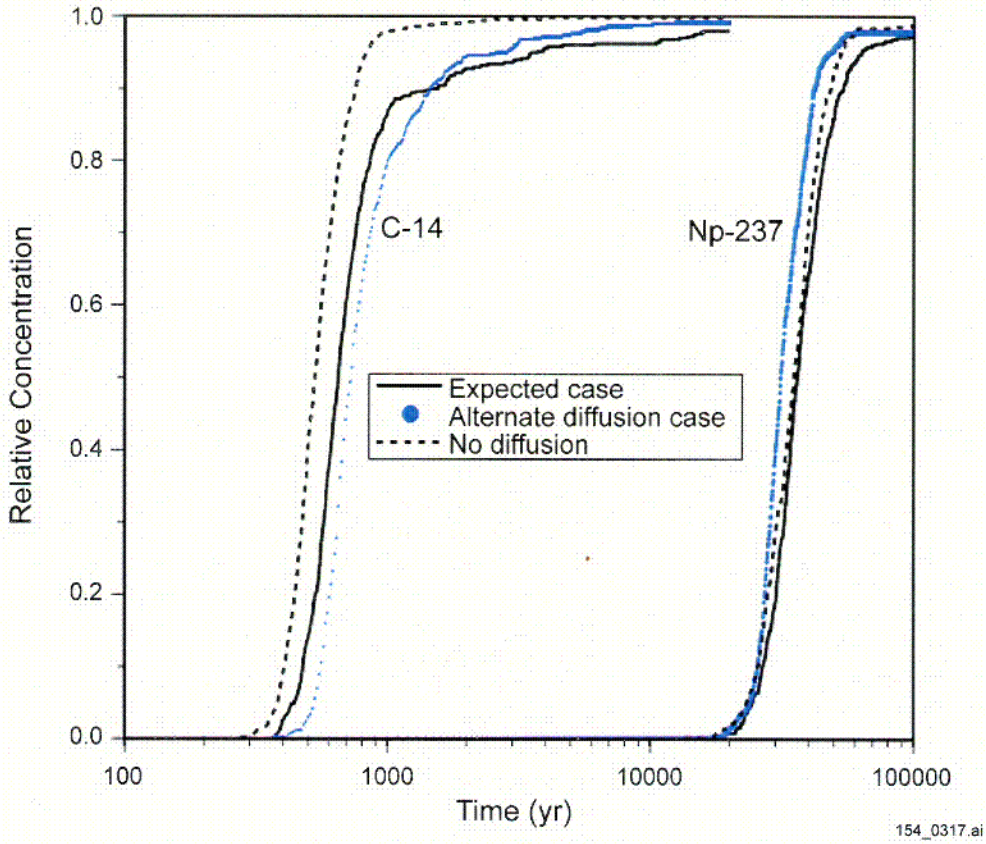

154_0317.ai

Source: Robinson 2001 [DIRS 154995], Filenames "fig8c-14.txt" and "fig8np-237.txt".

NOTE: C-14 = carbon-14; Np-237 = neptunium-237. The model used to generate the breakthrough curves is reasonably conservative for TSPA analyses, and furthermore, the resulting times only represent travel in the saturated zone portion of the system. Consequently, the results should not be used to evaluate the expected breakthrough of radionuclides or groundwater travel time at the point of compliance.

Figure 12.3.2.3-8. Matrix Diffusion Models for Carbon-14 (Conservative) and Neptunium-237 (Weakly Sorbing) Radionuclides

C13

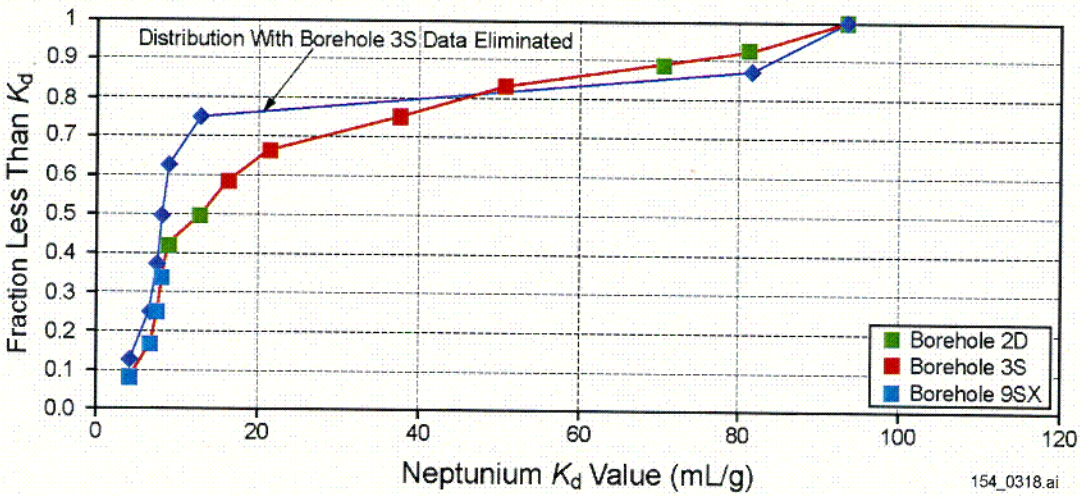

154_0318.ai

Source: Reimus 2001 [DIRS 154994], File "Neptunium Alluvium Sorption"; DTN: LA0003JC831341.001 [DIRS 147176].

NOTE: Alluvium samples for these sorption tests were obtained from NC-EWDP boreholes 2D, 3S, and 9SX. The red curve includes all data cited in the legend, and the blue curve includes all data cited in the legend except for the 3S data.

Figure 12.3.2.4-1. Neptunium Sorption Coefficients results from Batch Sorption Tests

C14

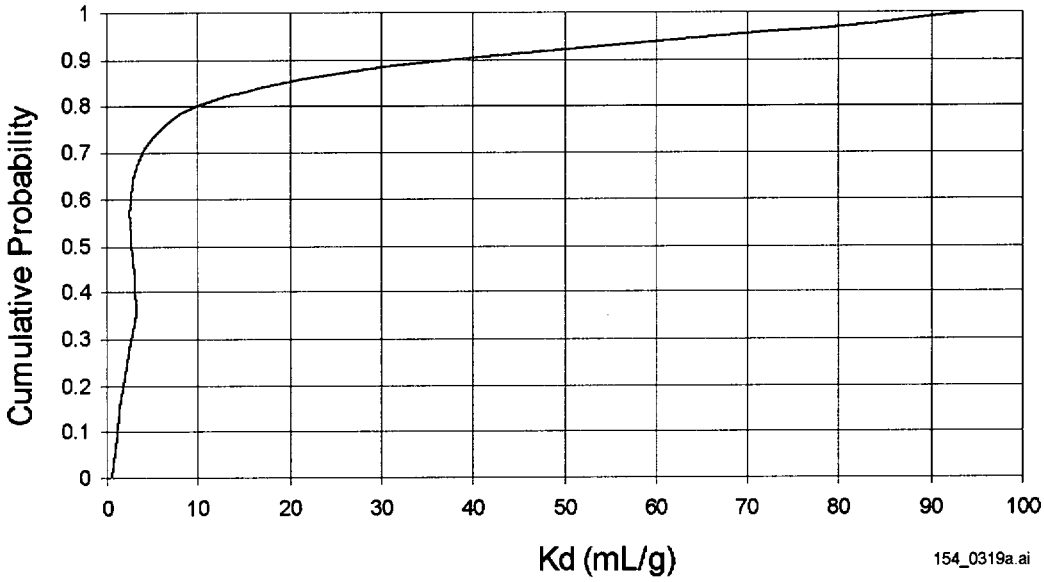

154_0319a.ai

Source: Kuzio 2001 [DIRS 154912], Filename "archive_sspa_v1_data/Np_cdf_uu".

Figure 12.3.2.4-2. Cumulative Distribution Function for Neptunium Sorption Coefficients (K_ds) used for Unquantified Uncertainty Calculations

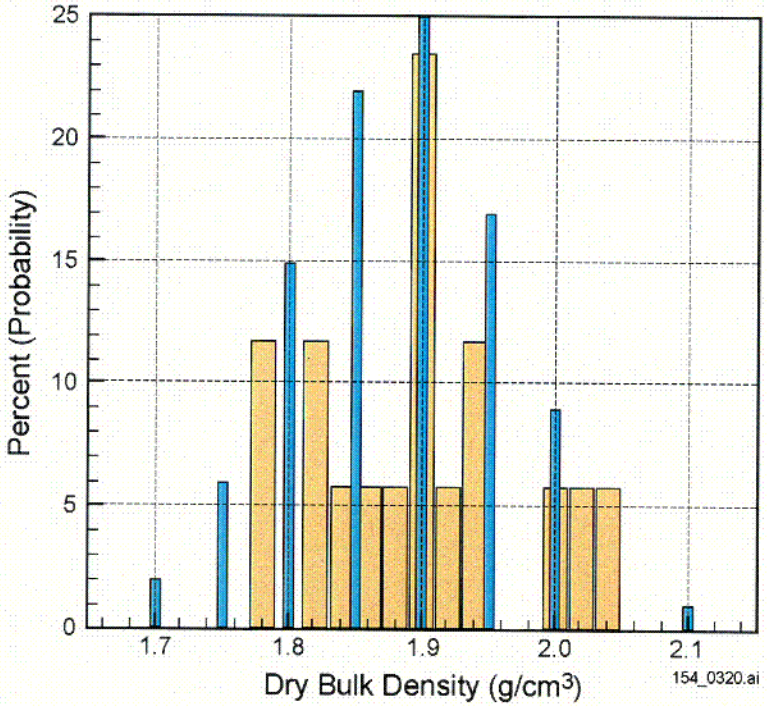

154_0320.ai

Source: Computed from saturated bulk densities presented by Black (2000 [DIRS 154704], p. 18).

NOTE: Thick bars represent measured data; thin bars represent data used in TSPA-SR supplemental analysis (McNeish 2001 [DIRS 155023]). The bars are located at the midpoint of the histogram interval.

Figure 12.3.2.4-3. Distribution of Simulated and Measured Dry Bulk Density for Alluvium

C15

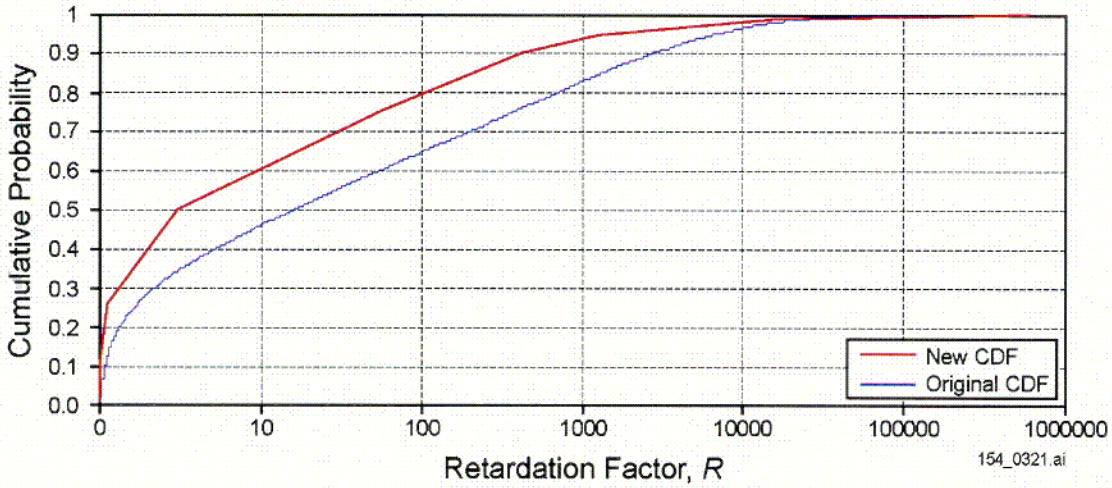

154_0321.ai

Source: Original CDF: CRWMS M&O 2000 [DIRS 129286], Figure 10, Curve B. New CDF: Kuzio 2001 [DIRS 155004], Filename "Grain_Size_Calcs_Submit", 5th Worksheet.

Figure 12.3.2.4-4. Original and new Cumulative Probability Density Functions for the Retardation Factor of Radionuclides Irreversibly-Sorbed to Colloids in the Alluvium.

C16

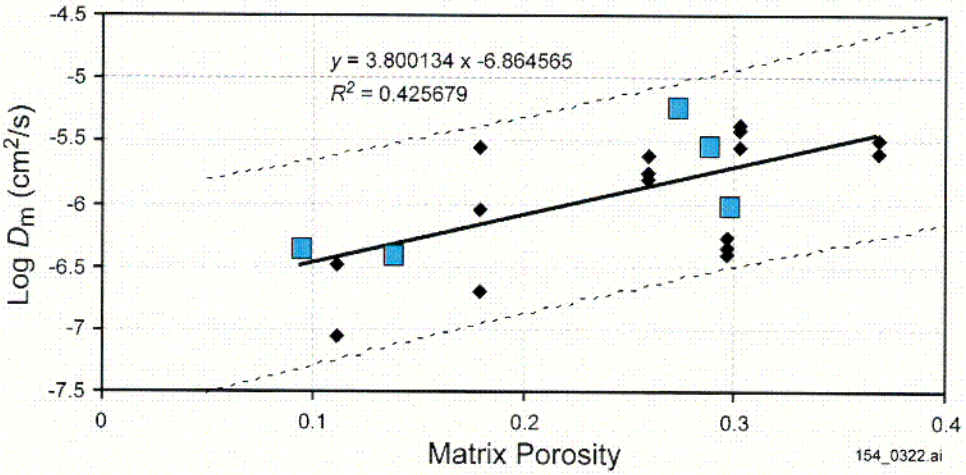

154_0322.ai

Source: Reimus 2001 [DIRS 154994], Filename "diffusion cell data for C-wells data"; C-wells data: DTN: LA9909PR831231.005 [DIRS 129624] (these data are non-Q because non-Q software was used to obtain diffusion coefficients from experimental data). Pahute Mesa data: Reimus et al. (1999 [DIRS 154689], p. 24, Table 2-2).

NOTE: D_m = matrix diffusion coefficient. Results of laboratory diffusion-cell experiments for bromide from C-wells cores (squares) and iodide from borehole ER-20-6 #1 on Pahute Mesa at the NTS (diamonds). Solid line is the best linear regression fit to all the data; dashed lines are 95 percent confidence intervals.

Figure 12.3.2.4-5. Matrix Diffusion Coefficients as a Function of Matrix Porosity

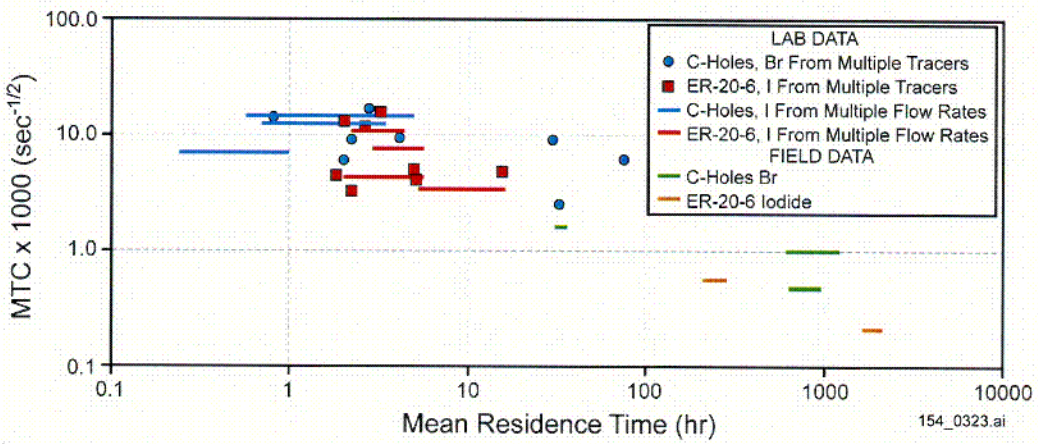

154_0323.ai

Source: Lab data for borehole ER-20-6 is from Reimus et al. 1999 [DIRS 154689], pp. 27 to 29, Tables 3-2 to 3-8; Reimus 2001 [DIRS 154994], Filename "Diffusion MTCs-Volcanics". Field data for borehole ER-20-6 is from Reimus and Haga 1999 [DIRS 154705], p.19. DTN: LA9909PR831231.003 [DIRS 140107]. DTN: LA9909PR831231.005 [DIRS 129624]. (C-wells data only).

NOTE: MTC = mass transfer coefficient. C-Holes refers to the C-wells Complex. Results from laboratory and field transport experiments in fractured volcanic rocks at the Nevada Test Site.

Figure 12.3.2.4-6. Matrix Diffusion Mass Transfer Coefficients as a Function of Mean Tracer Residence Time

C17

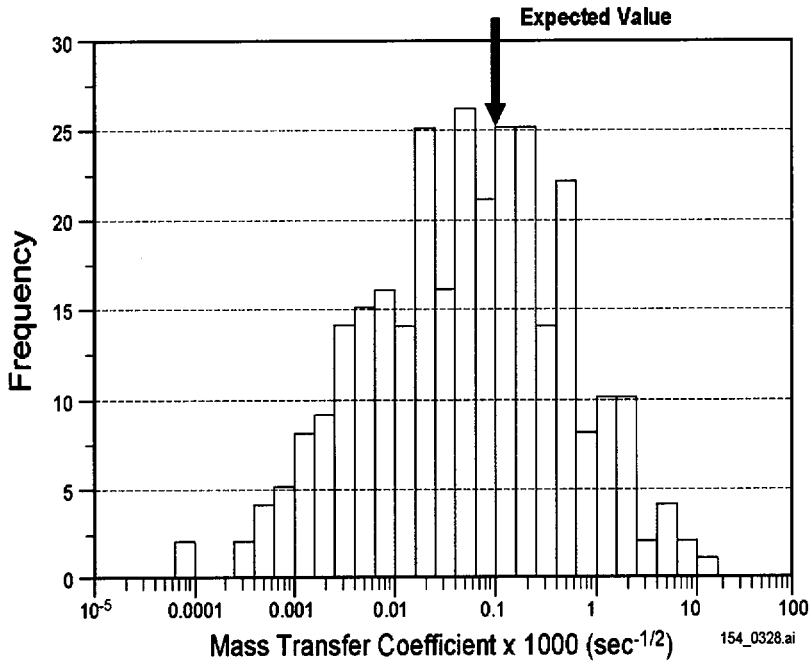

154_0328.ai

Source: Kuzio 2001 [DIRS 154912], Filename "archive_sspa_v1_data/mass_transfer_coeff/mass_transfer_coeff_300_fp_dc.xls".

NOTE: Data from 300 realizations of the site-scale SZ flow and transport model for TSPA.

Figure 12.3.2.4-7. Histogram of Mass Transfer Coefficient Values

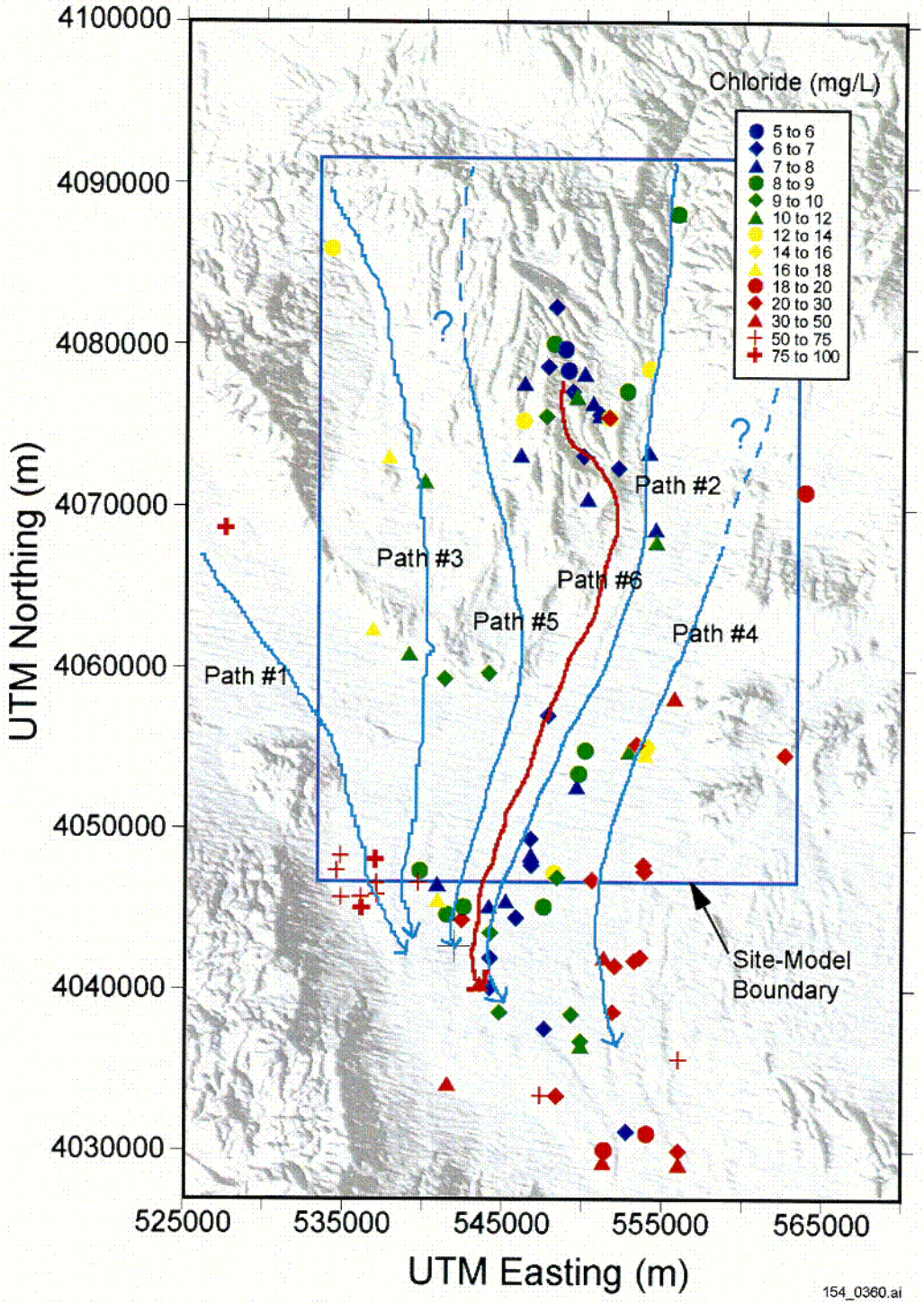

154_0360.ai

Source: Adapted from CRWMS M&O 2001 [DIRS 154795], Figure 17.

Figure 12.4-1. Groundwater Flow Paths Determined from Hydrochemical and Isotopic Data

C18

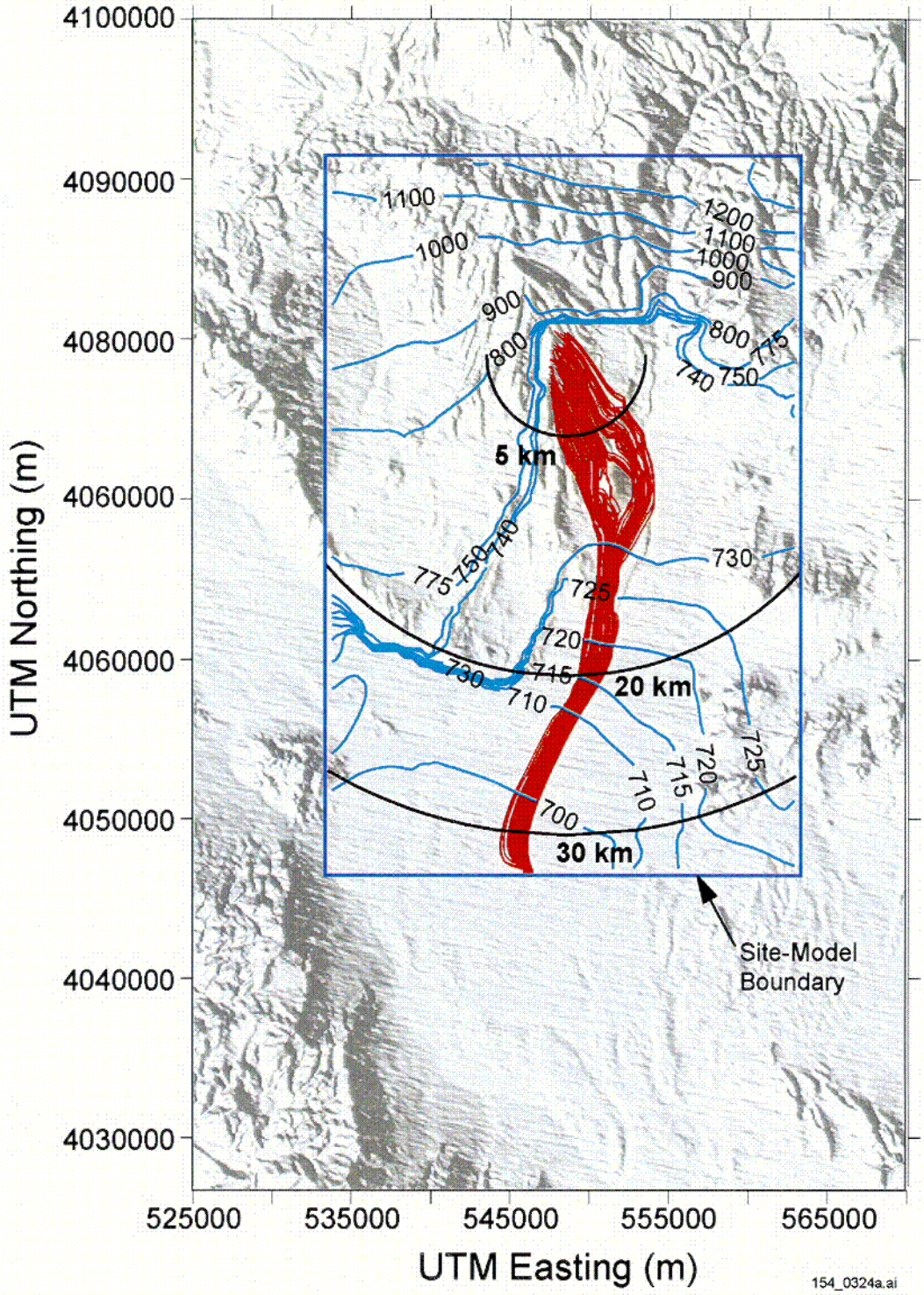

154_0324a.ai

Source: Adapted from CRWMS M&O 2000 [DIRS 139582], Figure 87.

NOTE: Blue lines are hydraulic head contours (m); red lines are the particle pathlines.

Figure 12.4-2. Groundwater Flow Paths Determined from Simulated Particle Pathlines

C19

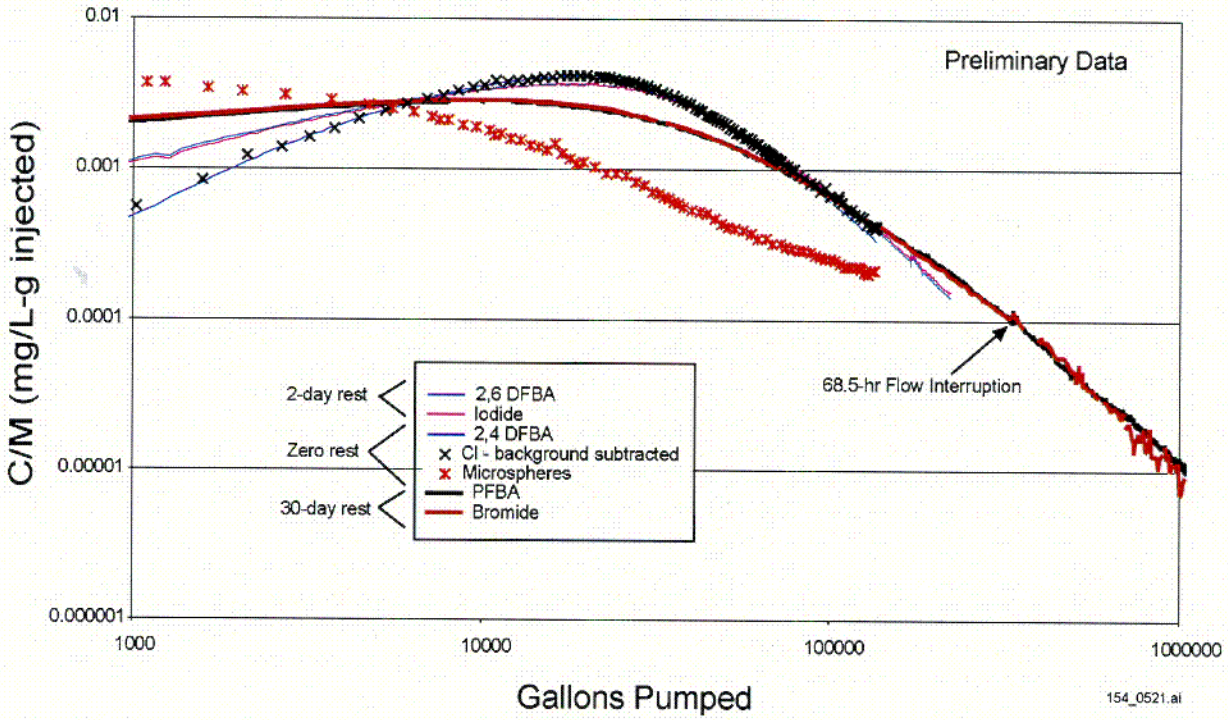

154_0521.ai

Source: Reimus 2001 [DIRS 155251], Filename "ATC Tracers – 1st Test", "ATC Tracers – 2nd Test", and "ATC Tracers – 3rd Test".

NOTE: The vertical axis is normalized concentration, which is concentration divided by injection mass. Tracers injected in earlier tests continued to be recovered in subsequent tests, but only the responses obtained prior to the injection of additional tracers are shown here.

Figure 12.4-3. Normalized Tracer Concentration Versus Gallons Pumped in Three Single-Well Tracer Tests Conducted in the Uppermost Screened Interval of Well NC-EWDP-19D1

C20

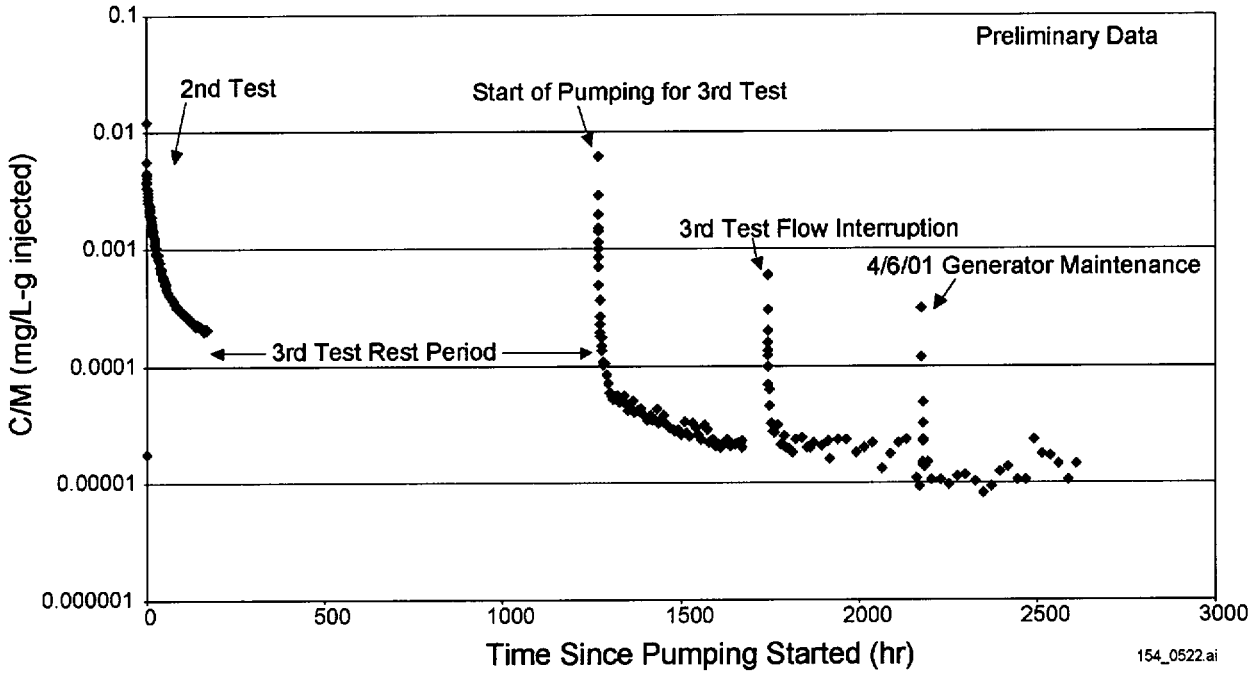

154_0522.ai

Source: Reimus 2001 [DIRS 155251], Filename "ATC Tracers – 2nd Test" and "ATC Tracers – 3rd Test".

NOTE: The vertical axis is normalized concentration, which is concentration divided by injection mass. Microspheres were injected only in the second test. However, the concentrations increased dramatically for a short time each time the pump was restarted after a shutdown.

Figure 12.4-4. Normalized Microsphere Concentrations Versus Time During the Second and Third Single-Well Tests in the Uppermost Screened Interval in Well NC-EWDP-19D1.

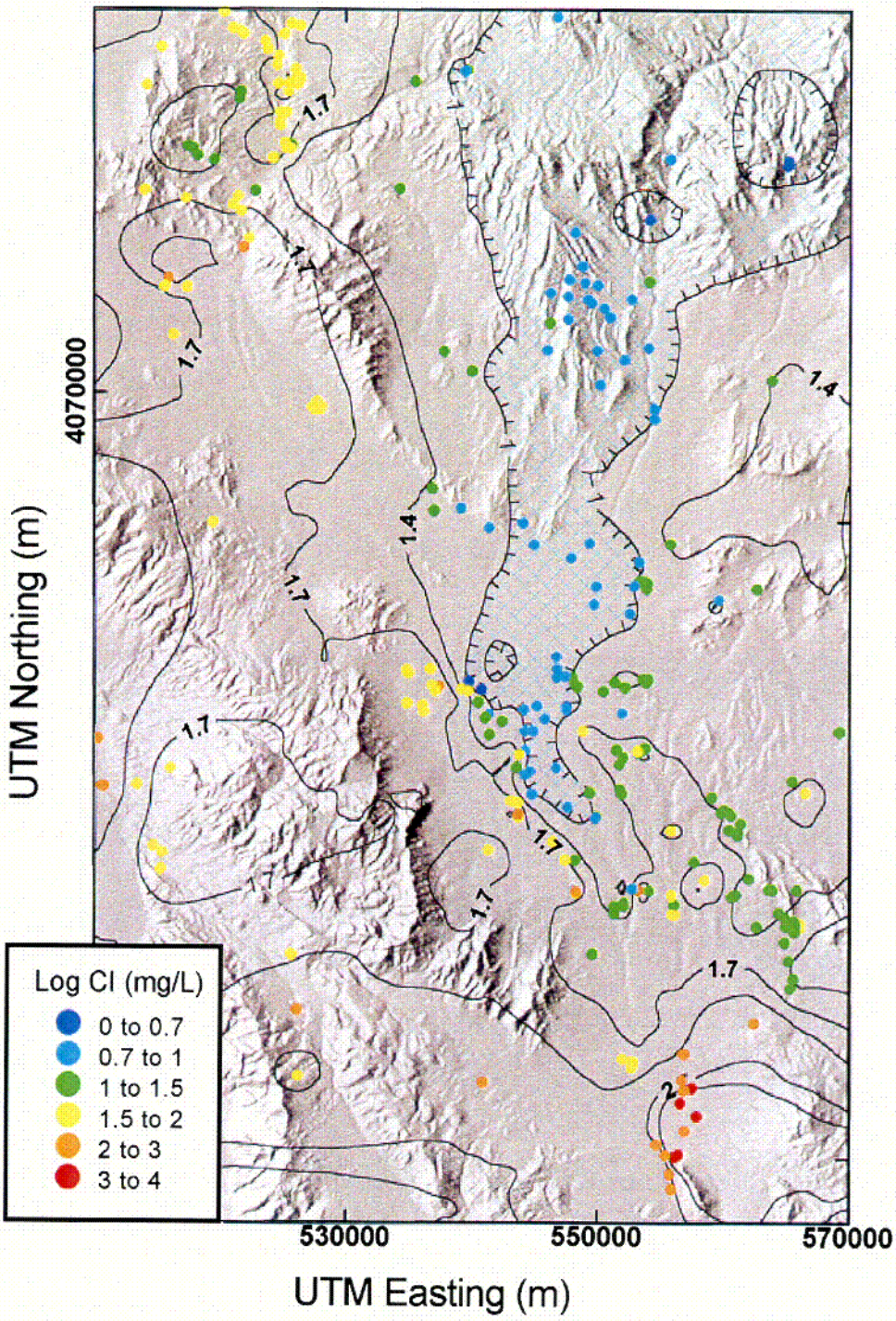

154_0505.ai

Source: Adapted from CRWMS M&O 2001 [DIRS 154795], Figure 5.

NOTE: Contours denote waters of similar composition.

Figure 12.4-5. Chloride Concentration in Groundwater

C21

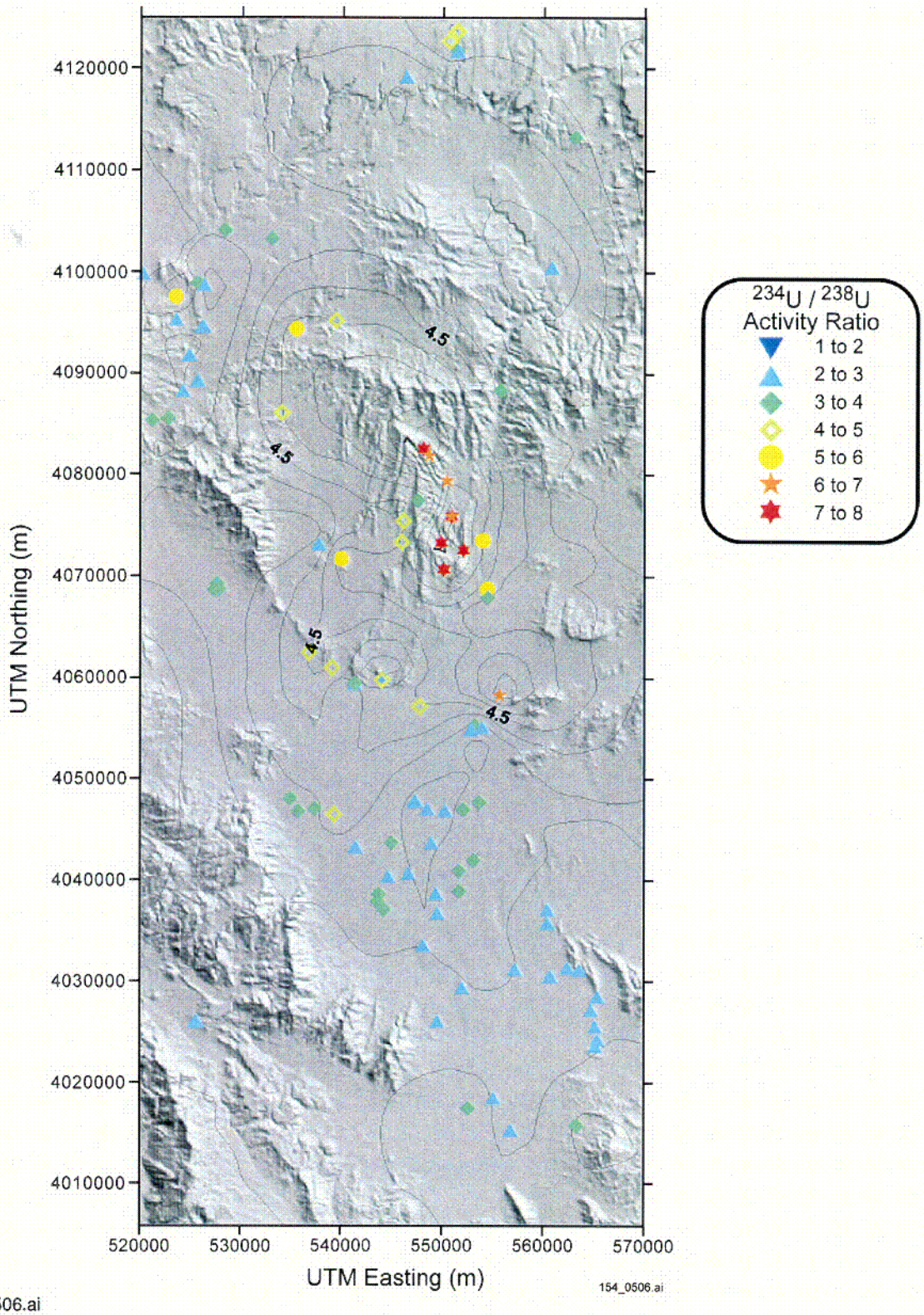

154_0506.ai

Source: Adapted from CRWMS M&O 2001 [DIRS 154795], Figure 18.

NOTE: Contours denote waters of similar composition.

Figure 12.4-6. Uranium Activity Ratios in Saturated Zone Waters

C22

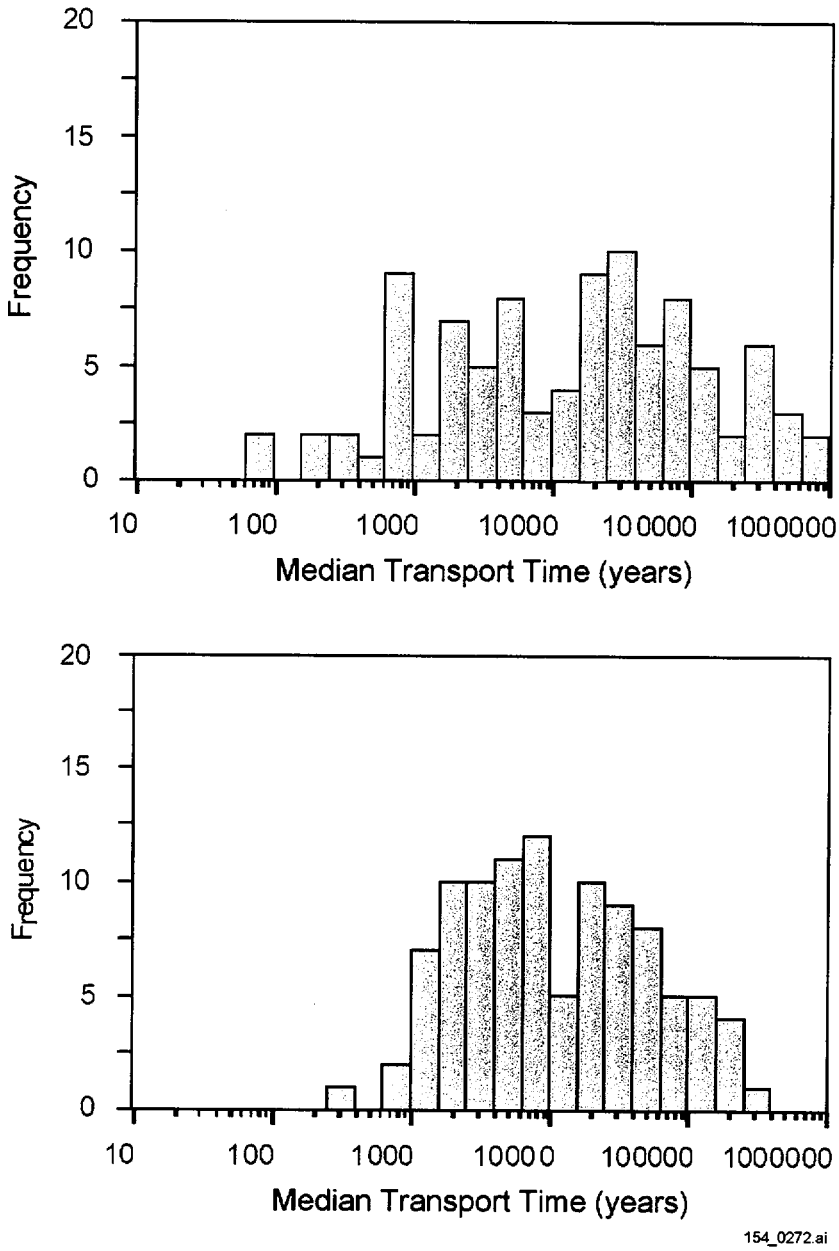

154_0272.ai

Source: Kuzio 2001 [DIRS 154912], Filenames "archive_sspa_v1_data/uu/btc_medians_Np_01.dat" and "archive_sspa_v1_data/nominal_case/btc_medians_Np_01.dat".

NOTE: Results of the supplemental science and performance analysis (upper) (McNeish 2001 [DIRS 155023]) and unquantified uncertainty (lower) cases based on 100 realizations of the site-scale saturated zone flow and transport model. The model used to generate the breakthrough curves is reasonably conservative for TSPA analyses, and furthermore, the resulting times only represent travel in the saturated zone portion of the system. Consequently, the results should not be used to evaluate the expected breakthrough of radionuclides or groundwater travel time at the point of compliance.

Figure 12.5.1-1. Simulated Median Transport Times of Neptunium for the Supplemental Science and Performance Analysis and the Unquantified Uncertainty Cases

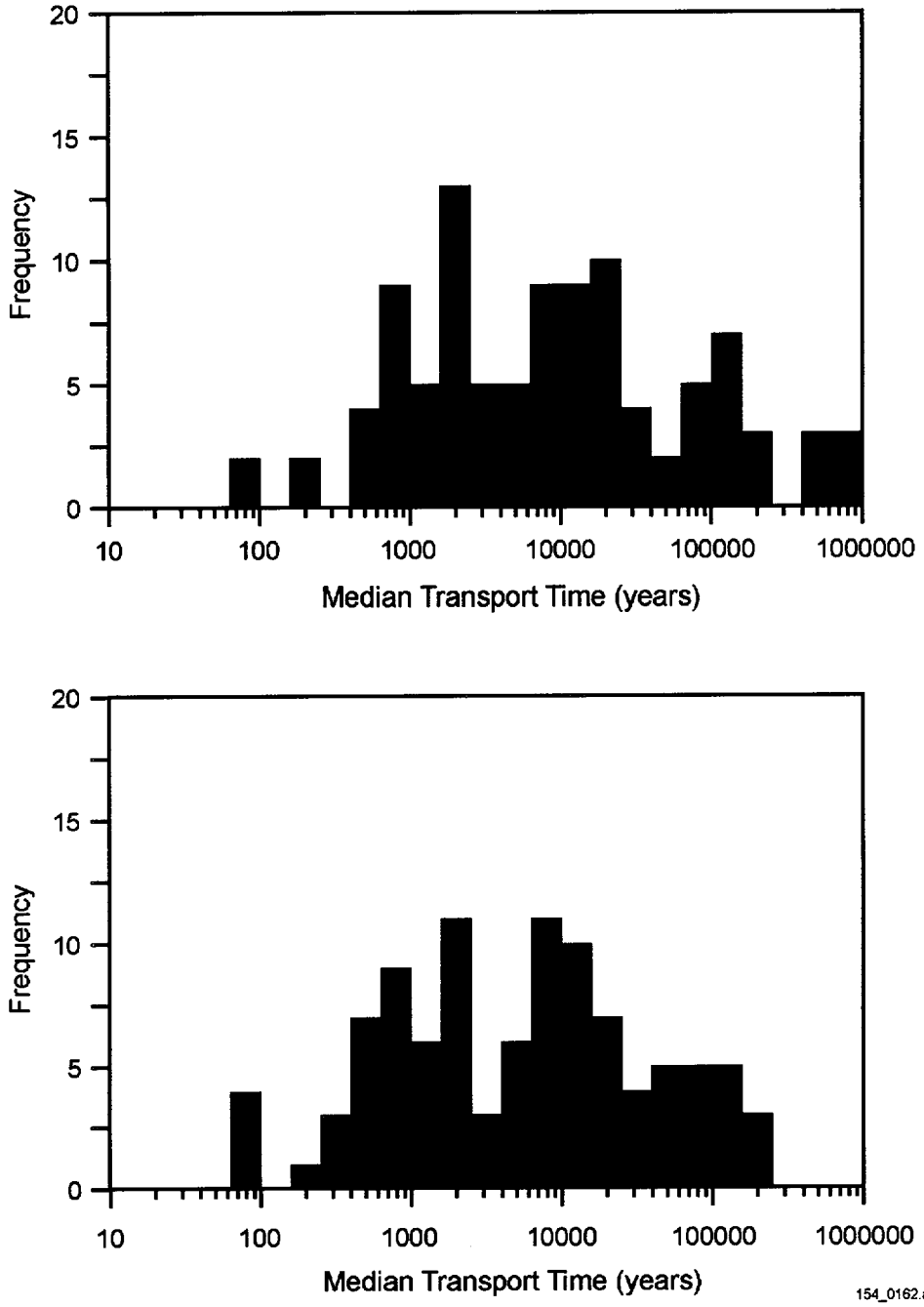

154_0162.ai

Source: Kuzio 2001 [DIRS 154912] Filename "archive_sspa_v1_data/no_diff/btc_medians_U_01.dat" and "archive_sspa_v1_data/nominal_case/btc_medians_U_01.dat".

NOTE: Histograms for 100 realizations of the supplemental science and performance analysis (upper) (McNeish 2001[DIRS 155023]) and no-matrix-diffusion (lower) cases from the site-scale saturated zone flow and transport model. The model used to generate the breakthrough curves is reasonably conservative for TSPA analyses, and further, the resulting times only represent travel in the saturated zone portion of the system. Consequently, the results should not be used to evaluate the expected breakthrough of radionuclides at the point of compliance.

Figure 12.5.2-1. Simulated Median Transport Times of Uranium for the Supplemental Science and Performance Analysis and the No-Matrix-Diffusion Cases

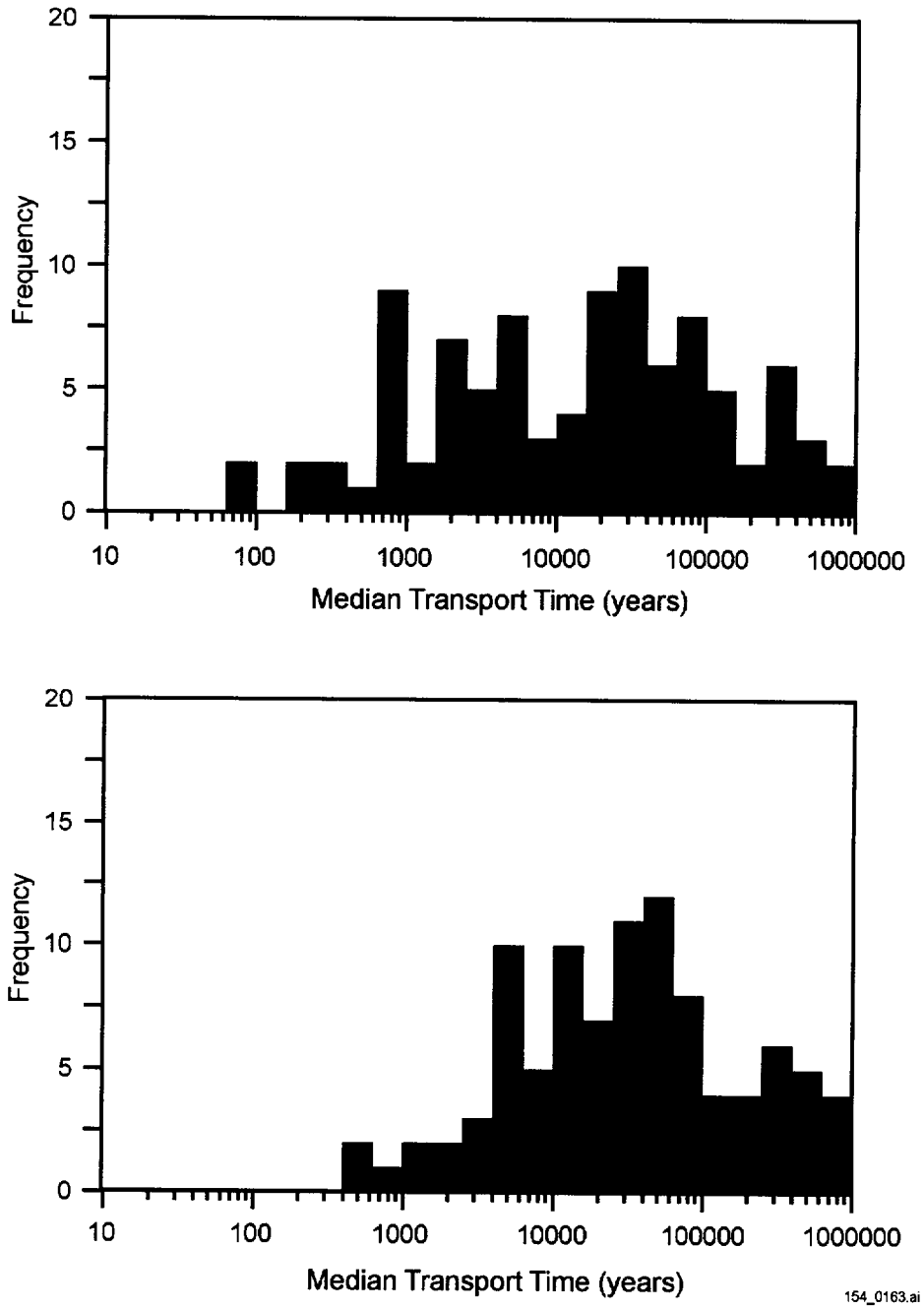

154_0163.ai

Source: Kuzio 2001 [DIRS 154912], Filename "archive_sspa_v1_data/high_diff/btc_medians_Np_01.dat" and "archive_sspa_v1_data/nominal_case/btc_medians_Np_01.data".

NOTE: Histograms for 100 realizations of the supplemental science and performance analysis (upper) (McNeish 2001 [DIRS 155023]) and enhanced-matrix-diffusion (lower) cases from the site-scale saturated zone flow and transport model. The model used to generate the breakthrough curves is reasonably conservative for TSPA analyses, and further, the resulting times only represent travel in the saturated zone portion of the system. Consequently, the results should not be used to evaluate the expected breakthrough of radionuclides at the point of compliance.

Figure 12.5.2-2. Simulated Median Transport Times of Neptunium for the Supplemental Science and Performance Analysis and Enhanced Matrix Diffusion Cases

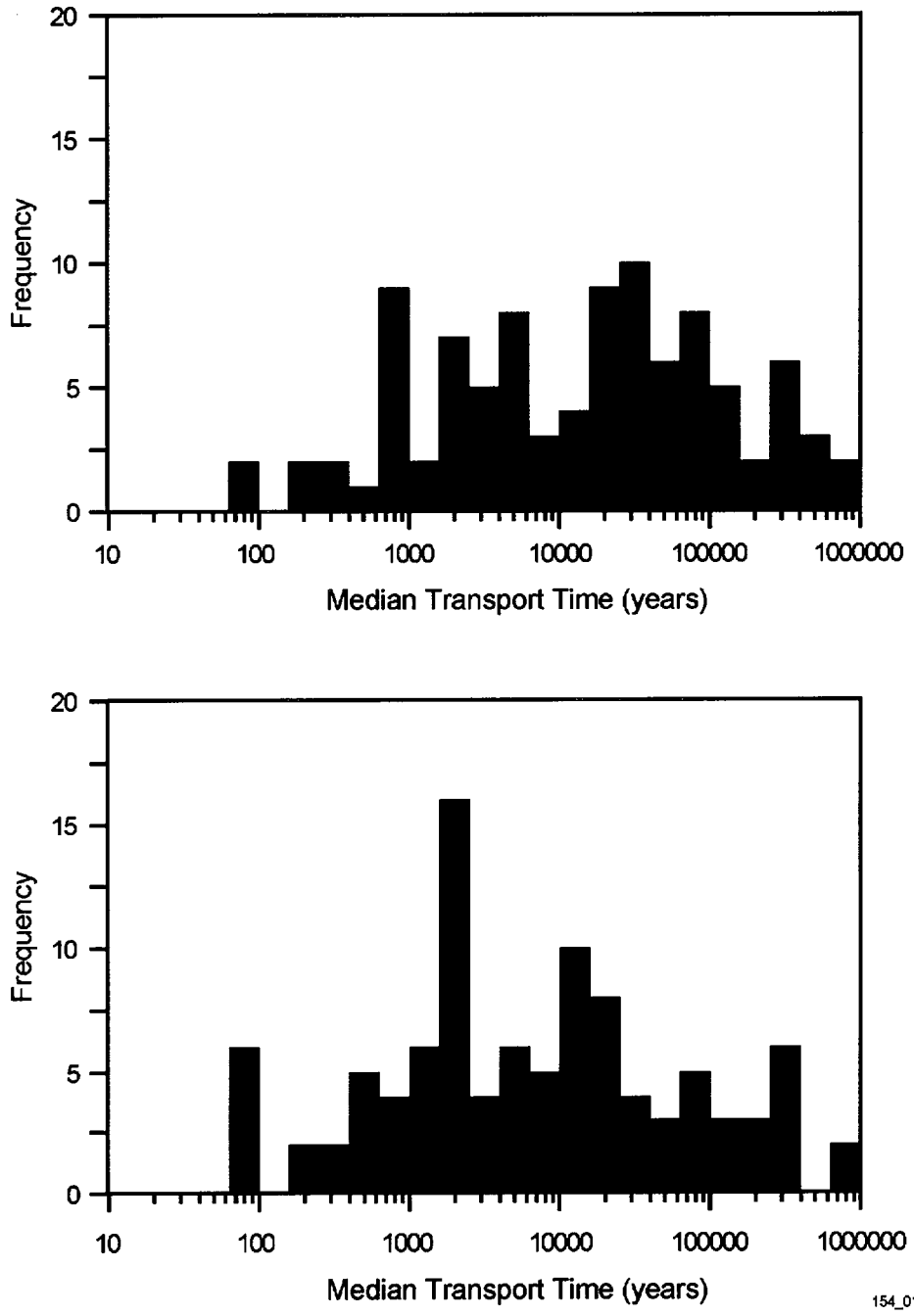

154_0164.ai

Source: Kuzio 2001 [DIRS 154912] Filename "archive_sspa_v1_data/no_alluv/btc_medians_Np_01.dat" and "archive_sspa_v1_data/nominal_case/btc_medians_Np_01.dat".

NOTE: Histograms for 100 realizations of the supplemental science and performance analysis (upper) (McNeish 2001 [DIRS 155023]) and minimum-alluvium (lower) cases from the site-scale saturated zone flow and transport model. The model used to generate the breakthrough curves is reasonably conservative for TSPA analyses, and further, the resulting times only represent travel in the saturated zone portion of the system. Consequently, the results should not be used to evaluate the expected breakthrough of radionuclides at the point of compliance.

Figure 12.5.2-3. Simulated Median Transport Times of Neptunium for the Supplemental Science and Performance Analysis and the Minimum Alluvium Cases

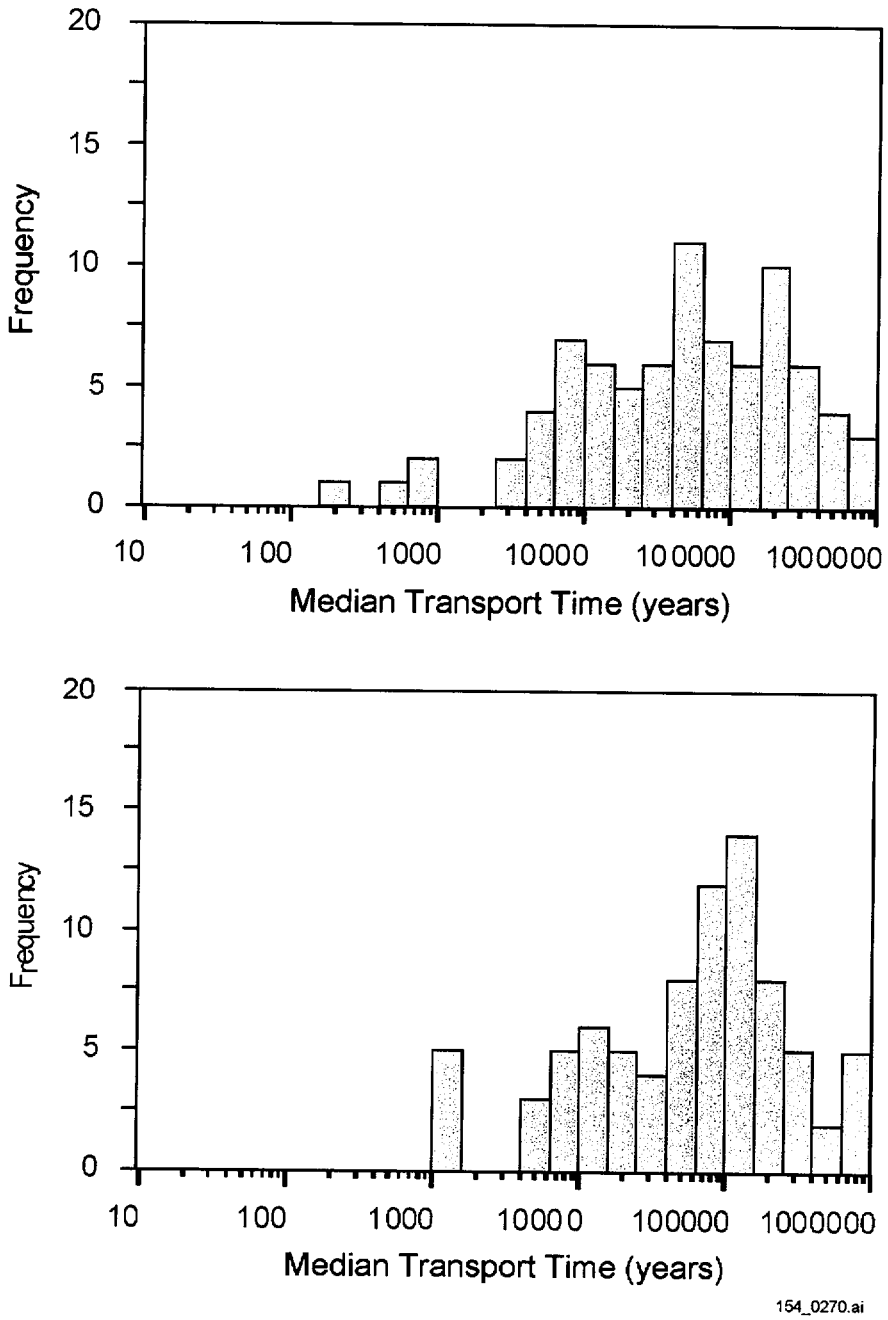

154_0270.ai

Source: Kuzio 2001 [DIRS 154912] Filename "archive_sspa_v1_data/alt-colloids/btc_medians_kc_01.dat" and archive_sspa_v1_data/nominal_case/btc_medians_kc_01.dat".

NOTE: Histograms for 100 realizations of the supplemental science and performance analysis (upper) (McNeish 2001 [DIRS 155023]) and increased uncertainty in colloid-facilitated transport (lower) cases from the site-scale saturated zone flow and transport model. The model used to generate the breakthrough curves is reasonably conservative for TSPA analyses, and further, the resulting times only represent travel in the saturated zone portion of the system. Consequently, the results should not be used to evaluate the expected breakthrough of radionuclides at the point of compliance.

Figure 12.5.2-4. Simulated Median Transport Times of Plutonium Reversibly Sorbed onto Colloids (K_c Model)

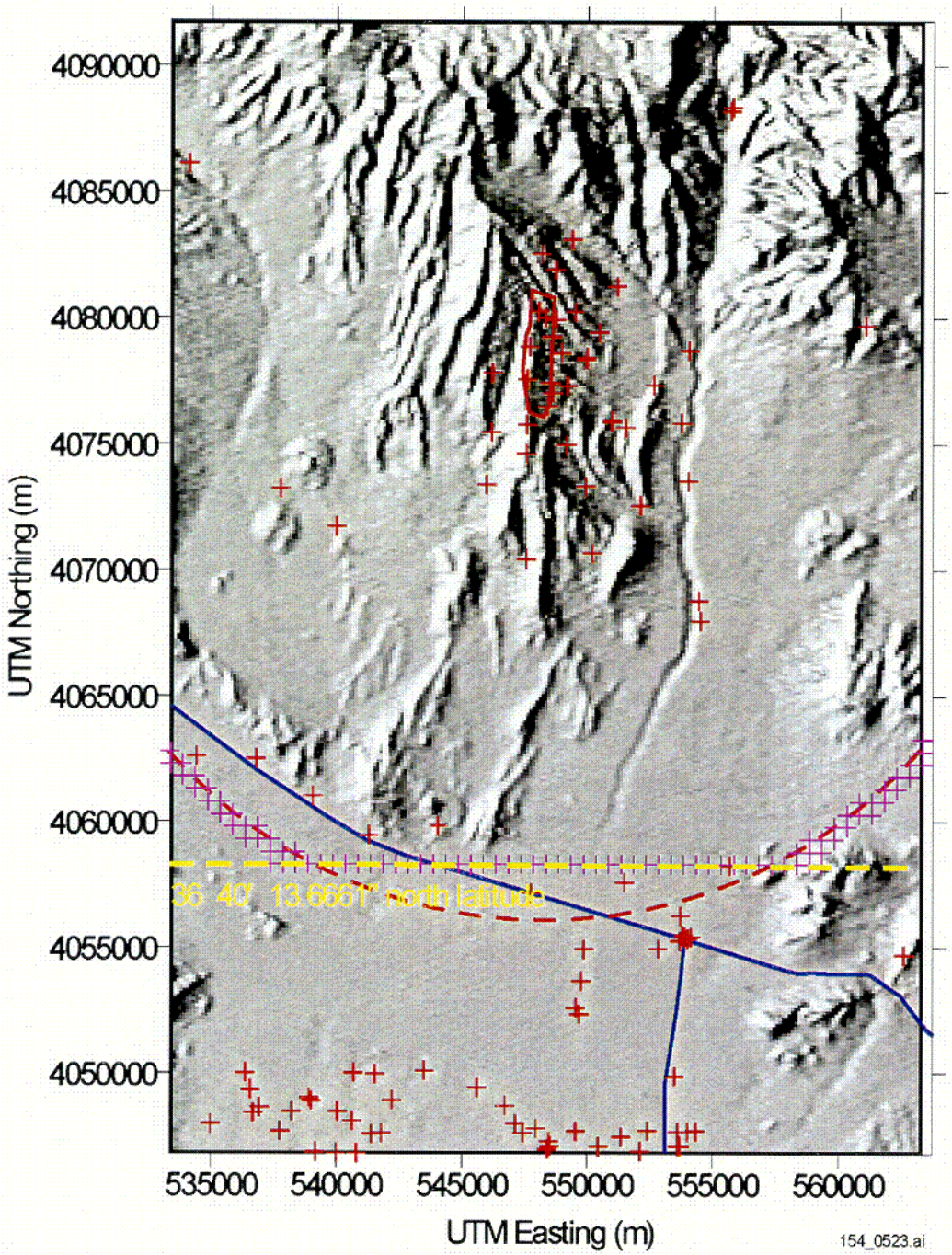

154_0523.ai

Source: Kuzio 2001 [DIRS 155244], Appendix 1.

NOTE: The yellow dashed line represents the southernmost boundary between the controlled area and accessible environment (36° 40' 13.6661" North latitude as per EPA 40 CFR 197.12 (66 FR 32074 [DIRS 155216])). The red dashed line represents the 20-km fence used in TSPA-SR to evaluate compliance with proposed EPA and NRC regulations. The purple crosses represent the intersection of the new southernmost boundary with the 20-km fence used in TSPA-SR evaluations. The red crosses are well locations, and the blue lines represent Highway 95 and Highway 373.

Figure 12.5.3-1 Southernmost Boundary of the Controlled Area and the Accessible Environment

C23

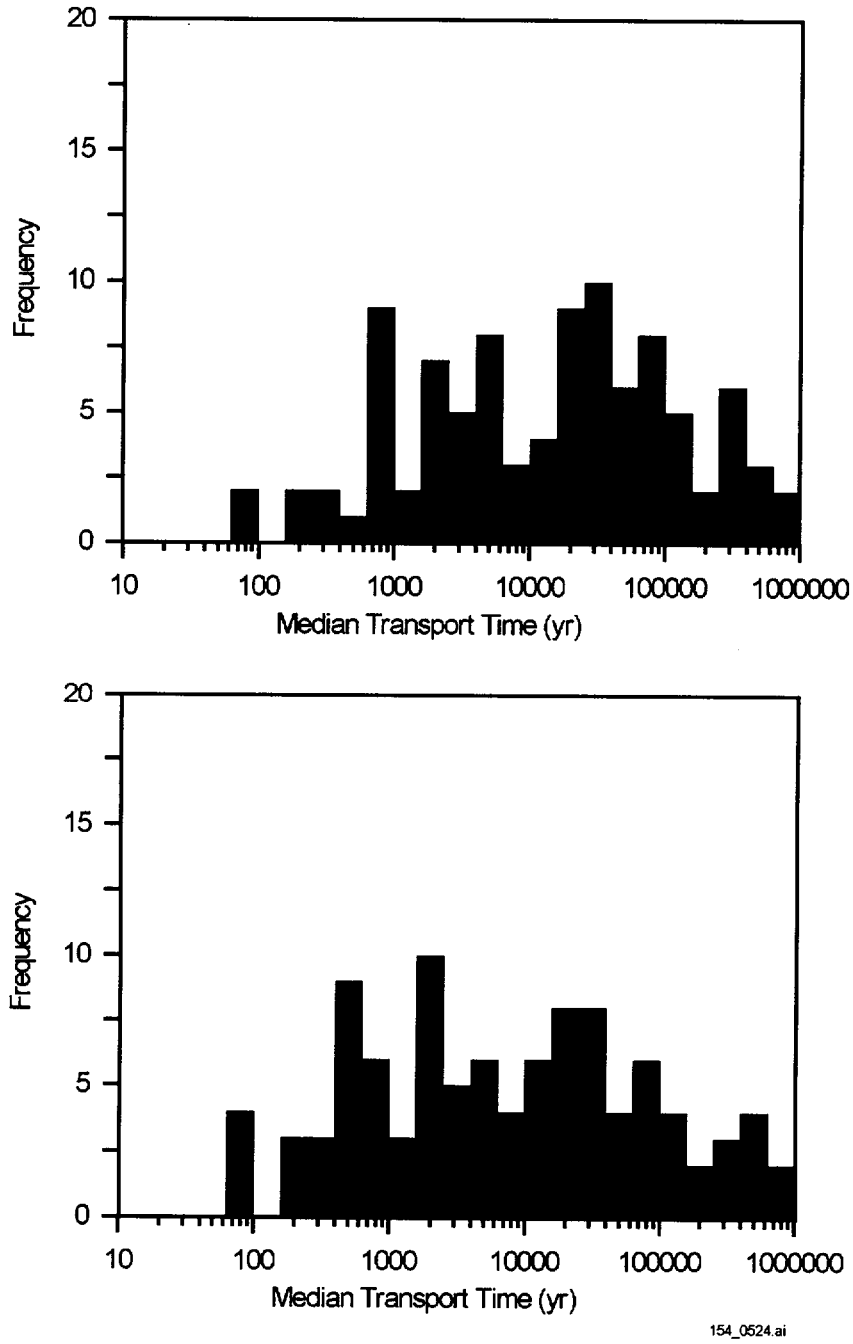

154_0524.ai

Source: Kuzio 2001 [DIRS 155244], Appendix 2.

Note: Upper panel is histogram for breakthrough 20 km from the potential repository, and lower panel is histogram for 18 km. The model used to generate the breakthrough curves is reasonably conservative for TSPA analyses, and furthermore, the resulting times only represent travel in the saturated zone portion of the system. Consequently, the results should not be used to evaluate the expected breakthrough of radionuclides or groundwater travel time at the point of compliance.

Figure 12.5.3-2. Frequency of Breakthrough for Simulated Median Transport Times of Neptunium-237

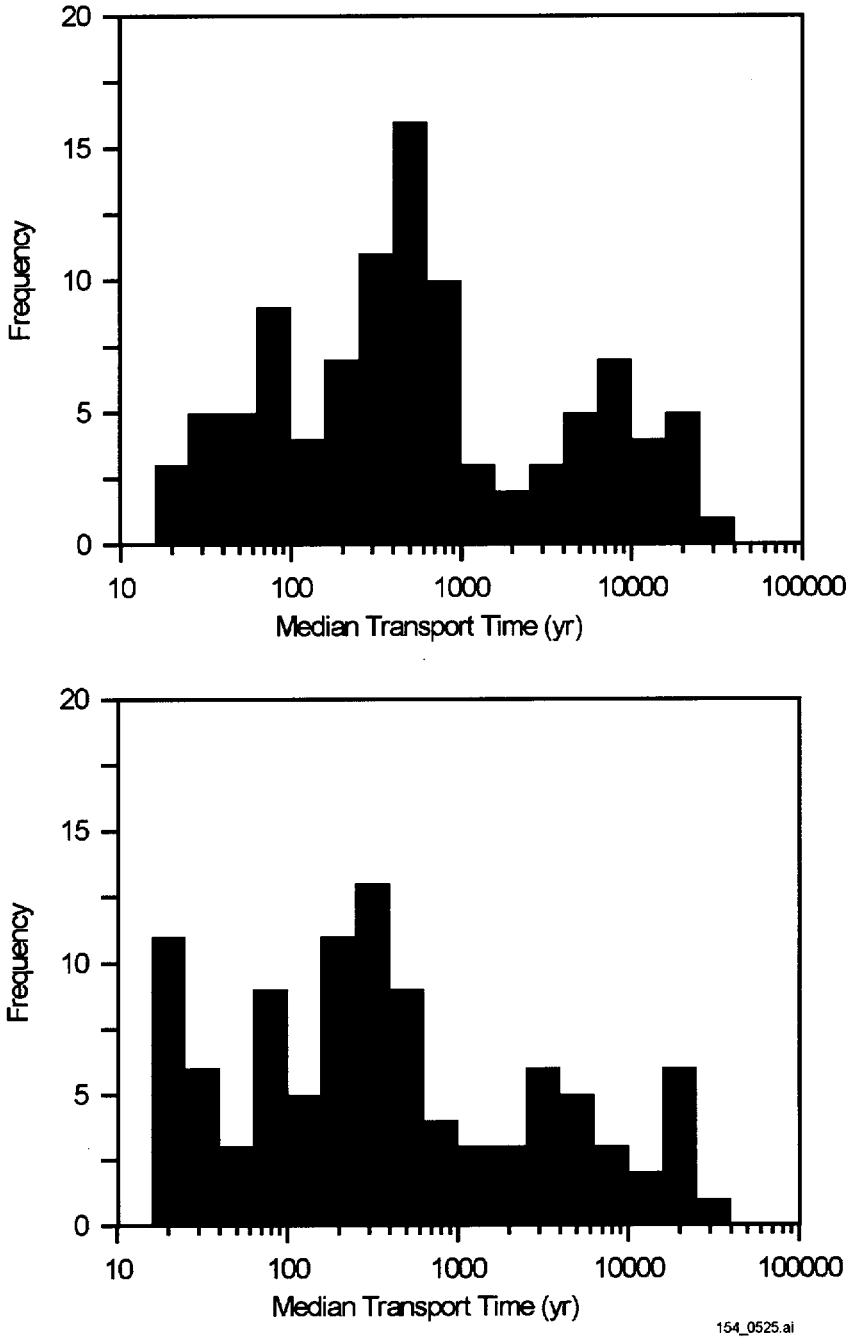

154_0525.ai

Source: Kuzio 2001 [DIRS 155244], Appendix 3.

Note: Upper panel is histogram for breakthrough 20 km from the potential repository, and lower panel is histogram for 18 km. The model used to generate the breakthrough curves is reasonably conservative for TSPA analyses, and furthermore, the resulting times only represent travel in the saturated zone portion of the system. Consequently, the results should not be used to evaluate the expected breakthrough of radionuclides or groundwater travel time at the point of compliance.

Figure 12.5.3-3. Frequency of Breakthrough for Simulated Median Transport Times of Carbon-14

INTENTIONALLY LEFT BLANK